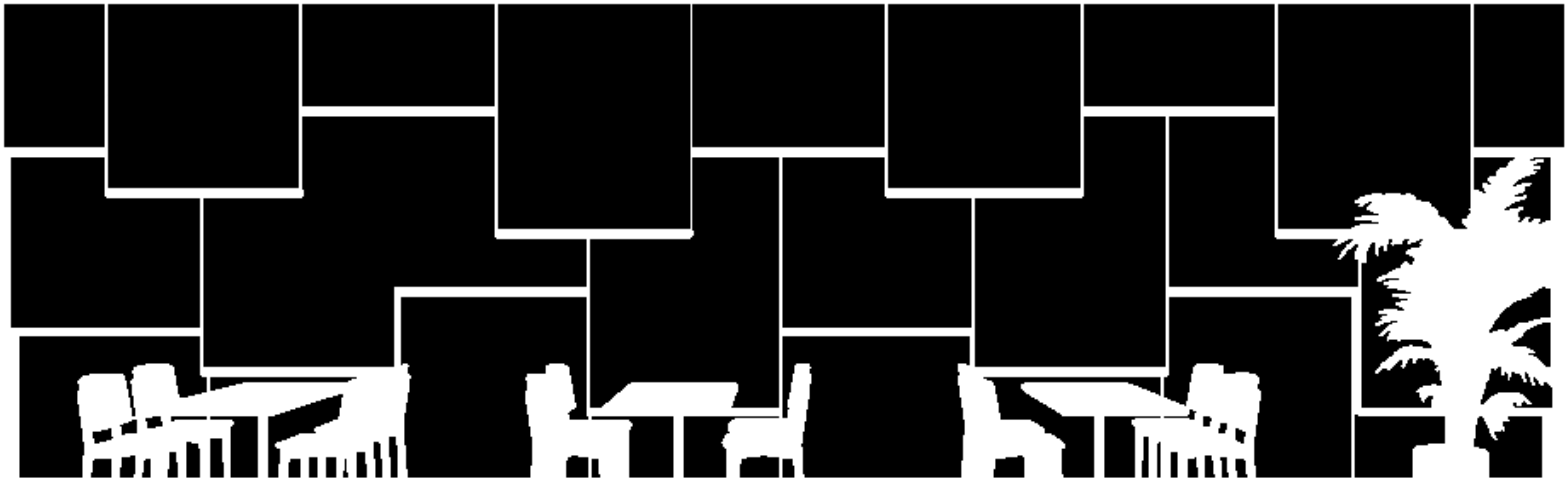


Comparative Analysis of Energy Saving and
Comfort Strategies in Glass Façade Buildings
System Modifications, Retrofitting, and Their Combination



Thesis Report

Building Technology Graduation Studio
Alya Farah Taufiqoh | 5564379

2024



Delft University of Technology

Building Technology Graduation Studio

Mentors:

Dr. Regina M.J. Bokel, Dr. Telesilla Bristogianni, Dr. Chujie Lu

External Delegate:

Drs. D.J. Dubbeling

P4 and P5 date:

29th May 2024 and 25th June 2024

Abstract

Inefficiencies in HVAC control and poorly designed glass façades can significantly impact energy demand and thermal comfort in buildings with extensive glass façades. Two potential solutions are the implementation of smart systems and retrofitting the glass façade. However, when considering these options in building design, it is often unclear which strategy is more effective. This thesis investigates the performance of smart systems using grey-box model predictive control (MPC) and the effectiveness of glass façade retrofitting strategies concerning energy savings and occupant thermal comfort. The case study for this research is an educational building with a vast glass façade. The study commenced with a review of relevant literature, followed by the development of the MPC system and an evaluation of its performance against various retrofitting strategies. The MPC system utilized a grey-box model for predictions and local optimization algorithms for control. The retrofitting strategies included the addition of films and curtains on the interior side of the glass façade. Results indicated a trade-off regarding the energy saving and thermal comfort between the two approaches. Compared to MPC, curtains did not reduce energy demand as significantly, but they provided better indoor thermal comfort. The study also found that the lumped model used in the MPC system had limitations for summer calculations and that some algorithms tended to be aggressive. In terms of retrofitting strategies, the application of curtains enhanced thermal comfort more effectively than adding films to the glass.

Keywords: Model Predictive Control, Grey-box Model, Glass Retrofitting Strategies, Glass Façade, Energy Efficient Buildings, Thermal comfort, Educational Buildings

Acknowledgments

First and foremost, I would like to thank God Almighty for His blessings and guidance throughout this thesis journey.

This endeavor would not have been possible without the support of my three mentors: Dr. Regina M.J. Bokel, Dr. Telesilla Bristogianni, and Dr. Chujie Lu. Their endless feedback, supervision, and, most importantly, patience, have been invaluable. Without their support, this thesis and I would have remained a big ball of overthinking and "what ifs."

I also owe a debt of gratitude to my external delegate, Drs. D.J. Dubbeling, who has been exceptionally kind and understanding throughout this journey. I would also like to thank the manager of the Pulse building for providing the necessary details.

Words cannot express my deep appreciation for the personal support and help from Milka van der Valk Bouman. Special thanks also go to my supportive friends: my "bondo bismillah" buddy Aprisia, my "panic buddy" Gargi, and my sweetest buddy Bernice. I am also grateful for the virtual presence of my family, *mama*, *ayah*, and *Pipo*, throughout this time. A special thanks to Firman, who consistently challenged me to complete tasks and encouraged me to stop worrying.

I would also like to extend my sincere thanks to my Indonesian study buddies who stayed late at the TU Delft Central Library every day. Lastly, thank you to all my BouT and Building Technology friends for keeping my spirits high.

A good thesis is a done thesis. A great thesis is a submitted thesis. A perfect thesis is neither. This too shall pass.

Alya Farah Taufiqoh
Delft, June 2024

To my family; whatever family means.
Thank you for believing in me. This is for you.

Contents

1. Introduction	1
1.1 Background	2
1.2 Problem Statement	2
1.3 Research Questions	3
1.4 Research Objectives	3
1.5 Research Methods	3
2. Literature Study	5
2.1 Energy Demand in Buildings	6
2.2 Thermal Comfort	8
2.3 Enhancing Existing Glass' Performance	13
2.4 Building Energy Modeling Approach	16
2.5 Building Control Strategies	22
3. Methodology	25
3.1 Case Study: Pulse (Building 33), TU Delft Campus	26
3.2 RC-modeling	30
3.3 Model Predictive Control	37
3.4 Glass Retrofitting Strategies	39
3.5 Comparison and Analysis	40
4. Changing the Existing System into Model Predictive Control (MPC)	41
4.1 Building Model (RC-modeling)	42
4.2 Model Predictive Control	46
5. Retrofitting the Existing Glass	49
5.1 Identifying the Impact on Window's Resistance and Absorptance Value	50
5.2 Impact on Heat Loss/gain for Winter and Summer through Window	51
5.3 Impact on Energy Demand and Comfort in Building	54
6. Fixing Pulse	60
6.1 Smart System vs Retrofitting	61
6.2 Materiality	61
6.3 Position	64
6.4 Composition	66

7. Conclusions	68
Reflections	71
References	74
Appendices	89

Chapter 1

Introduction

1.1 Background

According to the International Energy Agency's report in 2023, building activities are responsible for 30% of global final energy consumption (with 8% of emissions coming directly from buildings and 18% from generating heat and electricity used in buildings) (IEA, 2023). Heating, ventilation, and air conditioning (HVAC) systems, among other energy-demand components within building infrastructures, contribute significantly to energy consumption at 40-60% (Solano et al., 2021). Inefficiencies in their operation or suboptimal thermostat settings can lead to considerable energy wastage. In addition, the façade, as the interface between indoor and outdoor climate, plays an important role in determining HVAC energy demand (Mărginean, 2019). Having a vast area of glass as a façade can be a problem when it generates a lot of heat transfer between the indoor and outdoor environment. Therefore, it is also important to consider the suitable façade properties and/or design to prevent energy waste.

Apart from energy usage, thermal comfort is a crucial factor in building design, influencing both energy consumption and occupant comfort (Hensen & Centnerova, 2001). The mean radiant temperature (MRT) plays a pivotal role in determining the operative temperature, a key metric for thermal comfort (Chaiyapinunt et al., 2005). When buildings use glass facades, MRT is significantly impacted due to the higher thermal radiation exchange between occupants and the building envelope and then to the outdoor environment. In addition, glass façades are also affected by solar radiation more than opaque elements. This thermal radiation exchange can lead to a decrease or increase in the perceived temperature, making occupants feel colder or warmer, respectively, and potentially leading to discomfort. This issue becomes particularly evident in buildings with large glass surfaces.

To that end, two methods, among many others, became the focus of this research to reduce the energy demand and improve the thermal comfort of a building: improving the HVAC system and the façade. The former applies a smart control system, while the latter is retrofitting the existing façade. Recent research regarding smart control and façade solutions focuses on only one scope, no cross-comparison (Balali et al., 2023; Sarihi et al., 2021). When a building design considers these options, which strategy should be chosen? Should the system be changed, should retrofitting be added, or should both be done?

1.2 Problem Statement

Based on the background mentioned above, it is clear that there is a gap in knowledge on which strategy provides better performance. Therefore, the formulated problem statement is:

There is a lack of understanding of how effective the application of Model Predictive Control (MPC), compared to glass retrofitting strategies, influences the energy demand

and thermal comfort of a glass facade building.

1.3 Research Questions

This thesis was driven by the curiosity of whether it is more effective to change the building's system, implement retrofitting, or perhaps both, for glass façade buildings. Based on this and the problem statement, the main question of this research is:

What is the optimal strategy for reducing energy demand and maintaining thermal comfort in glass façade buildings: modifying the existing building system, implementing retrofitting strategies, or employing a combination of both approaches?

To answer that main question, several sub-research questions have been formulated to investigate various aspects concerning energy demand, thermal comfort, MPC, and retrofitting strategies. The formulated sub-research questions are:

- 1. What are the aspects influencing energy demand?*
- 2. How is thermal comfort measured? What are the influencing parameters?*
- 3. How can a model be developed for model prediction, and what is the problem formulation for the control?*
- 4. How does the integration of MPC affect energy efficiency and occupant comfort?*
- 5. What are the retrofitting options, and how do they impact energy consumption and thermal comfort?*
- 6. What are the advantages and disadvantages of modifying building systems versus implementing retrofitting strategies (concerning energy demand and thermal comfort)?*
- 7. What is the effectiveness of combining building system modifications with retrofitting strategies in achieving optimal energy savings and comfort levels?*

1.4 Research Objectives

The primary purpose of this thesis is to evaluate the energy and comfort performance of MPC and retrofitting strategies in glass façade buildings. To get there, this study aims to develop an MPC model that can operate a building to minimize energy consumption while maintaining optimal thermal comfort. Additionally, retrofitting strategies for glass façades will be selected and assessed using both the existing system and the MPC model. A case study will be employed to develop the model, as well as to test, calibrate, and evaluate its performance.

1.5 Research Methods

This study was conducted using simulations to achieve the main goal. First, the Pulse Building (Building 33, TU Delft Campus) was selected as the case study. Using that building, an RC-thermal network was constructed. This model served as the prediction model in MPC. The building model was then calibrated through parameter estimation

until validated. Next, a control strategy was designed, which involved optimization as the final part of the MPC process. This MPC was then applied to both the baseline and retrofit strategies, which were selected based on their performance when applied to the baseline. Ultimately, the use of MPC in several alternatives was compared with alternatives using the existing system concerning the energy demand and thermal comfort. The illustration in Fig 1.1 depicts the research framework from the literature study to data analysis.

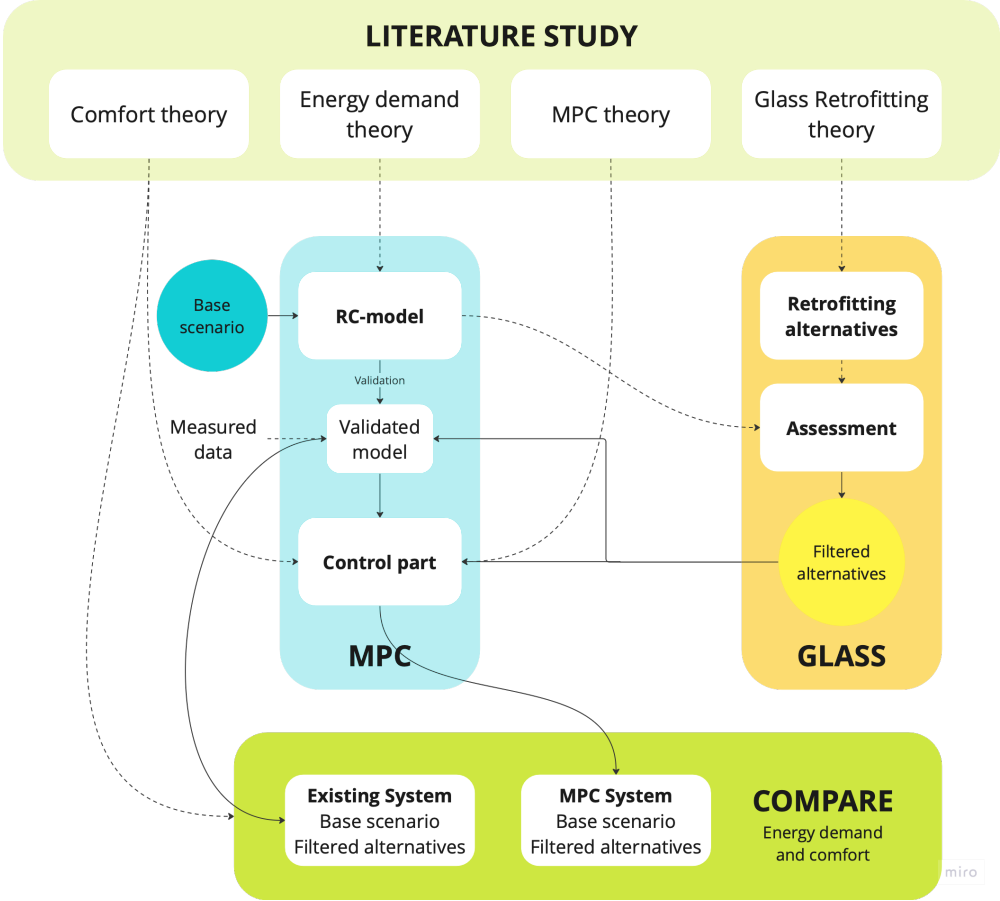


Fig 1.1 Research framework.

Chapter 2

Literature Study

2.1 Energy Demand in Buildings

Operational Energy vs Embodied Energy

Energy serves diverse functions within the built environment, including heating, cooling, ventilating, and cooking. However, it is crucial to recognize that the energy utilization of a building extends beyond its operational phase. The production of building materials and energy-related components also needs energy. Consequently, a building's energy consumption can be categorized into two main segments: "operational energy," which represents the energy consumed during the active use of the building, and "embodied energy" for the energy required for the production of its materials. Calculating embodied energy typically involves employing Life Cycle Analysis methodologies, as seen in Fig 2.1. This thesis will focus more on the operational energy.

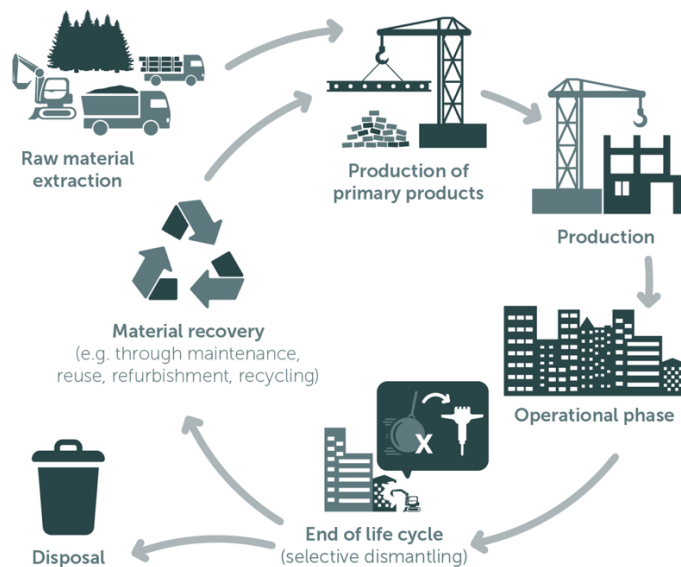


Fig 2.1 Building life cycle. Source: Hollenbeck & Naumann, 2023.

Energy Supply Chain

The energy cycle begins with the demand, often referred to as the energy "that is required." This demand represents the specific form of energy needed, whether it be heat, cold, light, or any other form, and it ultimately should be met using renewable resources as they are accessible on Earth. In the intermediate stages, various technical components come into play to convert, store, and/or distribute the energy into the appropriate form, ensuring it is available at the right time and in the right location.

In the context of the built environment, the technical supply chain can be divided into distinct levels, namely energy demand, final energy, and primary energy. Fig 2.2 illustrates this energy chain. It is crucial to have a clear understanding of these levels and their respective meanings to assess energy systems accurately. For example, when

discussing the energy consumption of a specific building, it is essential to specify whether we are referring to the energy demand, final energy, or primary energy, as each of these concepts has distinct implications and significance in the evaluation process.

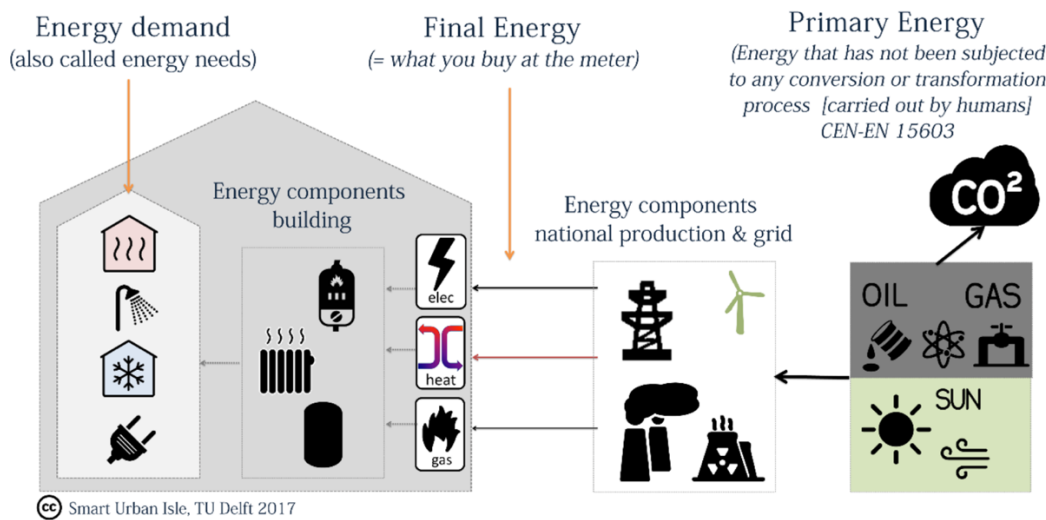


Fig 2.2 Energy supply chain: from energy demand to primary energy. Source: Jansen, 2020.

This thesis defines energy consumption as the energy demand. It means the heat and cold that need to be supplied or removed from a conditioned space to keep the desired temperature. The energy demand functions as an indicator of the building's intrinsic characteristics, including insulation and air tightness, in combination with how the building is used, regardless of the specific technical systems or equipment utilized to satisfy this demand.

Energy Needs in Building

The energy balance serves as the initial step in determining a building's energy requirements. The energy balance of a room encompasses all the heat flows that either enter or exit that particular space. Various types of heat flows are involved in this calculation, as seen in Fig 2.3.

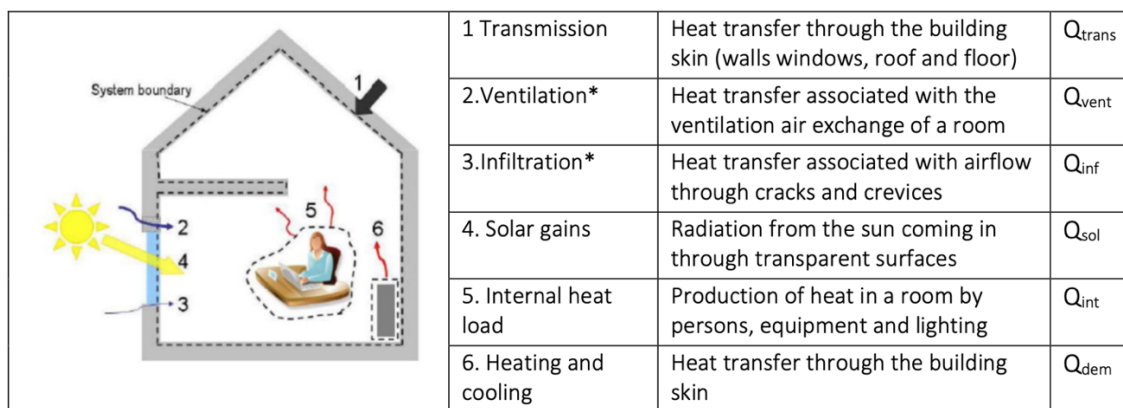


Fig 2.3 Heat flows that enter and leave the room. Source: Jansen, 2020.

The heat transfer required to alter the temperature of the air is incorporated into the heat balance as either a heat loss or gain. In a steady state condition, equations 1 and 2 can be applied as the heat flows are not dynamic. There are two main equations for analyzing the energy system, as shown in equations 3 and 4. From the equations, it can be concluded that when the energy balance is not 0 (zero), the building either has excess heat or needs more heat, which leads to a cooling and heating demand.

$$Q_{in} = Q_{out} \quad (1)$$

$$Q_{trans} + Q_{vent} + Q_{sol} + Q_{int} + Q_{dem} = 0 \quad (2)$$

$$Q_{trans} = U_{value} \times A \times \Delta T \quad (3)$$

$$Q_{vent} = \dot{m} \times C_p \times \Delta T \quad (4)$$

Here, A is the surface area [m^2], \dot{m} is the mass (air) flow rate [kg/m], and C_p is specific heat capacity [$kJ/kg/C$]. The minimum airflow for a person in an educational building is 8.5l/s.

2.2 Thermal Comfort

High-performance buildings typically prioritize reducing energy consumption to achieve energy efficiency. However, the indoor quality, especially the occupant's comfort, is often overlooked (Mousavi et al., 2023). Thus, including the comfort aspect when designing these buildings is also crucial.

Thermal comfort is a condition where individuals do not feel compelled to adjust their surroundings through actions or behavior (Hensen, 1991). Another definition of comfort by ASHRAE in 1992 is "the condition of the mind in which satisfaction is expressed with the thermal environment. It can be expressed into observable parameters". Six parameters that influence thermal comfort, which include physical and personal variables, were published by Machperson in 1962 and can be seen in Fig 2.4 (Z. Lin & Deng, 2008).

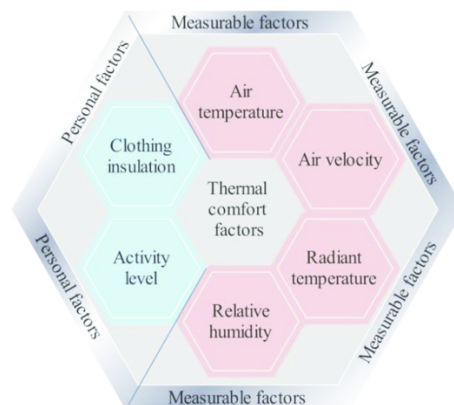


Fig 2.4 Six influencing parameters of thermal comfort. Source: Simion et al., 2016.

Current knowledge has two different approaches to defining thermal comfort, namely the static approach and the adaptive approach (Doherty & Arens, 1988). This section will review these two thermal comfort approaches.

Static Model

The static model is an approach where it uses the heat balance concept. The proposed method by Fanger centers on the six key parameters that impact thermal comfort: humidity, air velocity, mean radiant temperature, air temperature, occupants' metabolic rate, and clothes. Thermoregulation theory, which is the base of this approach, explains that humans exchange heat with the environment by sweating, shivering, and regulating blood flow to the skin to uphold a heat equilibrium (Charles, 2003).

Fanger combined several experimental investigations in climate chambers, which incorporated over a thousand participants, resulting in the predicted mean vote (PMV) index. The PMV index, which projects the average reaction of a large population, is associated with ASHRAE's thermal sensation scale: -3 cold, -2 cool, -1 slightly cool, 0 neutral, +1 slightly warm, +2 warm, and +3 hot. The integration of PMV led to the development of the predicted percentage of dissatisfied (PPD) index. The PPD anticipates the proportion of individuals who expressed dissatisfaction by rating outside the central range of three points on the ASHRAE scale (ratings of -3, -2, +2, +3). The relation between PPD and PMV values can be seen in Fig 2.5.

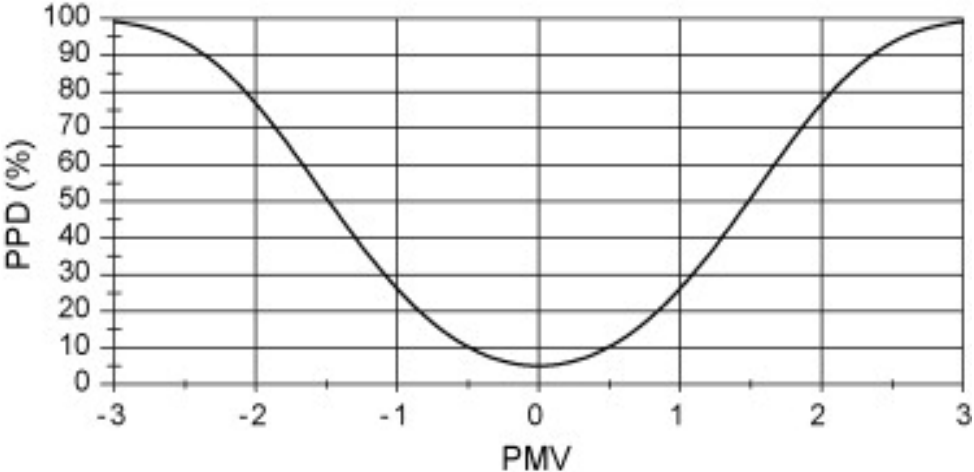


Fig 2.5 Relation of PMV and PPD. Source: Djongyang et al., 2010.

Adaptive Model

While the heat balance approach considers occupants to act as passive recipients towards thermal conditions, the adaptive model of thermal comfort encompasses various strategies individuals employ within buildings to attain a comfortable thermal environment. These adjustments can be grouped into three distinct sets of responses: behavioral adaptation, physiological adaptation, and psychological adaptation (Kwok

& Rajkovich, 2010). Individuals typically respond in one to two categories, aligning with the three aforementioned categories (Roaf et al., 2010).

Through the analysis of field survey data from various locations worldwide, there is a discovery of a strong correlation between the comfort temperature and the average indoor temperature (Nicol et al., 2012; M. Humphreys, 1976). Furthermore, it was observed that there exists a significant correlation between the indoor comfort temperature and the outdoor temperature (M. Humphreys, 1978). Equation 5 and Fig 2.6 illustrate a linear equation to express the relationship between comfort temperature and monthly mean outdoor air temperature.

$$T_n = 11.9 + 0.534 T_o \quad (5)$$

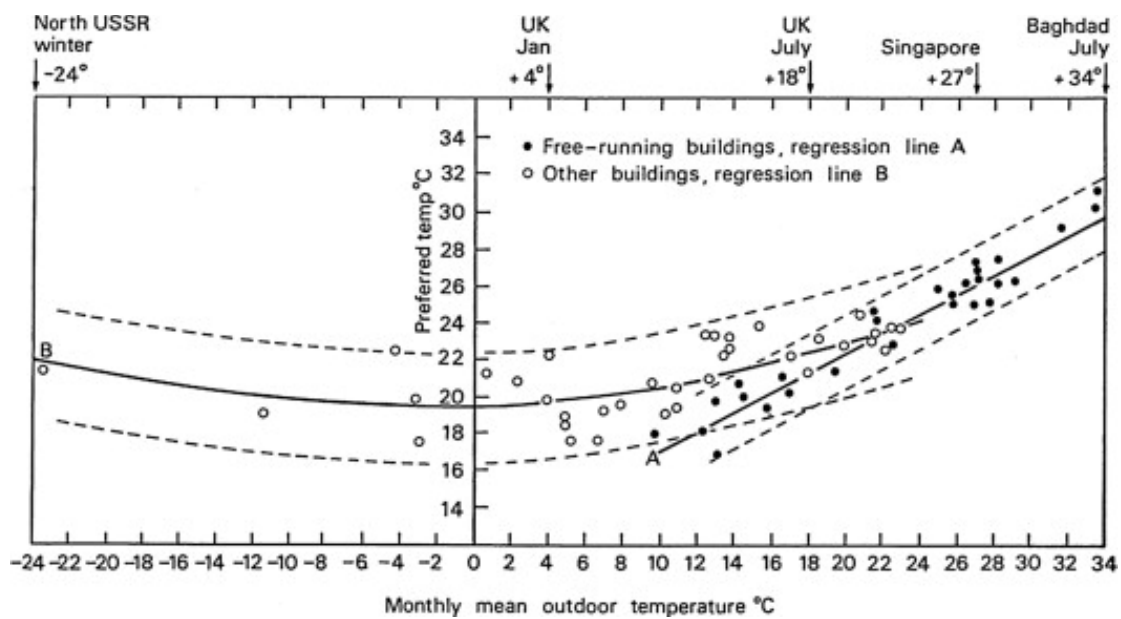


Fig 2.6 The relationship between preferred temperature and monthly mean outdoor temperature. Source: M. A. Humphreys et al., 2013.

Here, T_n is the preferred indoor temperature [C] and T_o is the outdoor monthly mean temperature [C] for a specific region. As stated in ASHRAE 55, this approach also has a relationship with PMV and PPD, as seen in Fig 2.7. The figure below uses indoor operative temperature [C] as the y-axis, which includes surfaces temperatures, view factor, and indoor air temperature, instead of indoor air temperature only (see equations 6 and 7). In the mentioned equations, surfaces temperatures are represented as T_s [K] and the view factors as F_s in mean radiant temperature MRT . The relationship between MRT and indoor temperature T_{indoor} can be seen in indoor operative temperature T_{op} equation, where hr is radiation coefficient and hc is convection coefficient.

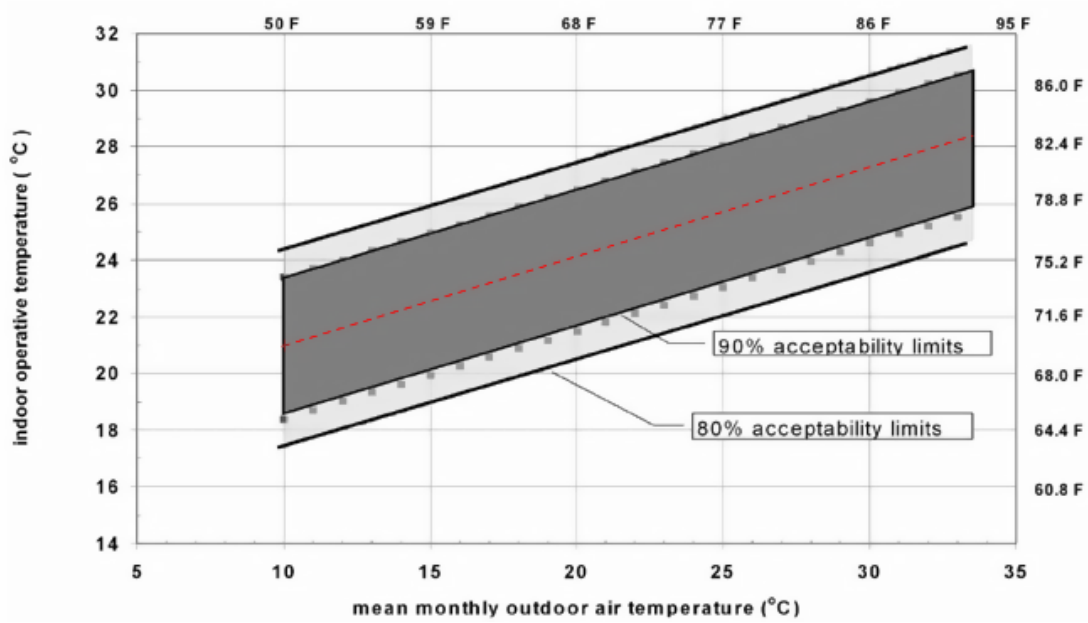


Fig 2.7 Relation with PMV and PPD. Source: ANSI/ASHRAE Standard, 2017.

$$T_{op} = \frac{hr MRT + hc T_{indoor}}{hr + hc} \quad (6)$$

$$MRT = \left(\sum_{i=1}^n F_{si} \times T_{si}^4 \right)^{\frac{1}{4}} \quad (7)$$

While the static approach is suitable for designing HVAC systems for modern buildings as it helps set the setpoint, the adaptive approach acknowledges the dynamic and interactive nature of thermal comfort. The adaptive one emphasizes real-world variability and individual adaptability, which makes it more suited to diverse and changing environments. Unlike the static model, this approach provides a range of setpoints in relation to outdoor temperature.

Dutch Thermal Comfort Model

The adaptive temperature limit value (ATG) method, an evolution of the Dutch thermal comfort metrics, was further refined in 2014, establishing the current guidelines for adaptive thermal comfort in the Netherlands (Boerstra et al., 2015). Aligned with international comfort standards such as NEN-EN 15251 and NEN-EN-ISO 7730, the revised ATG method employs Operative temperature to assess comfort limits. Buildings are categorized based on alpha or beta types and their classification level (Class A/B, C, D). The adaptive thermal comfort limits for each class are detailed in Fig 2.8, while the relationship between comfort class limits and outdoor running mean temperature for alpha and beta buildings is depicted in Fig 2.9.

Class (bandwidth)	Explanation	PPD	PMV analogy (bandwidth)
A	High level of expectation. Select this category as a reference when designing spaces for people with limited load capacity (for instance, sensitive people or persons who are diseased) or when there is a higher demand for comfort	Max. 5%	–
B	Normal level of expectation. Select this category as a reference when designing or measuring new buildings or in the case of substantial renovations	Max. 10%	$-0.5 < PMV < +0.5$
C	Moderate level of expectation. Select this category as a reference in the case of limited renovations or when measuring older existing buildings	Max. 15%	$-0.7 < PMV < +0.7$
D	Limited level of expectation. Select this category as a reference in the case of temporary buildings or limited use (for instance, one to two hours of occupation per day)	Max. 25%	$-1.0 < PMV < +1.0$

Fig 2.8 Buildings categorization and classification description. Source: Boerstra et al., 2015.

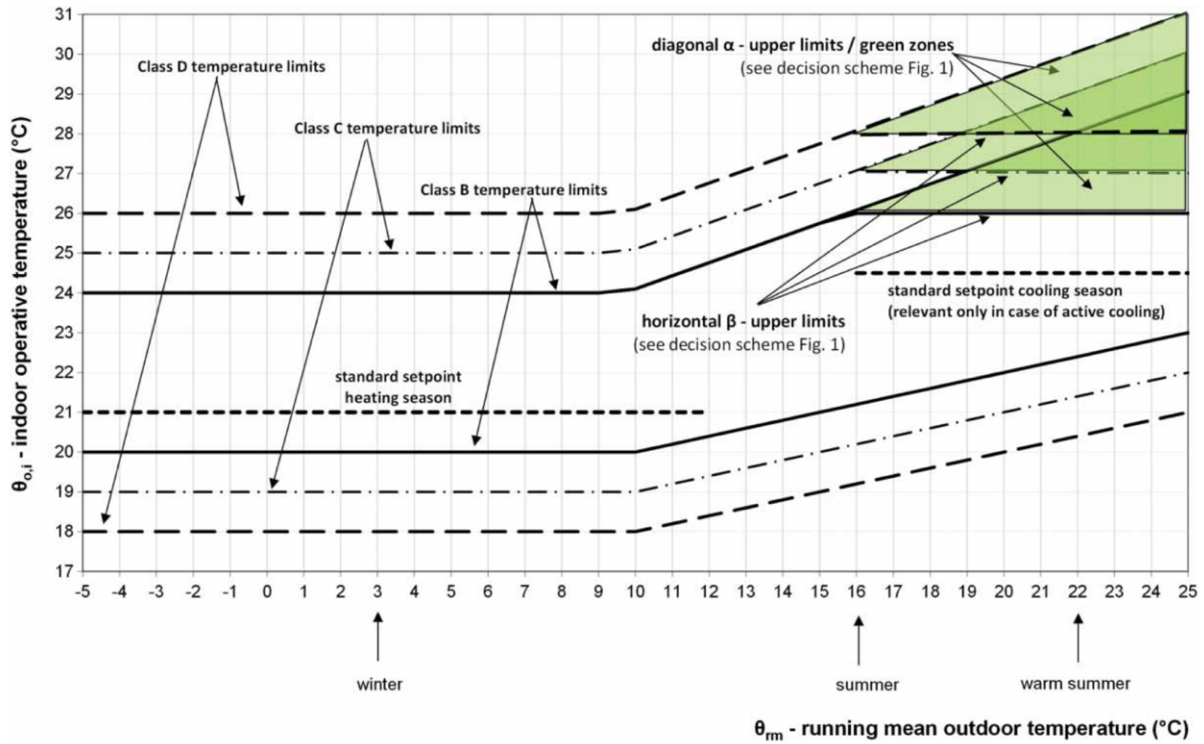


Fig 2.9 The adaptive temperature limit value (ATG) model. Source: Boerstra et al., 2015.

$$\theta_{rm} = (0.2) \cdot \theta_{ed-1} + (0.8) \cdot \theta_{rm-1} \quad (8)$$

$$\theta_{rm} = 0.253 \cdot \left(\begin{array}{l} \theta_{ed-1} + (0.8) \cdot \theta_{ed-2} + (0.8)^2 \cdot \theta_{ed-3} \\ + (0.8)^3 \cdot \theta_{ed-4} + (0.8)^4 \cdot \theta_{ed-5} \\ + (0.8)^5 \cdot \theta_{ed-6} + (0.8)^6 \cdot \theta_{ed-7} \end{array} \right) \quad (9)$$

According to Boerstra et al., the RMOT or running mean outdoor temperature θ_{rm} can be calculated using equation 8. Here, the θ_{rm} and θ_{rm-1} are the RMOT for today and the day before, respectively. θ_{ed-1} denotes the DMOT or daily mean outdoor temperature for the previous set day. In case of unavailable DMOT records, equation 9 can be used.

2.3 Enhancing Existing Glass' Performance

As mentioned earlier, most of the heat transfer occurs at the building envelope. Glass plays a significant role as heat quickly passes through due to the low thermal mass of glass. Therefore, having a glass façade can pose challenges for energy demand and thermal comfort. This section will explore the impact of glass in buildings and discuss some retrofitting options to improve glass performance.

Overcooling and Overheating

The buildup of heat within the structure can lead to discomfort among occupants, which is defined as overheating. Sensitivity to temperature varies, but most individuals feel warm at 25 °C and hot at 28 °C, while temperatures exceeding 35 °C can induce significant discomfort (Gupta & Gregg, 2018). Some research indicates that the efforts to enhance energy efficiency in winter through strategies like improved insulations and airtightness to reduce heat loss contribute significantly to overheating during summer months. The main factors contributing to overheating issues include external heat gain (heat accumulation from the building envelope), underestimate of internal heat gain (heat accumulated from occupants, lighting, appliances, and building services), and inadequate ventilation approaches (Barbosa et al., 2015; Gupta & Gregg, 2018; Kazanci & Olesen, 2016).

On the other hand, the precise definition and quantification of overcooling concerning thermal comfort have yet to undergo systematic investigation. However, some literature, as stated in (Alnuaimi et al., 2022), often describes "overcooling" as the excessive use of active cooling systems within a space. The paper categorized three definitions of overcooling, at which one explains overcooling as the occurrence when the air temperature drops below a predetermined criterion, typically the setpoint temperature. Furthermore, alongside single temperature points and temperature ranges, the study also outlines degree-time interval metrics like overcooling degree days. These metrics compare designed comfortable air temperatures, factoring in seasonal temperature ranges and humidity, with external air temperatures to gauge the extent of overcooling.

The other definition explains overcooling in terms of the thermal comfort metrics PMV and PPD where PMV below -0.5 is considered as too cold. In the adaptive approach, where the focus is on indoor operative temperatures, discomfort is not only assessed by looking at the air temperature itself but also by taking surface temperatures into account. Therefore, overcooling and overheating can occur not only when the indoor air temperature exceeds thermal comfort limits but also when the surface temperatures drop or increase, respectively. The phenomenon is especially common in buildings with full-glass façades. (Kontes et al., 2017).

Strategies to Enhance Glass Performance

Enhancing the building envelope can prove advantageous in mitigating the potential for both overheating and overcooling (Chvatal & Corvacho, 2009). Thermal discomfort in glass façade buildings is related to glass surface temperature and solar radiation, where the intensity of transmitted diffuse solar radiation emerges as the primary factor influencing discomfort levels (Chaiyapinunt & Khamporn, 2021). Nonetheless, in the case of windows with low transmittance, the significance of discomfort is more linked to surface temperature fluctuation rather than to solar radiation (Khamporn & Chaiyapinunt, 2014). According to (Wahi, 2020; Sarihi et al., 2021), there are some potential strategies that can be done to improve glass façade buildings, see Table 2.1.

Table 2.1 Potential strategies to improve glass façade building. Source: Wahi, 2020; Sarihi et al., 2021.

Goals	Actions	Strategies	Placement
Minimize solar gain	Reduce glazing ratios	Change façade composition	Façade
Minimize solar gain	Reduce SHGC values	Change glass, add films, coatings	Façade
Sun protection	Shade the glass	Add shading, shutters, greenery	External
Sun protection	Solar control	Change glass, add films, coatings, enamels	Façade
Sun protection	Prevent solar entering space	Add blinds, curtains, paints	External and internal
Insulate	Insulated glazing unit	Change glass, add films, coatings, curtain	Façade
Insulate	Triple glazing	Change glass	Façade
Add thermal mass	Exposed thermal mass	Add PCM	External and internal

However, renovating the building by changing the glass or adding a new structure adds to the energy in the building life cycle or the material life cycle (Ardente et al., 2011). This thesis tries to keep the glass in place, keep the embodied energy as minimal as possible, and maintain the façade's appearance. Therefore, not all retrofitting strategies are suitable. Façade composition, changing glass, and adding shade are no longer considered. An option like enamel requires a high temperature for the firing (minimum of 590 °C) (Beltrán et al., 2020). This option may not be suitable for all glass types, especially for existing glass, for which an assessment of the glass and the surrounding materials is needed. Therefore, adding enamel is also no longer considered an option.

From the explanations above and the strategies comparison matrix in Fig 2.10, strategies that remain mostly involve modifying the glass surfaces and adding blinds. The latter is to improve solar heat gain and add resistance between the indoor air and outdoor air (Wright et al., 2009; D. Wang et al., 2015). One approach for the glass surfaces' modification is adding a coating to the glass, while another is applying a film. Coating is a process where a very thin layer of liquid is applied to the original glass

surface, which can be done in controlled and uncontrolled environments using a spraying machine (controlled) or manual brushing (uncontrolled). This method requires curing to make the coating durable, which can be accomplished through either firing or UV curing (Trier & Ranke, 2007). However, coating that is applied directly to an existing window can lead to oxidation because of the direct contact between the silver and air. Wrong application can lead to ineffective performance. Direct spray coating improves the glass's performance (S. Lin et al., 2019), but it is better to keep the coating layer in sealed air also to improve its lifespan (Van Den Bergh et al., 2013).

As for filming, the process is less complex. It does not require special appliance treatment and no curing for finishing. Films can be placed inside or outside the windowpane (Yin et al., 2012), depending on the purpose and product requirements. However, placing an additional layer of film on the indoor surface is preferable to prevent it from being affected by the weather (EPD, 2024).

Retrofitting Strategies Comparison Matrix

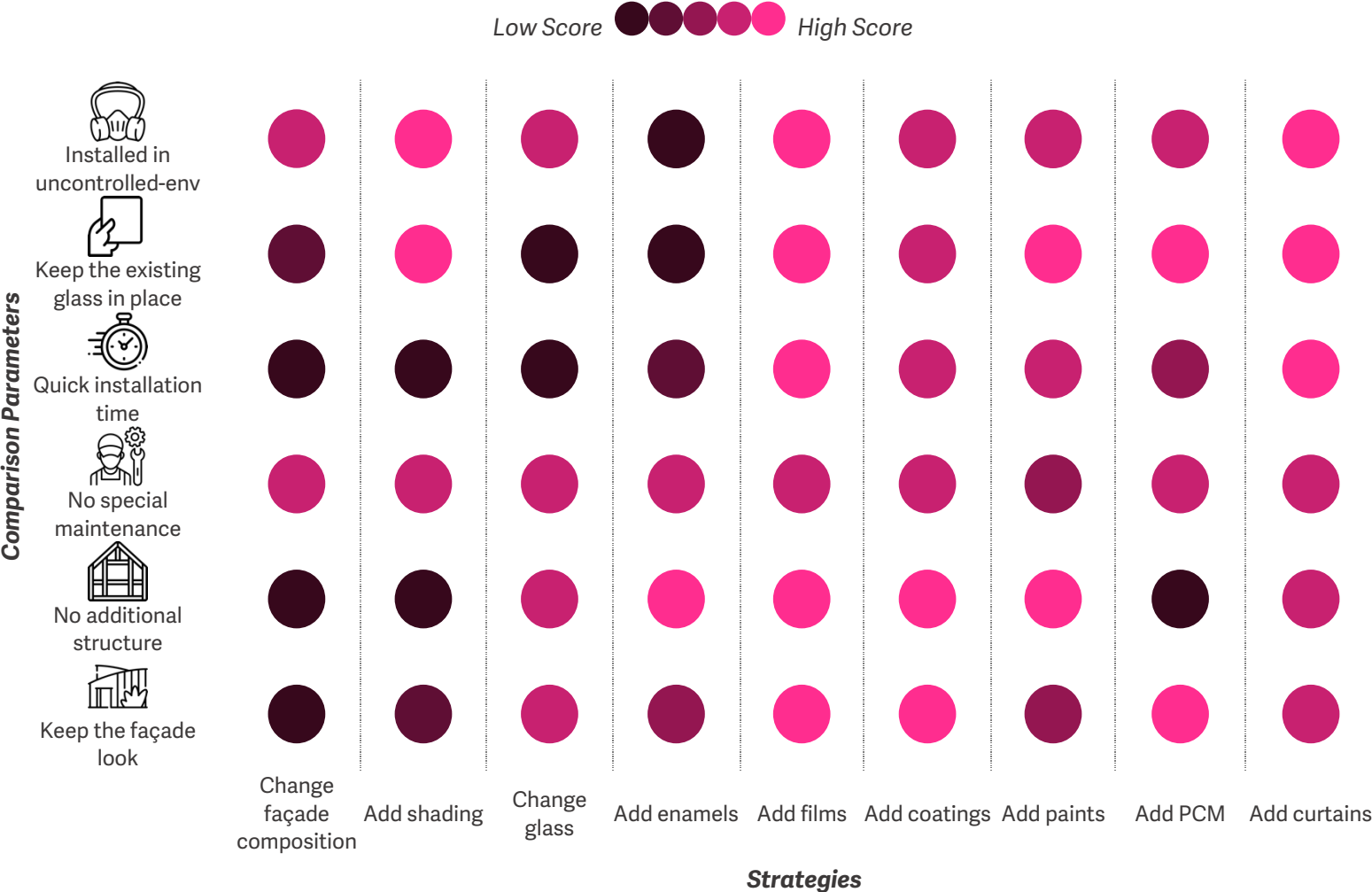


Fig 2.10 Retrofitting strategies comparison matrix.

2.4 Building Energy Modeling Approach

To assess the building's energy demand and thermal balance, various modeling techniques are developed. These models fall into three categories: white-box (physics-based), black-box (data-driven), and grey-box (hybrid) (Delcroix et al., 2021). The objective of these models is to create a digital twin of the actual building or the building that is under construction.

The model can be static or dynamic. The static or steady-state models are characterized by constant or unchanging parameters over time, whereas dynamic or unsteady-state models involve parameters that vary with time. Dynamic modeling addresses a range of issues associated with transient operations, which are essential for system startup, shutdown, and responses to disturbances (P. Li et al., 2014). Disruptions in HVAC systems can occur as a result of fluctuations in heating and cooling loads, human activities, or control interventions (Bendapudi, 2002). This section will discuss the three models and their characteristics.

White-box approach

In white-box technique, the buildings' thermal modeling can be approached by developing the physical properties of the materials within the structures through the application of either thermal dynamic equations or resistance-capacitance (RC) modeling (X. Zhang et al., 2020). These models are predominantly employed during the design phase, where the objective is to forecast and assess the performance of HVAC system components via simulation with tools, as seen in Fig 2.11 (Afroz et al., 2018).

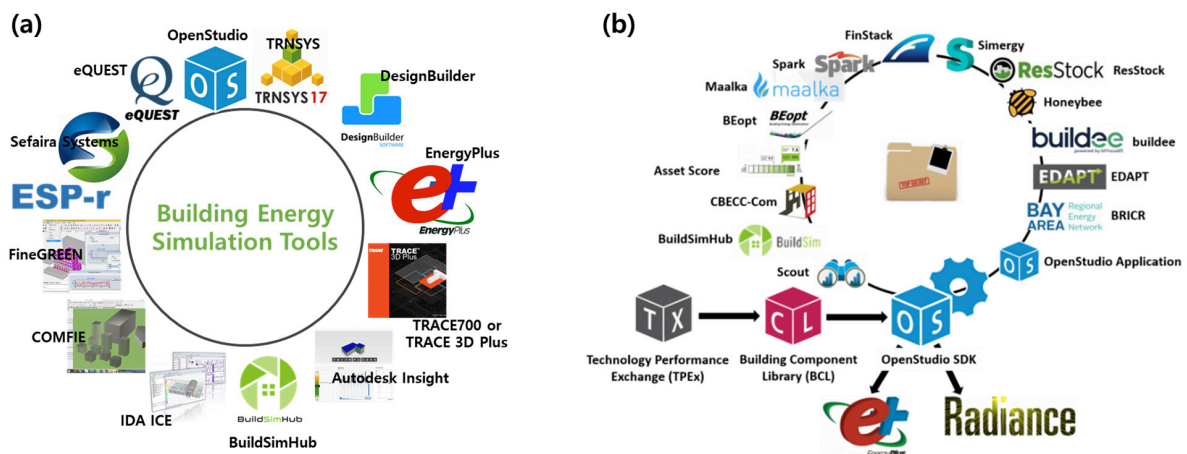


Fig 2.11 Building energy simulation tools used in white-box modeling approach. Source: Kim et al., 2022.

The white-box model is based on the concept of energy balance in the building, which influences energy demand if there is any imbalance. Cooling loads arise when the building accumulates excessive heat, necessitating cooling measures to restore equilibrium (indicated by a positive outcome in the heat balance equation). In contrast,

heating loads manifest when the building encounters heat deficiencies, causing a drop in temperature and requiring heating interventions to rectify the situation (indicated by a negative outcome from the heat balance equation) (Chwieduk, 2014; Stephens, 2019).

Black-box approach

Black-box or data-driven models are constructed by collecting real-world system performance data while also taking into account the prerequisites for measured chronologically ordered data, alongside considerations of accuracy and complexity levels (S. Zhang et al., 2021). Unlike the white-box method, this method is used when there's no physical data of the building, but there are sensors monitoring the building's behavior which often found in modern or smart buildings. Therefore, this approach neglects the physics phenomenon in the buildings (Lu et al., 2022). Subsequently, mathematical relationships between input and output variables are established using methods such as statistical regression or artificial neural networks (ANN) (Vaughn, 2014). A standard workflow of this data-driven modeling technique can be seen in Fig 2.12.

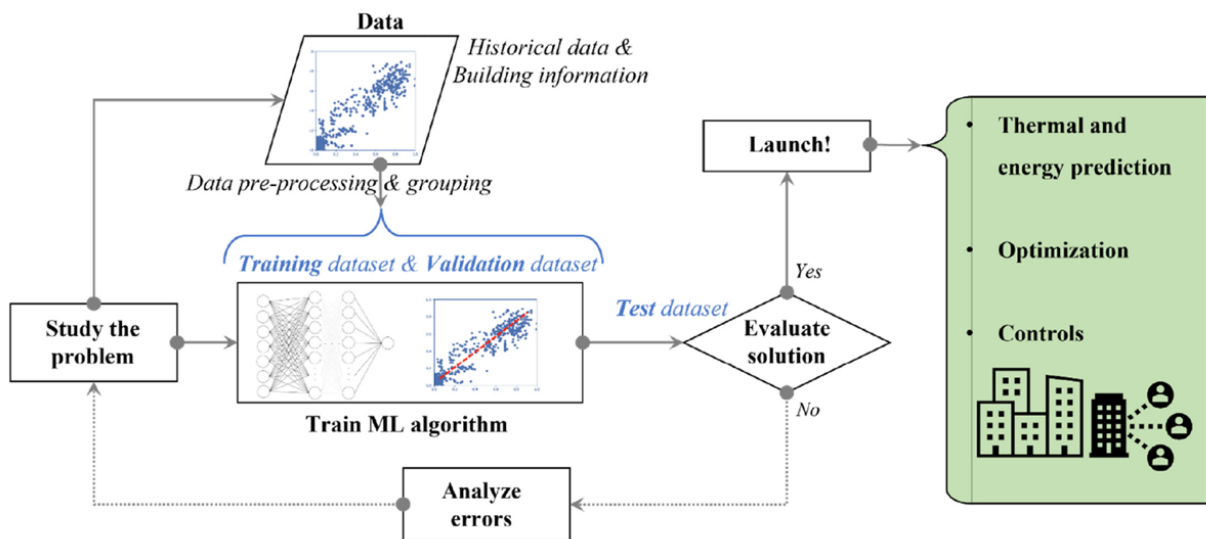


Fig 2.12 Diagram illustrating a standard black-box model approach using machine learning. Source: Kim et al., 2022.

While a white-box model simulates the energy balance conditions of a space, a black-box model focuses on predicting how future data (output) will appear based on historical data. The output can be electricity, heating or cooling demand, or hot water. Although the black-box approach does not need a physical formula, it still needs logical input data to help make a correlation with the output, such as weather data, occupancy data, indoor environment information, and building characteristic data (Lu et al., 2022). The details can be seen in Fig 2.13.

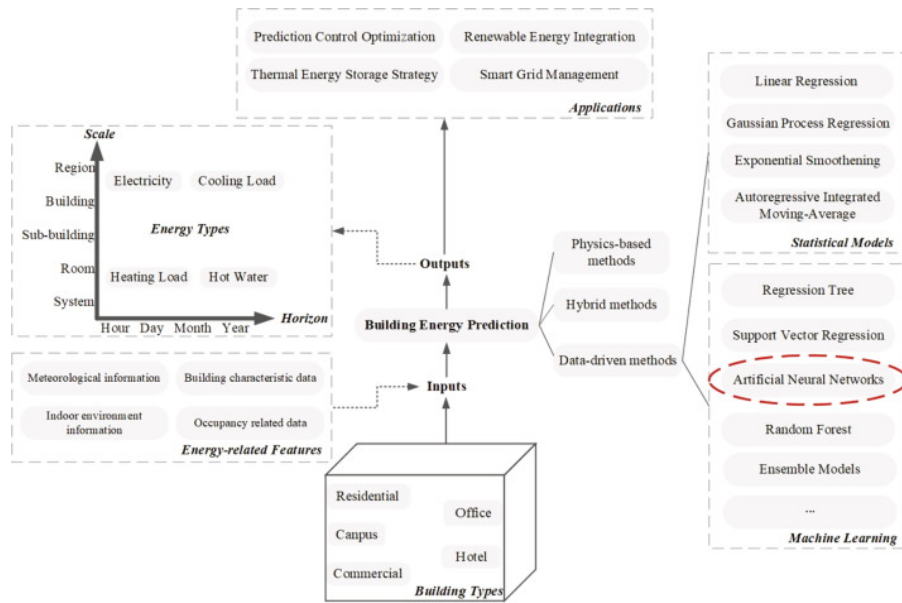


Fig 2.13 Inputs, outputs, and data-driven methods for black-box modeling. Source: Lu et al., 2022.

Grey-box approach

The gray-box category combines the white-box and black-box approach which includes simplified physical relationships and requires parameter estimation based on measured data (Shamsi et al., 2021). This approach is selected when both physical data and measured data are accessible, but there is discrepancy between the calculations derived from the physical data and the measured data. A diagram illustrating a standard grey-box model approach can be seen on Fig 2.14. Typically, gray-box models start by simplifying physics by reducing state-space dimensionality or linearizing them using RC analogy (similar to an electrical circuits). The RC is then combined and calibrated with measured data from the real building condition (Ljung, 2001). The process aims to get a physically logical model that resembles the real condition.

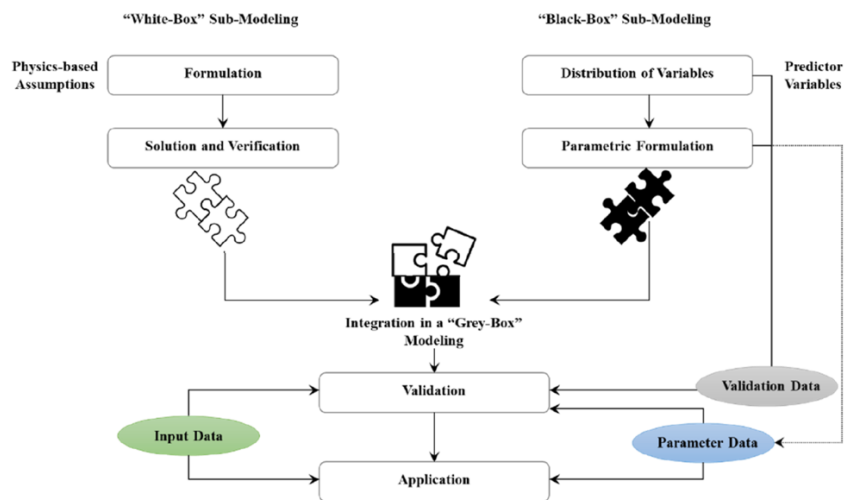
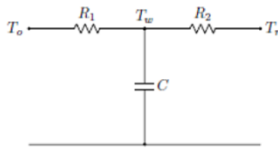


Fig 2.14 Diagram illustrating a standard grey-box model approach. Source: Kim et al., 2022.

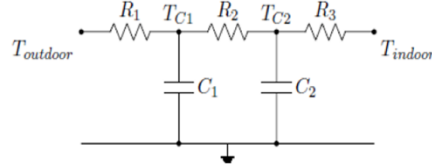
White-box sub-modeling

As mentioned before, the grey-box approach starts with white-box modeling. This step does not have to be as complicated as pure white-box model. In fact, most grey-box models use RC-model, where a model is defined based on its similarity to an electrical circuit with resistors and capacitors, as illustrated in Fig 2.15. Just like white-box modeling, the input of this RC-model is the building material information, where R being the resistance value and C being the capacitance. In this simple example, it represents the model of a building's envelope, where C_n represents the thermal capacity of the zone (the ability to store thermal energy) and R_n represents the building walls separating the ambient temperature $T_{outdoor}$ from the zone's temperature T_{in} (Boodi et al., 2022). In another example, there are also Q_h and gAQ_{sun} which represent thermal power from the building's heating system and solar irradiation, respectively (Y. Li et al., 2021).

1. 2R1C



2. 3R2C



3. 3R4C

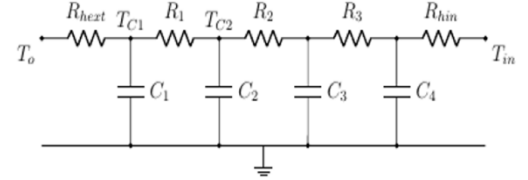


Fig 2.15 Example of RC-model of a building envelope. Source: Boodi et al., 2022.

There are some assumptions that need to be considered when making RC-model: natural ventilation and all three heat transfer coefficients (radiation, convection, and conduction) are constant (Z. Wang et al., 2019). Based on those assumptions, relationship between resistance and capacitance can be seen in equation 10.

$$C_1 \frac{dT_{C1}}{dt} = \frac{T_{outdoor} - T_{C1}}{R_1} + \frac{T_{C2} - T_{C1}}{R_2} \quad (10)$$

The equation above takes the second example of RC-model (3R2C) at node 1. Here, C_1 denotes thermal capacitance, T_{C1} and T_{C2} represents nodes temperatures, R_1 and R_2 are the thermal resistance between the temperatures. This equation is then converted into matrix form. Another example of RC-model, the equations, and the matrix can be seen on Fig 2.16.

Model Structure	
Differential Equations	$C_1 \frac{dT_1}{dt} = \frac{T_2 - T_1}{R_{1,2}} + w_1 Q_1 + w_2 Q_2$ $C_2 \frac{dT_2}{dt} = \frac{T_3 - T_2}{R_{2,3}} + \frac{T_1 - T_2}{R_{1,2}}$
State-Space Representation	$\frac{d}{dt} \begin{bmatrix} T_1 \\ T_2 \end{bmatrix} = \begin{bmatrix} -\frac{1}{C_1 R_{1,2}} & \frac{1}{C_1 R_{1,2}} \\ \frac{1}{C_2 R_{1,2}} & -\frac{1}{C_2 R_{2,3}} - \frac{1}{C_2 R_{1,2}} \end{bmatrix} \begin{bmatrix} T_1 \\ T_2 \end{bmatrix} + \begin{bmatrix} 0 & \frac{w_1}{C_1} & \frac{w_2}{C_1} \\ \frac{1}{C_2 R_{2,3}} & 0 & 0 \end{bmatrix} \begin{bmatrix} T_3 \\ Q_1 \\ Q_2 \end{bmatrix}$ $T_1 = [1 \quad 0] \begin{bmatrix} T_1 \\ T_2 \end{bmatrix}$
Variables	<p>Input: $\mathbf{u} = [T_3 \quad Q_1 \quad Q_2]'$; Output: $\mathbf{y} = T_1$; State: $\mathbf{x} = [T_1 \quad T_2]'$;</p> <p>Parameter: $\boldsymbol{\theta} = [R_{1,2} \quad R_{2,3} \quad C_1 \quad C_2 \quad w_1 \quad w_2]'$</p>

Fig 2.16. RC-model, differential equations, and the matrix. Source: Z. Wang et al., 2019.

Black-box sub-modeling

In the dynamic simulation, parameters such as T_a , T_z , Q_h , and Q_{sun} will vary from time to time and are commonly referred to time-series data. Depending on availability, those parameters are historical data that can be gathered from field measurements, sensors, or weather stations (Berthou et al., 2014). The involvement of historical data marks when the black-box modeling first comes into play. The simulation will still use the physical formulation from the white-box modeling, but specific parameters are sourced from historical data, as seen in the parametric formulation phase in Fig 2.14.

Black-box calibration

Depending on the model output, validation with measured data is crucial, as seen in the validation phase on Fig 2.14. For instance, if the model's output is energy demand, this calculated energy demand must be compared to the actual energy demand to identify discrepancies. If discrepancies occur, a calibration needs to be made (S. Wang & Xu, 2006).

Various approaches can be employed to compare the calculated and measured datasets, including sum-squared error, mean-squared error, mean-bias error, and others (Holst et al., 1992). ASHRAE provides guidelines for calibrating energy models using monthly and hourly data (Ruiz & Bandera, 2017; Leitão, 2017). Key metrics for this evaluation include the Mean Bias Error (MBE) and the Coefficient of Variation of the Root Mean Square Error (CV(RMSE)) as seen in Table 2.2. The calculation for both metrics can be found in equations 11 and 12.

Table 2.2 Calibration criteria for simulation model. Source: Ruiz & Bandera, 2017.

Time-series data	Calibration Matrix	
	CV(RMSE)	MBE
Monthly calibration	<15%	<5%
Hourly calibration	<30%	<10%

$$CV(RMSE) = \frac{\sqrt{\frac{\sum_{i=1}^n (m_i - s_i)^2}{n - p}}}{\bar{m}} \times 100\% \quad (11)$$

$$MBE = \frac{\sum_{i=1}^n (m_i - s_i)}{\sum_{i=1}^n m_i} \quad (12)$$

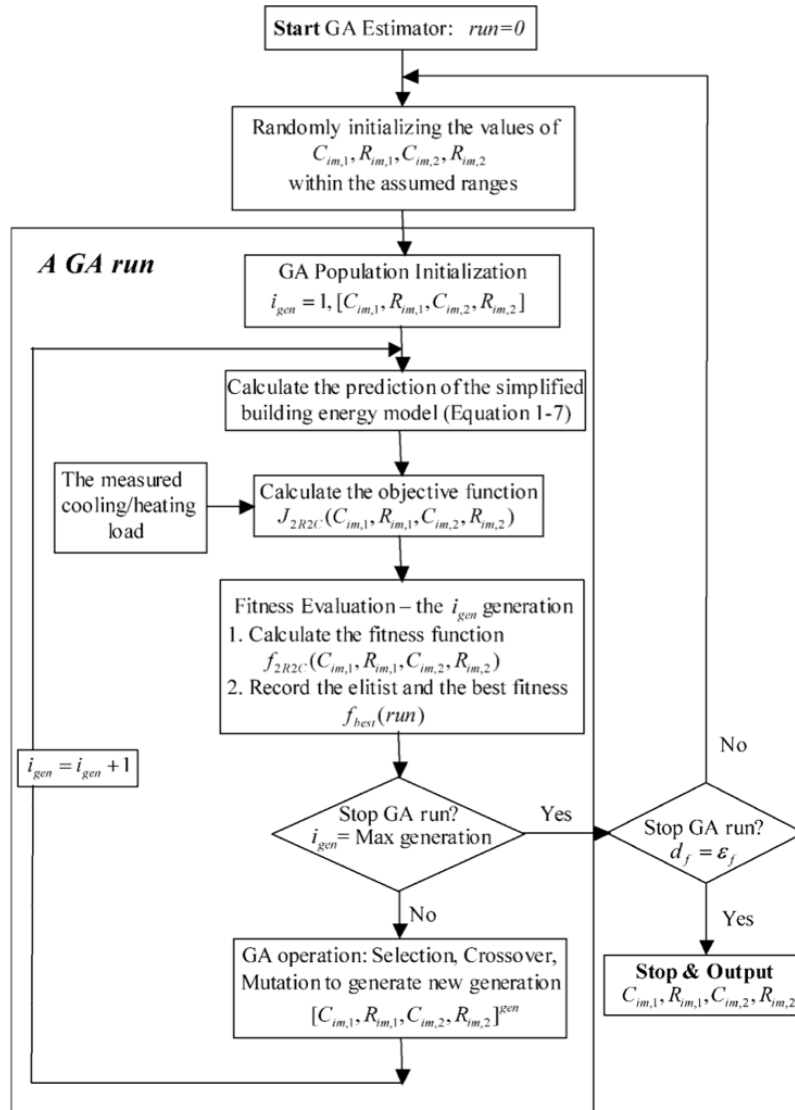


Fig 2.17 Diagram illustrating an example of parameter estimation workflow. Source: Wang & Xu, 2006.

The calibration process involves adjusting specific constant parameters, a procedure known as parameter estimation (Kristensen et al., 2004). This adjustment is carried out to align the calculated output with the measured data. The essence of this method lies in systematically testing new parameter sets to minimize the error matrix or maximize the accuracy, as seen in “calculate objective function” in Fig 2.17. The calibration algorithms are optimization algorithms. Therefore, the approach can be either derivative-based or non-derivative (Farag et al., 2024). Some well-known methods for selecting the next sets of parameters include genetic algorithms, first and second-order derivatives, Bayesian optimization, and others. The choice depends on the nature of the data or the function. After the calibration, the new (validated) parameters will be used for the model instead of the initial parameters.

2.5 Building Control Strategies

BMS or building management system is a control system that regulates either the HVAC or electrical systems in the building (Joseph, 2018, p. 45). For HVAC system, BMS can control some variables such as air pressure, humidity, temperature, etc., which can vary over time. The general workflow of this control system can be seen in Fig 2.18. From the illustration, the function of this control system is to monitor or gather the building conditions, detecting discrepancies between the measured and the setpoint, and control the system to minimize the error or accessing alarm for manual tuning (Liu et al., 2023).

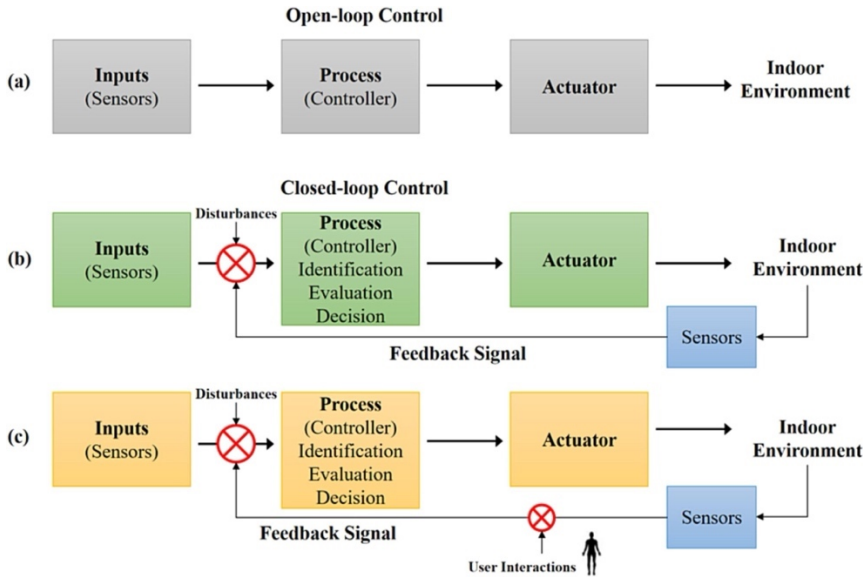


Fig 2.18 General workflow of building control system.

Conventional building control relies on rule-based feedback mechanisms, employing predetermined logic and schedules for the operation of building equipment. These control strategies are typically implemented using classical control techniques like on/off control and Proportional-Integral-Derivative (PID) control. However, the growing complexity of building control tasks, such as integration with the grid,

occupancy-based control, and prediction-based control, has presented challenges to these conventional approaches. Based on the current research, one of the popular advance control methods is model predictive control which can outperform the traditional PID control (Drgoňa et al., 2020;Salcan-Reyes et al., 2024).

Model Predictive Control (MPC)

MPC system is usually a closed loop system as seen in Fig 2.19. The workflow includes gathering the building current state and disturbances, forecasting the future behavior of the building, and optimizing the control input to meet certain objectives while satisfying the constraints (Drgoňa et al., 2020).

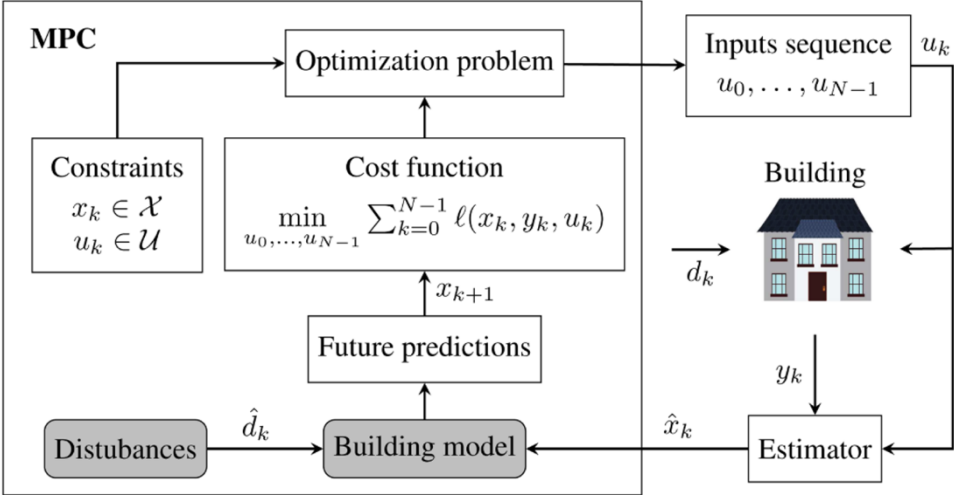


Fig 2.19 Closed loop system of MPC. Source: Drgoňa et al., 2020.

Objective

A cost function or an objective function serves as the target of the MPC, which may involve minimizing or maximizing a certain variable (Drgoňa et al., 2020). The goals set for this method are not restricted to being singular or linear. In some cases, multi-objective MPC involves opposing objective functions. The most popular trade-off case is minimizing energy consumption while maximizing occupant comfort. The formulation of the optimization will find a way to balance the two or more goals.

Choosing the objective function for MPC depends on several things, one of them is the level of detail of the modeling. For instance, the objective of minimizing heat transfer is commonly used when the model captures only the building envelope. On the other case, where the HVAC system is modeled, the objective can be minimizing the energy consumption. However, the objectives are not limited to occupant comfort and energy consumption. Some research shows that monetary cost, greenhouse emissions, and energy storage can also be the objectives.

In order to achieve the objective, as suggested in the system name, there will be

something that is controlled. Some MPCs are designed to control the HVAC component such as the temperature setpoint, the valve opening for air, or water flow rate. For the building model with only the façade, the control can be the heating or cooling amount delivered into the room or the setpoint for the supply air or water. In general, the objective and control are formulated according to how detailed the model is (Drgoňa et al., 2020).

Constraints

Unlike the objective function, constraints in MPC needs to be defined typically as a set of ranges and can be set on input, output, or any variables (Maciejowski & Huzmezan, 1997). The purpose of constraints is to keep certain variable within specified limits. There are hard constraints that have to be satisfied by the system and soft constraints that can be more flexible as it only adds penalty. Examples of constraints include room temperature, comfort metrics, air flow rates, etc. Occasionally, constraints may need to be softened to prevent infeasibility during the optimization. In adaptive MPC, the constraints can also vary in time, requiring “if-else” statements in the formulation.

Chapter 3

Methodology

3.1 Case Study: Pulse (Building 33), TU Delft Campus

Pulse (Fig 3.1) is the first energy-neutral edifice within the TU Delft campus, boasting an impressive energy label of A++++. The rooftop is equipped with 490 solar panels, covering an area of 750 square meters, and these panels generate an annual yield of 150,000 kWh. This solar array is proficient in supplying all the building's energy needs. Moreover, Pulse incorporates a system of heat and cold storage underground (ATES) and is fitted with high-grade insulating glass. The building is managed by active BMS, a sophisticated system that intelligently regulates renewable energy, ventilation, lighting, cooling, and heating at the level of individual rooms. The design of the façade openings maximizes the use of natural daylight, thereby reducing the reliance on artificial lighting and further diminishing energy consumption.



Fig 3.1 Pulse (Building 33), TU Delft Campus. Source: ectorhoogstad.com

Despite the impressive energy efficiency of the building, my personal experience highlights a significant issue with thermal comfort, particularly in study areas near the glass façade. Depending on the season, these areas can become uncomfortably cold or hot. This observation underlines the importance of not just focusing on energy efficiency but also paying close attention to thermal comfort within the building. Balancing these two aspects is crucial for creating a sustainable and comfortable environment for occupants.

Building Façade

This building adheres to passive-house regulations, boasting impressive R-values. Opaque elements on the facade and roof have an R-value of $7 \text{ m}^2\text{K/W}$, while the ground floor and external floors have a value of $5 \text{ m}^2\text{K/W}$. Internal walls, since they are not directly exposed to outdoor temperatures, possess a slightly lower resistance at $3 \text{ m}^2\text{K/W}$. In terms of transparent elements, which dominate the facade, the buildings employ triple-glazing units with a U-value of 1.65 and a g-value of 0.4. Fig 3.2 provides

a visual depiction of the building façade. Appendix A provides the material details.

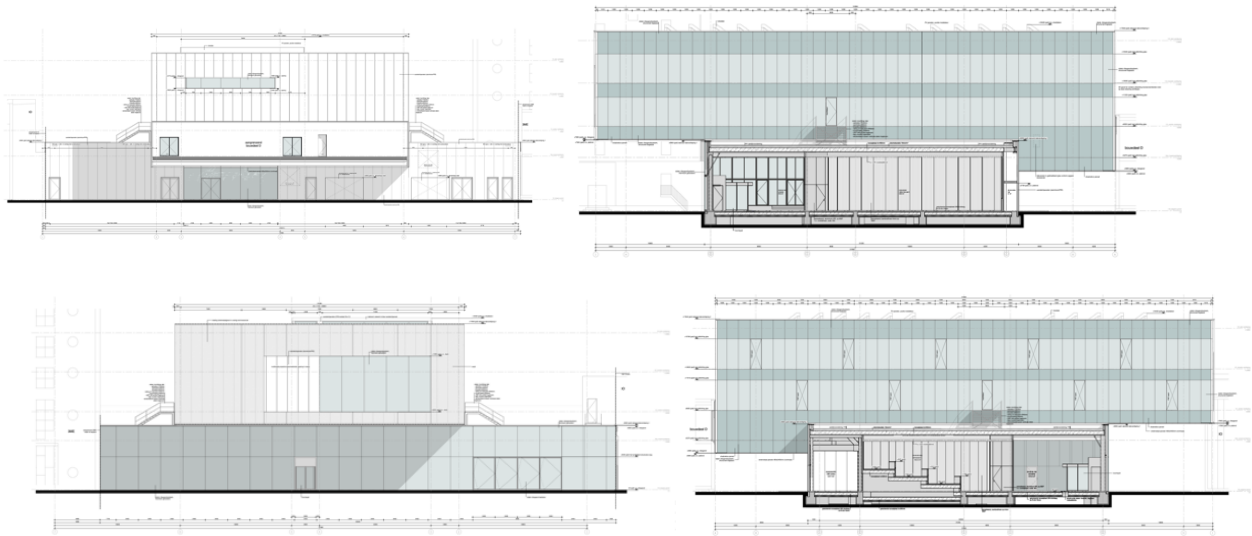


Fig 3.2 Pulse façade.

Building Management System

Pulse Building stands as a sustainable and energy efficiency building. It uses the power of an Aquifer Thermal Energy Storage (ATES) system to regulate its internal temperature. With a coefficient of performance (COP) of 4.5 for heating and 30 for cooling, Pulse maximizes the efficiency of its energy usage. Its climate control infrastructure is comprehensive, including climate ceilings in lecture halls and study areas, as well as floor-based heating and cooling systems in corridors. Additionally, mechanical ventilation also plays a role in maintaining optimal indoor temperatures in summer, further enhancing the building's energy performance.

The Pulse building uses active BMS, which means it is equipped with various sensors, including one that measures the CO₂ levels in each room. This sensor is utilized to regulate the amount of ventilation required for the indoor space. The minimum ventilation rate per person is set at 30m³/h. The building also features operable windows that occupants can use for natural ventilation. However, this study does not take into account this feature; it only includes infiltration (0.5L/s/m²) as part of the ventilation system.

The data obtained from Pulse's BMS includes energy demands, indoor temperatures, and outdoor temperatures for winter and summer. Since the case study involves numerous sensors, outdoor and indoor temperatures were gathered from them and averaged. The available dataset is hourly data and spans from 2019 to 2022. Compared to other years, 2019 does not represent the actual energy demand behavior (the flat lines); therefore, this particular year was not considered. The graph of 2020's energy consumption is relatively flat, indicating that the weather was not too extreme. Energy consumption in 2021 and 2022 was significantly more fluctuating.

However, looking at the peak winter and summer periods, 2022 had higher energy consumption. Therefore, this study uses the building and weather conditions from winter (January) and summer (July) of 2022. The periods were chosen to determine whether the proposed alternatives can withstand extreme weather based on the available data. A comparison of energy consumption across the four years can be seen in Fig 3.3.

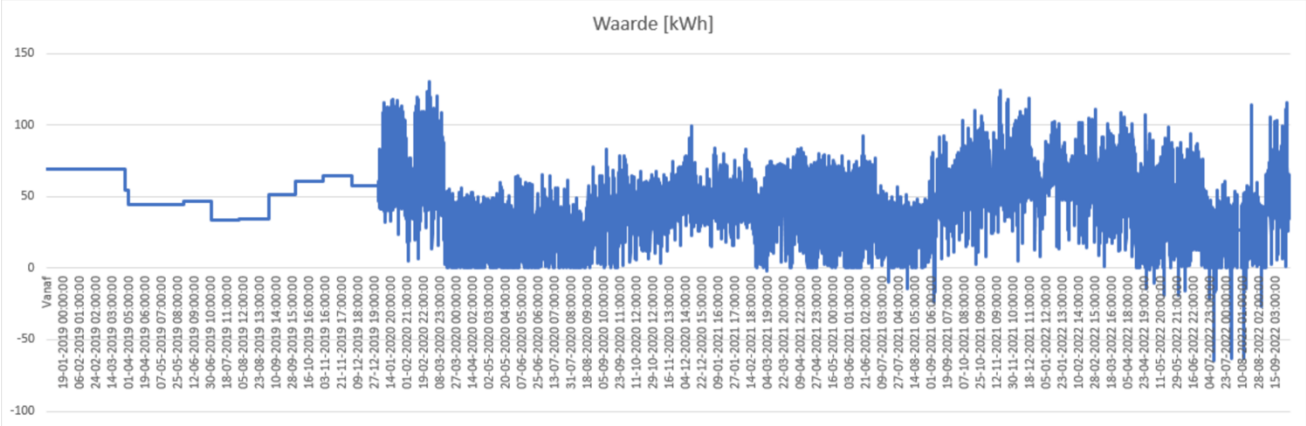


Fig 3.3 Pulse's energy consumption from 2019 to 2022.

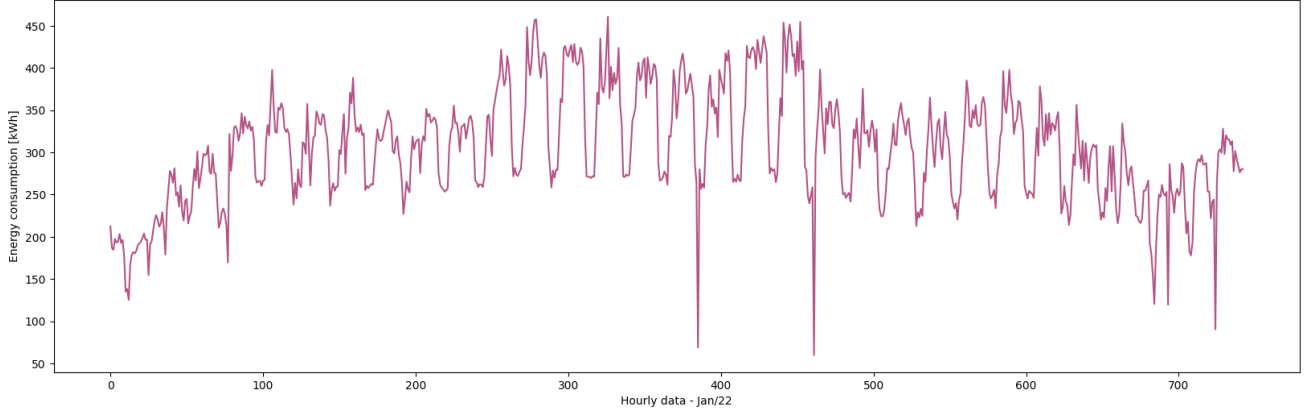


Fig 3.4 Pulse's energy consumption in winter, January 2022.

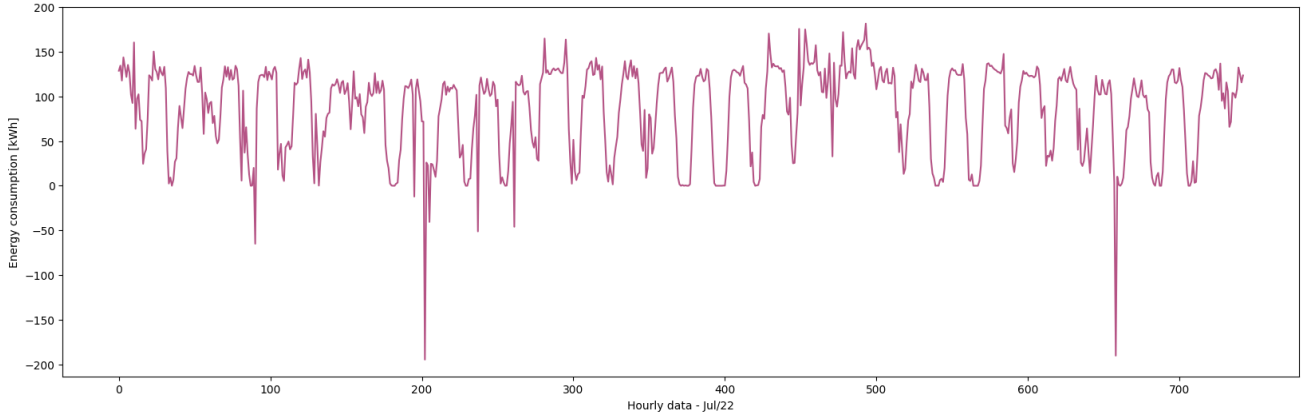


Fig 3.5 Pulse's energy consumption in summer, July 2022.

As seen in Fig 3.4 and Fig 3.5, there are several extreme drops in both winter and summer. Since these drops appear extreme, it is assumed there was either a reset or

an error in the sensor. Therefore, drops resulting in negative values during summer are assumed to be equal to those at the previous timestep. Since the drops do not reach negative values for winter, they need to be chosen manually. It appears that there are six drops in the winter. Those drops are also assumed to be equal to the value at the previous timestep.

Occupancy Schedule

This facility serves not only as a classroom but also as a study space for students. Teaching activities are scheduled from 8:00 to 16:00, while the building remains open from 8:00 to 24:00 to accommodate student needs. Although few students typically stay late, it is common for them to remain until closing time during exam weeks. There are approximately 13 classrooms with capacities ranging from 40 to 130 seats. Study areas are situated on the intermediate floor (mezzanine), first floor, and second floor, mainly near the large glass façade. The combined capacity of these study areas totals approximately 150. Additionally, on the ground floor, there is a *horeca* space that functions as a cafeteria area at certain times on the day and can also serve as a study area. Since there are no sensors for occupancy counting, the occupancy schedule for 2022 is obtained from TU Delft’s academic calendar, room capacitance, and personal experience. A comparison between winter and summer occupancy in January and July 2022 can be seen in Fig 3.6 and Fig 3.7. The academic calendar and assumptions made for the occupant amounts can be seen in appendix B and C.

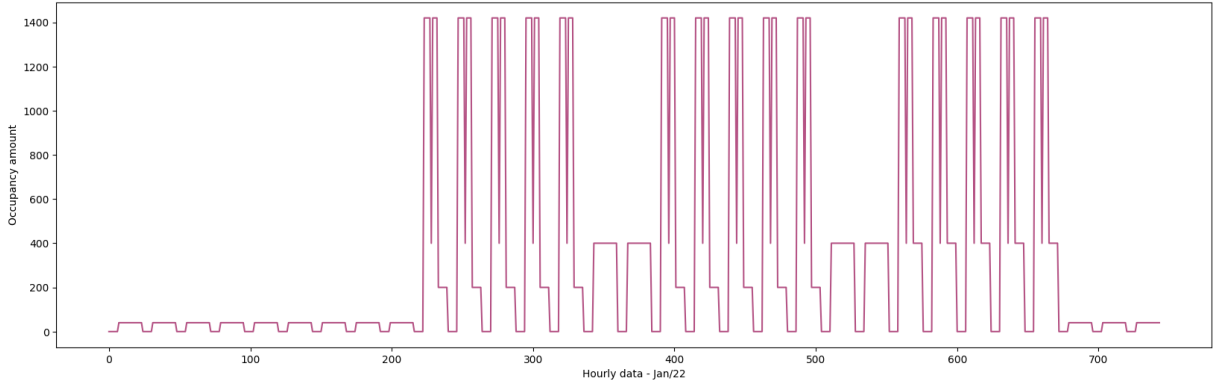


Fig 3.6 Pulse’s occupancy estimations in January 2022.

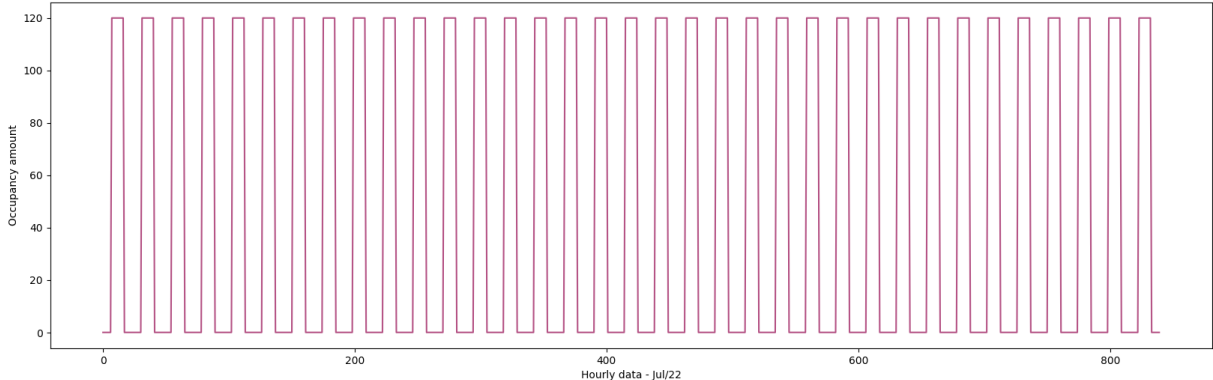


Fig 3.7 Pulse’s occupancy estimations in July 2022.

3.2 RC-modeling

RC-thermal Network

To accurately capture the dynamic effects of changing disturbances such as solar radiation and outside temperature, a dynamic simulation approach is employed. This simulation not only tracks the fluctuations in indoor temperature but also monitors the variations in surface temperatures, taking into account the thermal capacity of the materials. Such dynamic simulation proves to be more accurate in assessing the changes in climate and occupancy schedules of the building, offering an improvement over static models, particularly for time series analysis. This section discusses the workflow and matrices utilized for RC modeling to evaluate the accuracy of the models associated with different node quantities.

RC-modeling workflow

As outlined in the literature review, the RC-model serves as the initial stage in making an MPC to make a digital twin for the building. The selected case study was transformed into a matrix format in Python. This matrix facilitates the calculation of heat transfers over time, allowing for the computation of the energy demand and surface temperatures of all times. The simulations were conducted during January and June 2022 at 1-hour intervals. The workflow for the dynamic simulation is presented visually in Fig 3.8.

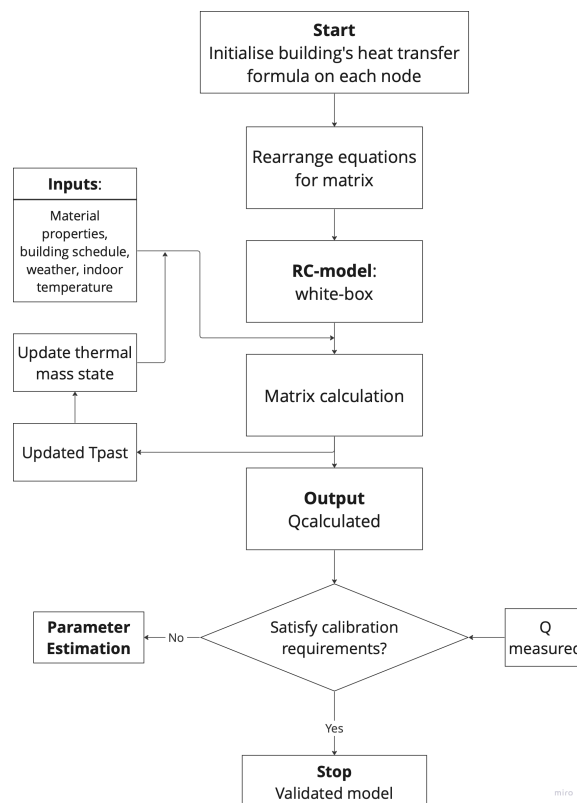


Fig 3.8 Workflow of the RC-modeling for dynamic simulation.

Matrix arrangement

The matrix for RC-model in this thesis is based on the thermal networks and heat transfer equations, which can be seen in Table 3.1 and Table 3.2.

Table 3.1 Thermal networks symbols and equations.



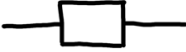



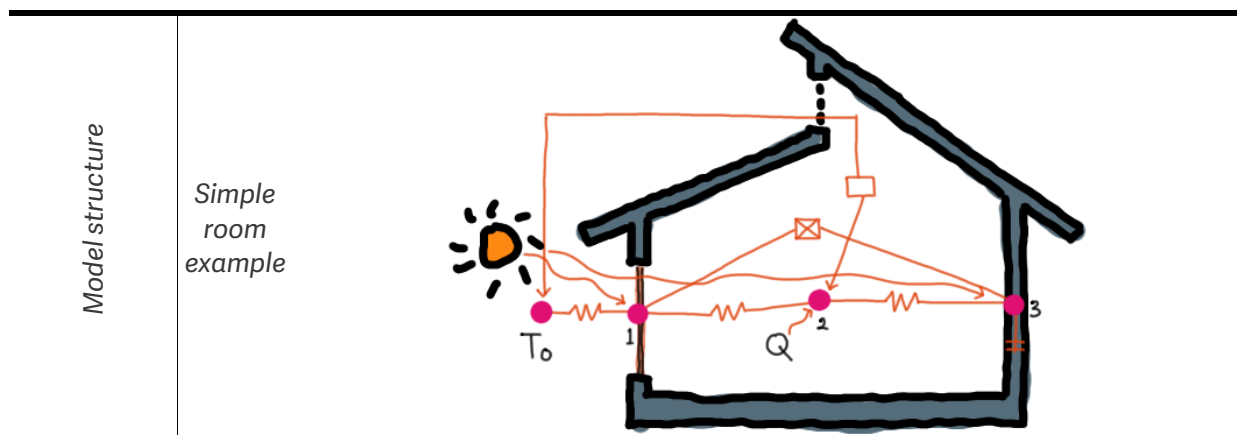
Symbols	Description	Equations
	Absorbed solar radiation	$A_1 \times A_{gl} \times Q_z$
	Heating	Q_{heat}
	Advection	$\rho_{air} \times V_{air} \times C_{p_{air}} \times \Delta T$
	Convection	$\alpha_{conv} \times A_s \times \Delta T$
	Radiation	$\alpha_{rad} \times F \times A_s \times \Delta T$
	Conduction and accumulation using response factor method	$A_s \left(\sum_{i=0}^N X_i \times T_s^{t-i} \right)$ $N = 50 \times d_s$ $X_0 = 2/\pi \sqrt{\frac{k \times \rho \times C_{ps}}{3600}}$ $X_n = -X_0 (2\sqrt{n} - \sqrt{n+1} - \sqrt{n-1}) ; n > 0$ $X_{n_{cor}} = X_n - \frac{Error}{N-1} ; n > 2$ $Error = \sum_{n=0}^N X_n$

Table 3.2 Matrix arrangement based on thermal networks.



Differential equations	Node 1	$\alpha_{conv_o} \cdot A_{gl} \cdot (T_o - T_1) + \alpha_{conv_i} \cdot A_{gl} \cdot (T_2 - T_1) + \alpha_{rad} \cdot A_{gl} \cdot F_{13} (T_3 - T_1) + A_1 \cdot A_{gl} \cdot Q_z = 0$
	Node 2	$\alpha_{conv_i} \cdot A_{gl} \cdot (T_1 - T_2) + \alpha_{conv_i} \cdot A_w \cdot (T_3 - T_2) + \rho_{air} \cdot V_{air} \cdot C_{p_{air}} \cdot (T_o - T_2) + Q_{heat} = 0$
	Node 3	$\alpha_{conv_i} \cdot A_w \cdot (T_2 - T_3) + \alpha_{rad} \cdot A_w \cdot F_{31} (T_1 - T_3) + D_1 \cdot A_{gl} \cdot Q_z = A_w (X_0 \cdot T_3 + X_1 \cdot T_3^{(t-1)} + X_2 \cdot T_3^{(t-2)} + X_3 \cdot T_3^{(t-3)} + \dots + X_n \cdot T_3^{(t-n)})$
Rearranged equations	Node 1	$\begin{aligned} & (-\alpha_{conv_o} \cdot A_{gl} - \alpha_{conv_i} \cdot A_{gl} - \alpha_{rad} \cdot A_{gl} \cdot F_{13}) \cdot T_1 \\ & + \alpha_{rad} \cdot A_{gl} \cdot F_{13} \cdot T_3 \\ & = -A_1 \cdot A_{gl} \cdot Q_z - \alpha_{conv_o} \cdot A_{gl} \cdot T_o \\ & - \alpha_{conv_i} \cdot A_{gl} \cdot T_2 \end{aligned}$
	Node 2	$\begin{aligned} & \alpha_{conv_i} \cdot A_{gl} \cdot T_1 + Q_{heat} + \alpha_{conv_i} \cdot A_w \cdot T_3 \\ & = (\alpha_{conv_i} \cdot A_{gl} + \alpha_{conv_i} \cdot A_w + \rho_{air} \cdot V_{air} \cdot C_{p_{air}}) \cdot T_2 \\ & - \rho_{air} \cdot V_{air} \cdot C_{p_{air}} \cdot T_o \end{aligned}$
	Node 3	$\begin{aligned} & \alpha_{rad} \cdot A_w \cdot F_{31} \cdot T_1 + (-\alpha_{conv_i} \cdot A_w - \alpha_{rad} \cdot A_w \cdot F_{31} - A_w \cdot X_0) \cdot T_3 \\ & = -D_1 \cdot A_{gl} \cdot Q_z + A_w (X_1 \cdot T_3^{(t-1)} + X_2 \cdot T_3^{(t-2)} + X_3 \cdot T_3^{(t-3)} + \dots + X_n \cdot T_3^{(t-n)}) \\ & - \alpha_{conv_i} \cdot A_w \cdot T_2 \end{aligned}$
Matrix	Equation	$T = M^{-1}B$
	T	$\begin{bmatrix} T_1 \\ Q_{heat} \\ T_3 \end{bmatrix}$
	M	$\begin{bmatrix} -A_{gl} \cdot (\alpha_{conv_o} \cdot -\alpha_{conv_i} \cdot -\alpha_{rad} \cdot F_{13}) & 0 & \alpha_{rad} \cdot A_{gl} \cdot F_{13} \\ \alpha_{conv_i} \cdot A_{gl} & 1 & \alpha_{conv_i} \cdot A_w \\ \alpha_{rad} \cdot A_w \cdot F_{31} & 0 & -A_w \cdot (\alpha_{conv_i} + \alpha_{rad} \cdot F_{31} + X_0) \end{bmatrix}$
B	$\begin{bmatrix} -A_1 \cdot A_{gl} \cdot Q_z - \alpha_{conv_o} \cdot A_{gl} \cdot T_o - \alpha_{conv_i} \cdot A_{gl} \cdot T_2 \\ (\alpha_{conv_i} \cdot A_{gl} + \alpha_{conv_i} \cdot A_w + \rho_{air} \cdot V_{air} \cdot C_{p_{air}}) \cdot T_2 - \rho_{air} \cdot V_{air} \cdot C_{p_{air}} \cdot T_o \\ -D_1 \cdot A_{gl} \cdot Q_z + A_w (X_1 \cdot T_3^{(t-1)} + X_2 \cdot T_3^{(t-2)} + X_3 \cdot T_3^{(t-3)} + \dots + X_n \cdot T_3^{(t-n)}) - \alpha_{conv_i} \cdot A_w \cdot T_2 \end{bmatrix}$	

The following matrix in equation 13 acts as the core calculation of the dynamic simulation. With n representing the number or sequence of the nodes, matrix T serves as a pivotal repository where all variables are yet to be determined. These variables include surface temperatures alongside the desired output variable, Q. Conversely, matrix B is designated to house known variables that go with solar radiation, $T_{outdoor}$, and T_{indoor} after the equation rearrangement. This matrix also contains the capacitance C of the materials, which will be updated during the simulation process. Matrix M plays a crucial role in conducting the heat transfer analysis, where most of the calculations of thermal balance are placed. Each row within matrix M delineates the nodes, thereby enabling examination of the thermodynamic phenomena occurring in the building.

$$\begin{bmatrix} T_{s1} \\ \vdots \\ T_{sn-1} \\ Q_{calc} \end{bmatrix} = \begin{bmatrix} M_{1,1} & \cdots & M_{1,n-1} & 0 \\ \vdots & \ddots & \vdots & \vdots \\ M_{n-1,1} & \cdots & M_{n-1,n-1} & 0 \\ M_{n,1} & \cdots & M_{n,n-1} & 1 \end{bmatrix}^{-1} \begin{bmatrix} B_1 \\ \vdots \\ B_n \end{bmatrix} \quad (13)$$

Input parameters

As stated in the literature study chapter, the input parameters for the matrix include material properties (envelope and thermal mass), building schedule, outdoor temperature, solar radiation, and indoor temperature. Building envelope and thermal mass data were obtained from detailed drawings and estimated for the lumped-model version. The complete parameters are detailed in Table 3.3, appendix D, and appendix E.

Table 3.3 Input parameters for matrix calculation.

Parameters	Description	Units
T_o	Outdoor temperature	°C
T_i	Indoor temperature	°C
A	Area of the building surfaces	m ²
U-value Glass	Reciprocal of resistance for glass	W/m ² K
A_1	Absorption value of glass; use g-value or Solar Heat Gain Coefficient (SHGC)	-
F	View factor	-
α_{conv_o}	Outdoor convective coefficient	W/m ² K
α_{conv_i}	Indoor convective coefficient	W/m ² K
α_{rad}	Radiative coefficient	W/m ² K
U-value Opaque	Reciprocal of resistance for opaque element	W/m ² K
D_1	Absorption value for opaque surfaces	-
d	Thickness for opaque element	m
R	Thermal resistance for opaque element	m ² K/W
k	Thermal conductivity for opaque element	W/mK
ρ_s	Density for opaque element	Kg/m ³
C_{ps}	Specific heat capacity for opaque element	J/kgK
Q_z	Solar energy	MJ/m ²
Vent	Ventilation per person	m ³ /s/person
ρ_{air}	Density of air	Kg/m ³

$C_{p\text{air}}$	Specific heat capacity of air	J/kgK
Q_{int}	Internal heat gain per person	W/m ²

The mentioned parameters are utilized consistently across all model versions. The subsequent sections will explain the different model versions. Certain parameters undergo modifications due to alterations in the thermal networks, particularly in the lumped version. The parameters held constant throughout are T_o , T_i , Q_z , vent, ρ_{air} , $C_{p\text{air}}$, and Q_{int} .

Different model versions

Three different versions of the RC-model were employed in this study. The aim of these three models is to compare the simulation accuracy against the measured data and to get a model that can calculate quickly. The latter goal is considered because this model will be used by MPC to forecast in real-time.

The first version of the RC-model is called V.1. This model only includes the building envelope, recognizing it as the primary place of heat transfer phenomena. Each element of the envelope, including walls, windows, roofs, and indoor air, is assigned as a unique node within the model. This configuration, which can be seen in the appendix F, results in a matrix of dimensions 20x20 corresponding to the approximately 20 nodes employed. Fig 3.9 illustrates the distribution of nodes in the building section.

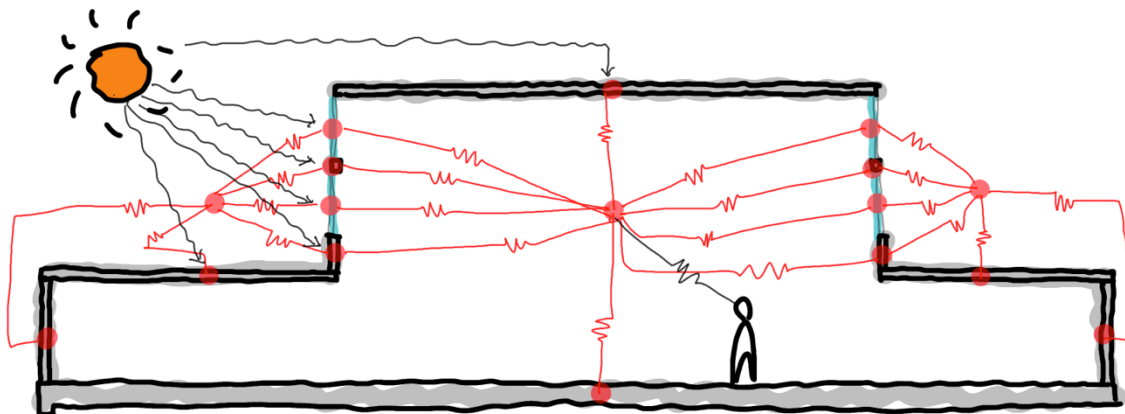


Fig 3.9 V.1 nodes distribution on Pulse's section.

The next version of the RC-model is called V.2. This model not only includes the building envelope, but also the inner walls and floors as internal mass. This model aims to see how accuracy increases or decreases with the presence of a thermal mass in the calculation. All internal walls or floors are assigned as one node within the model, as they have the same material properties on the surfaces. The additional nodes details can be seen in the appendix G. The glass walls inside Pulse are negligible due to their low thermal capacitance. The matrix configuration is the same as V.1 but with the

addition of 2 rows and columns for the internal mass. Fig 3.10 illustrates the distribution of nodes in the building section.

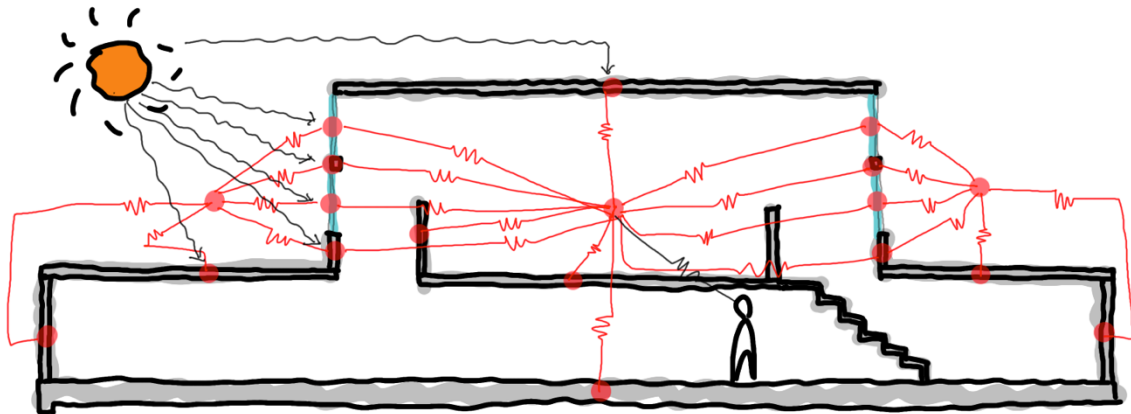


Fig 3.10 V.2 nodes distribution on Pulse's section.

The third version of the RC-model is called V.3. Compared to the last two versions, this model only has five lumped nodes: opaque envelope (including walls and roof), external windows, indoor floors, indoor walls, and indoor air (Fig 3.11). The nodes' details can be seen in the appendix H. This model is way more simplified than the other two. The objective of this model is to evaluate whether the simplification affects the calculation accuracy and to determine if the computational time can be reduced.

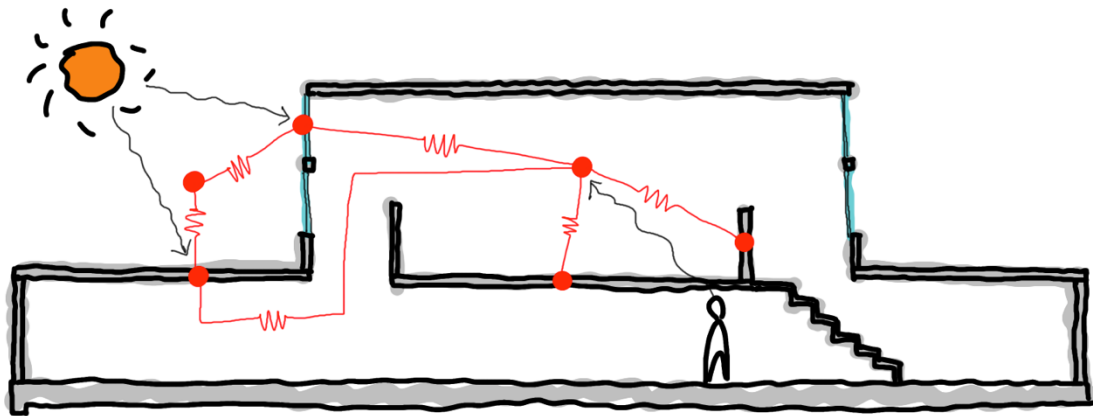


Fig 3.11 V.3 nodes distribution on Pulse's section.

Model Calibration (Parameter Estimation)

Calibration is performed by changing parameters (inputs) until the simulation results closely align with real-world scenarios. The calibration process can be accomplished through manual or black-box methods. Manual tuning, such as adjusting the building schedule and ventilation amount, is taken prior to the black-box process. The calibration using the black-box method is aimed to perceive CV(RMSE) and MBE values within the threshold, as stated in the literature study. The workflow for parameter

estimation is visually depicted in Fig 3.12. The problem formulation in this optimization process starts with initiating values of the parameters that will be estimated. These initial guesses can be depicted from technical drawings, the rule of thumb, and assumptions. Some parameter bounds need to be stated in order to avoid nonsensical estimations. The bounds estimation can be seen in equation 14.

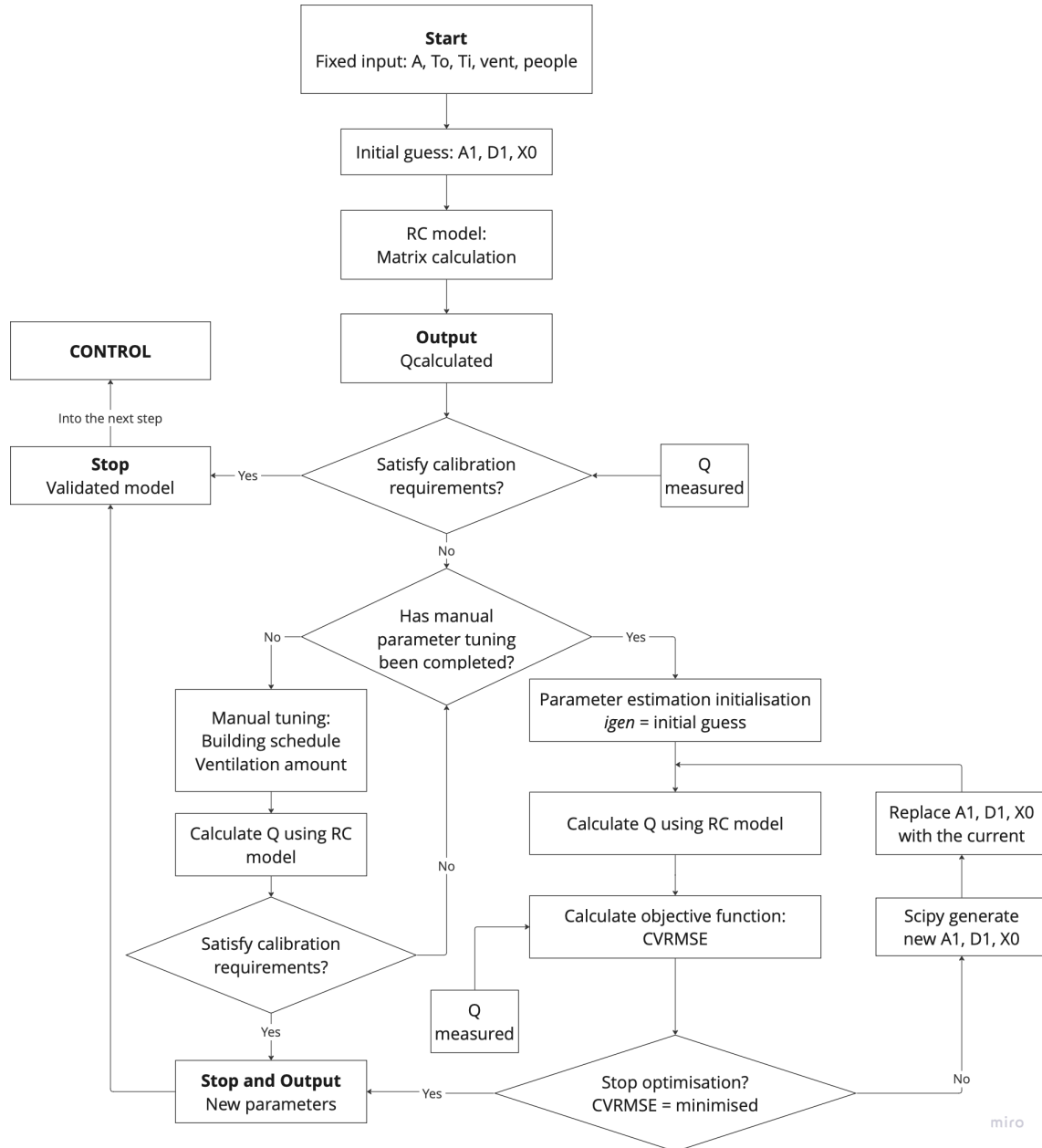


Fig 3.12 Workflow of the parameter estimation.

$$\frac{guess}{2} \leq guess \leq (guess \times 2) \quad (14)$$

This study tries three different algorithms. Two of the algorithms are derivative-based, namely L-BFGS-B and SLSQP. The other one is non-derivative and is called Nelder-Mead. These three algorithms are employed to evaluate the accuracy of the estimation

and the convergence speed.

3.3 Model Predictive Control

The validated building model was then utilized as the predictive model in the Model Predictive Control (MPC) framework. The objective of this MPC was to reduce energy demand while adhering to thermal comfort constraints. In terms of control, it also employed optimization but with a different algorithm from that used in parameter estimation. The control algorithm needed to include constraints, whereas parameter estimation only required bounds. The input to the MPC consists of the current state of the building, and its output is the control input for the building over a predicted time horizon.

MPC Workflow

The inputs for the prediction model include T_{indoor} , ventilation, and weather data. The first two are obtained from building meters or sensors, while the latter is collected from the weather forecast from weather station. This predictive model will predict with a horizon length of 12 hours and a time step of 1 hour, predicting 12 hours into the future. Subsequently, the MPC model will optimize variable controls, which are the temperature setpoints, for each data within the horizon range. The model then takes the first state from the prediction, denoted as $k+1$ (where k is the current state), and uses it as input for the building. The entire workflow is visualized in Fig 3.13.

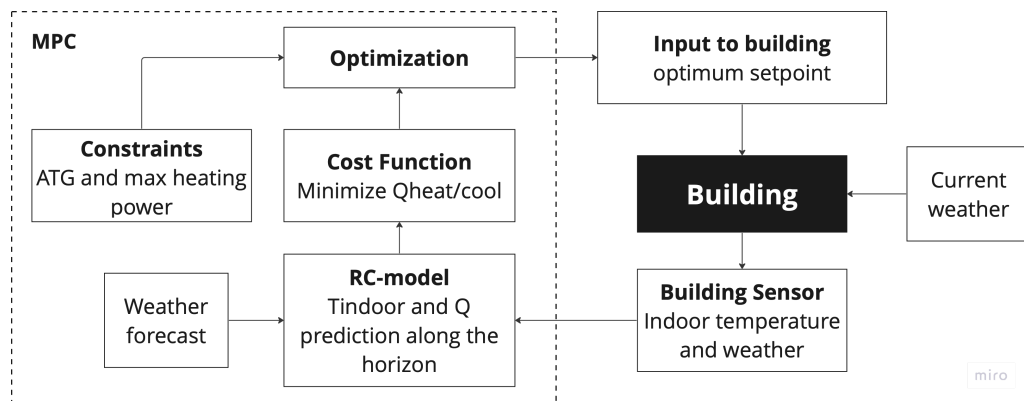


Fig 3.13 Model predictive control (MPC) workflow.

Problem Formulation and Algorithm

The problem formulation for the control part of MPC is essentially the same as the optimization process conducted during parameter estimation. The objective of this control model is to minimize Q (Equation 18). The difference in this optimization lies in the inclusion of several constraints, not only bounds. The algorithms capable of accepting inequality constraints in the Python library *Scipy* are SLSQP and COBYLA, both of which will be used in this study. The two optimizers are known best as local optimizers, meaning they only find the best solutions near the first guess (Faílde et al.,

2023). The local optimizers are chosen because the jump on the setpoint temperature cannot be too high.

The constraints in this thesis are divided into three categories: constraints to limit the results of the objective function u_k , constraints for the parameters T_{indoor} , and comfort constraints. The maximum allowable Q for summer is 217 kWh, while for winter, it is 450 kWh. These values are derived from the maximum power used during peak moments in 2022. This MPC is aimed to reduce energy consumption; thus the energy produced by this smart system is not allowed to exceed the existing energy consumption, hence the maximum allowable Q. For indoor temperature constraints x_k , T_{indoor} parameter is restricted to have a maximum difference of 2.2°C from the T_{indoor} at the previous timestep, considering thermal comfort (Mtibaa et al., 2021). The x_k is used as bounds as well.

For comfort constraint z_k , it adopts the Dutch Adaptive Thermal Comfort (ATG) considering the running mean outdoor temperature and indoor operative temperature; thus, this constraint considers indoor operative temperature T_{op} and running mean outdoor temperature T_{or} . The f and g functions denote ATG's upper and lower limits, respectively. The Pulse building falls into the Beta category and class limit B. Equations for MPC problem formulations can be found in equations 15-18. However, there is some flexibility if the optimization cannot find a condition that falls within class B's upper and lower limits. If the class B comfort limit cannot be satisfied, it can consider class C and then class D. Additionally, if the comfort constraints cannot be satisfied at all, the model will revert to u_k .

$$u_k = f_{Qheat}(T_{i_k}, T_{o_k}, Q_{z_k}) \begin{cases} \text{Summer,} & u_k \leq 217 \text{ kWh} \\ \text{Winter,} & u_k \leq 450 \text{ kWh} \end{cases} \quad (15)$$

$$x_k = \begin{cases} T_{indoor_{t-1}} - T_{indoor_t} \leq 2.2^\circ\text{C} \\ T_{indoor_t} - T_{indoor_{t-1}} \leq 2.2^\circ\text{C} \end{cases} \quad (16)$$

$$z_k = \sum_{i=k}^n f(T_{or}) - \sum_{i=k}^n g(T_{or})$$

$$f(T_{or}) = \begin{cases} 24^\circ\text{C}, & 10^\circ\text{C} \leq T_{or} \leq 16^\circ\text{C} \\ ((0.2 \times T_{or}) + 18) + 4.8^\circ\text{C}, & 10^\circ\text{C} \leq T_{or} \leq 16^\circ\text{C} \\ 26^\circ\text{C}, & T_{or} > 16^\circ\text{C} \end{cases}$$

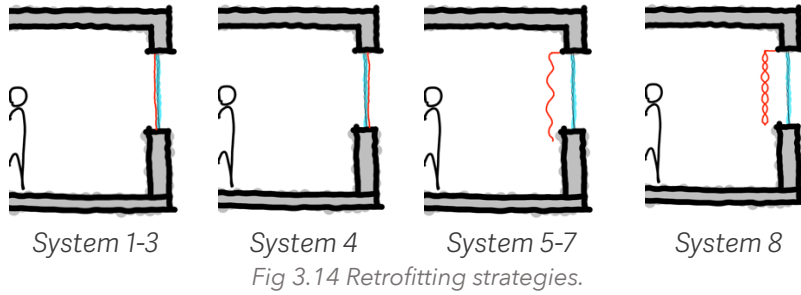
$$g(T_{or}) = \begin{cases} 20^\circ\text{C}, & T_{or} < 10^\circ\text{C} \\ ((0.2 \times T_{or}) + 18)^\circ\text{C}, & T_{or} \geq 10^\circ\text{C} \end{cases} \quad (17)$$

$$z_k = \begin{cases} (T_{op} - g(T_{or})), (f(T_{or}) - T_{op}) \\ (g(T_{or}) - 1) - f(T_{or}), & \text{if } (g(T_{or}) - T_{op}) < 0 \text{ or } (f(T_{or}) - T_{op}) < 0 \\ (g(T_{or}) - 2) - f(T_{or}), & \text{if } (g(T_{or}) - 2) - T_{op} < 0 \text{ or } (f(T_{or}) + 2) - T_{op} < 0 \\ u_k, & \text{if none of the three conditions satisfied} \end{cases}$$

$$\min_{u_k} \sum_{i=k}^n Optim(x_k, u_k, v_k, z_k) \quad (18)$$

3.4 Glass Retrofitting Strategies

The base window utilized in this study was a double-glazed Low-E glass. Retrofitting strategies added to the window include films, curtains, and air-pocket/bubble wrap curtains. Illustrations of the placement of the strategies can be seen in Fig 3.14. The details of these strategies can be found in Table 3.4 and appendix I.



Three strategies, namely phase-change material (PCM), electrochromic, and photochromic film, will not be considered in this study. PCM changes its material over time from solid to liquid and vice versa, leading to variations in thermal properties. Similarly, the two films change colors over time, resulting in changes in absorption properties depending on the environment. Due to the simplification of the model, simulating these materials' gradient values is challenging.

Table 3.4 The features of the retrofitting strategies.

System	Window Glass	Gap (m)	Retrofitting Strategy	Reference
Base	Low-E Double glazing	-	-	
1	Base	-	Low-E film	(EPD, 2022)
2	Base	-	Insulating film	(SS, 2024)
3	Base	-	Solar control film (inside)	(Yin et al., 2012)
4	Base	-	Solar control film (outside)	(Yin et al., 2012)
5	Base	0.07	Polyester thermal curtain, dark blue (0% openness)	(Sotex, 2024)
6	Base	0.07	Polyester thermal curtain, green (28% openness)	(Sotex, 2024)
7	Base	0.07	polyester sheer curtain, beige translucent (54% openness)	(Sotex, 2024)
8	Base	0.05	Transparent bubble wrap curtain	(BIS, 2013)

Those systems are evaluated regarding the impact on the window's resistance and absorptance value, the heat loss/gain through the systems, and the impact on energy demand and comfort in building.

3.5 Comparison and Analysis

The base case and the selected retrofitting strategies are tested using MPC. The obtained results, which are energy demand and thermal comfort, are then compared with those obtained using the existing system. This analysis began by examining the energy savings compared to the baseline. Subsequently, the analysis evaluated the comfort performance using the Dutch comfort matrix, ATG. From both factors, energy and comfort, conclusions and key lessons were drawn regarding the performance of MPC and retrofitting strategies for both summer and winter peaks.

Chapter 4

Changing the Existing System into Model Predictive Control (MPC)

4.1 Building Model (RC-modeling)

Different Models Evaluations

Using the same constant-input values across all models, the following figures represent the results obtained from each model compared to the measured heating/cooling demand [kWh]:

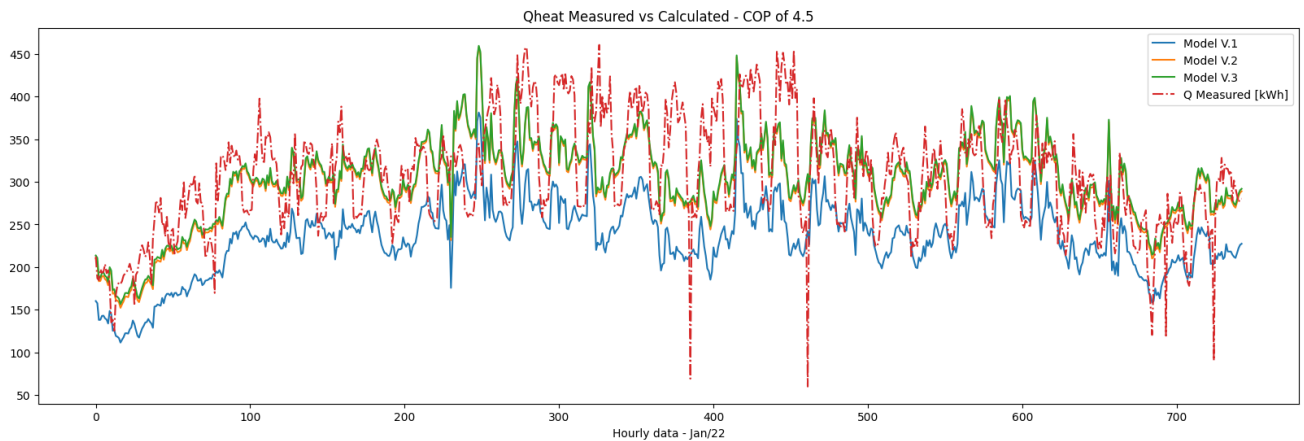


Fig 4.1 Comparison of measured and calculated heating demand in all models in 2022 climate scenario.

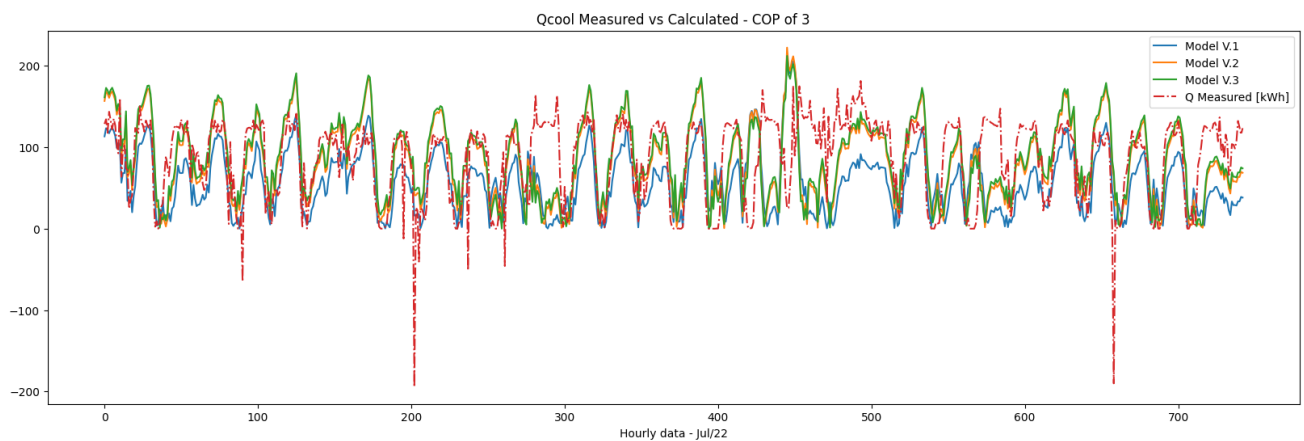


Fig 4.2 Comparison of measured and calculated cooling demand in all models in 2022 climate scenario.

All model versions display discrepancies with Q -measured, which was expected due to the simplifications inherent in the models. Additionally, several parameters not considered as inputs, such as hot water usage, wind, rain, differences in occupancy schedules, and other disturbances, can contribute to this disparity. The Q -measured graph also reveals noticeable extreme drops, indicating potential sensor, meter, or HVAC equipment resets. These instances imply human intervention in the control system, further complicating the alignment between Q -calculated and Q -measured values.

Hence, it is apparent that creating a digital twin of a building poses challenges.

ASHRAE recommends evaluating the accuracy of Q-calculated using the calibration matrix CV(RMSE) and MBE. Table 4.1 presents the scores of each model for both summer and winter seasons.

Table 4.1 Comparison of CV(RMSE), MBE, and execution time in all models using winter and summer months in 2022 climate scenario.

Rank	Model	Mode	Calibration Matrix*		Calibrated	Execution Time
			CV(RMSE)	MBE		
3	V.1	Winter	0.28	0.23	x	1h 1m
		Summer	0.66	0.33	x	1h 3m 9s
2	V.2	Winter	0.18	0.02	v	1h 13m 23s
		Summer	0.57	0.03	x	1h 11m 3s
1	V.3	Winter	0.17	0.01	v	50s
		Summer	0.56	0.01	x	51s

*CV(RMSE) should be <30% and MBE should be <10% for hourly calibration.

Model V.1 exhibits the poorest scores because of its sole consideration of the building envelope without any inner thermal mass. With the inclusion of thermal mass in V.2, scores decrease, indicating higher accuracy, with the winter score already falling within the acceptable range. Nonetheless, the CV(RMSE) for summer months still surpasses the permissible threshold. Despite Model V.3 outperforming the other two models in terms of accuracy and computing time, its CV(RMSE) for the summer month remains above the acceptable threshold. Consequently, further model calibration is needed, mainly due to the lumped parameters.

Parameter Estimation

The objective function of this parameter optimization is to minimize CV(RMSE) because the exceeding score for summer V.3 is that matrix. The allowable limit is 0.3; therefore, the objective function does not need to be minimized to 0. Instead, it is transformed into equation 19, ensuring that the resulting CV(RMSE) value is capped at 0.3.

$$\min \sum_{i=k}^n CV_{RMSE}(\text{parameters}) - 0.3 \quad (19)$$

1st attempt: Including only the absorption values

The input for the parameter estimation function comprises the parameters to be estimated. As the first attempt, the parameters utilized are only A_1 and D_1 which are the absorption values of glass and opaque materials, respectively. The two parameters were chosen because of the model's accuracy for the winter season, which implies that parameters related to heat transfer (conduction, convection, and radiation) are already precise. However, for the summer season, the total load is calculated not only from heat transfer but also from solar gain. Hence, in Model V.3, the solar absorption parameters become essential and need to be adjusted.

Given that the estimation process can lead to wide fluctuations, giving bounds to the parameters is crucial as explained in the methodology chapter. The absorption of a material typically ranges from 0 to 1. Consequently, the upper bounds are set to 1. However, one parameter may increase significantly during the estimation process while the other decreases to a very low value. Therefore, the lower bounds are defined as half of the guessed values. The formulas for the objective function and bounds are provided in equation 20.

$$CV_{RMSE}(A_1, D_1) = \begin{cases} A_1, & (0.5 \times A_1) \leq A_1 \leq (2 \times A_1) \\ D_1, & (0.5 \times D_1) \leq D_1 \leq (2 \times D_1) \end{cases} \quad (20)$$

After formulating the objective function and parameter bounds, A_1 and D_1 were optimized to ensure CV_{RMSE} of Q-calculated falls within the threshold. The optimized parameter values, number of iterations, and convergence speed for each algorithm are provided in Table 4.2 and appendix J.

Table 4.2 1st attempt: Comparison of performance for each algorithm.

	A_1	D_1	CV_{RMSE}	Iteration at Convergence	Convergence Speed
Base	0.4	0.25	0.56	-	-
L-BFGS-B	0.4	0.25	0.56	3	2m
SLSQP	0.4	0.25	0.56	3	3m 22s
Nelder-Mead	0.4	0.25	0.56	16	1h 6m 58s

The initial guess of A_1 and D_1 were taken from the previous graduation thesis and material specification, respectively. None of the three algorithms changed the initial guess, and the objective was not minimized. The derivative-based algorithms only reached three iterations and declared the convergence. While the non-derivative could reach 16 iterations, there were still no changes in the parameter values. This problem can occur because of the nature of the algorithm or an issue in the problem formulation.

2nd attempt: Different guesses values

For the second attempt, the same parameters were considered. However, the initial guesses were made differently to check if the issue was because of the guesses. Using the same bounds, the results showed that the parameters' value changed as seen in Table 4.3 and appendix K. However, the CV(RMSE) still has not changed. From this attempt, it is clear that the algorithms are sensitive to the initial guess as the number of decimal places matters. However, the CV(RMSE) was still too high and did not reduce significantly, although the parameters changed significantly. To that end, it can be observed that the chosen parameters do not significantly impact the objective.

Table 4.3 2nd attempt: Comparison of performance for each algorithm.

	A_1	D_1	CV_{RMSE}	Iteration at Convergence	Convergence Speed
Base	0.39	0.24	0.55	-	-
L-BFGS-B	0.389	0.239	0.55	6	2m
SLSQP	0.39	0.24	0.55	3	3m 22s
Nelder-Mead	0.20	0.125	0.55	22	1h 6m 58s

3rd attempt: Including thermal mass

The 3rd attempt was another effort to minimize the CV(RMSE) of the model. In this trial, the thermal masses are included with both A_1 and D_1 . X_{0-a} , X_{0-c} , and X_{0-d} denote the inner pane of the opaque envelopes, inner slabs, and inner walls. The additional parameters were chosen to analyze if the conduction and heat accumulation would impact the discrepancy between the calculated and measured Q. The bounds can be seen in equation 21.

$$CV_{RMSE}(A_1, D_1) = \begin{cases} A_1, & 0.2 \leq A_1 \leq 1 \\ D_1, & 0.125 \leq D_1 \leq 1 \\ X_{0-a}, & (0.5 \times X_{0-a}) \leq X_{0-a} \leq (2 \times X_{0-a}) \\ X_{0-c}, & (0.5 \times X_{0-c}) \leq X_{0-c} \leq (2 \times X_{0-c}) \\ X_{0-d}, & (0.5 \times X_{0-d}) \leq X_{0-d} \leq (2 \times X_{0-d}) \end{cases} \quad (21)$$

Table 4.4 3rd attempt: Comparison of performance for each algorithm.

	A_1	D_1	X_{0-a}	X_{0-c}	X_{0-d}	CV_{RMSE}	Iteration at Convergence
Base	0.39	0.24	3.916	11.002	3.916	0.55	-
L-BFGS-B	0.389	0.239	3.916	11.002	3.916	0.55	12
SLSQP	0.39	0.24	3.916	11.002	3.916	0.55	6
Nelder-Mead	0.2	0.125	7.832	18.335	7.832	0.55	198

Table 4.4 and appendix L show that some parameters were altered but the CV(RMSE) remained constant. From this point, the doubt of the algorithms and the problem formulation increased. Therefore, it is essential to manually check whether the resulting CV(RMSE) corresponds with the parameter values.

4th attempt: Monte-Carlo sampling

This last attempt was conducted to manually check if the alteration of the parameters would impact the CV(RMSE). A Monte-Carlo approach was employed to perform that evaluation. One hundred iterations were conducted by combining random samples from the values within each parameter's bounds. The result showed that the distributions of CV(RMSE) were very low, as seen in Fig 4.3. The result indicates that the algorithms worked fine, and the problem formulation was also not the problem. It is safe to say that the RC-model has limitations for summer calculation.

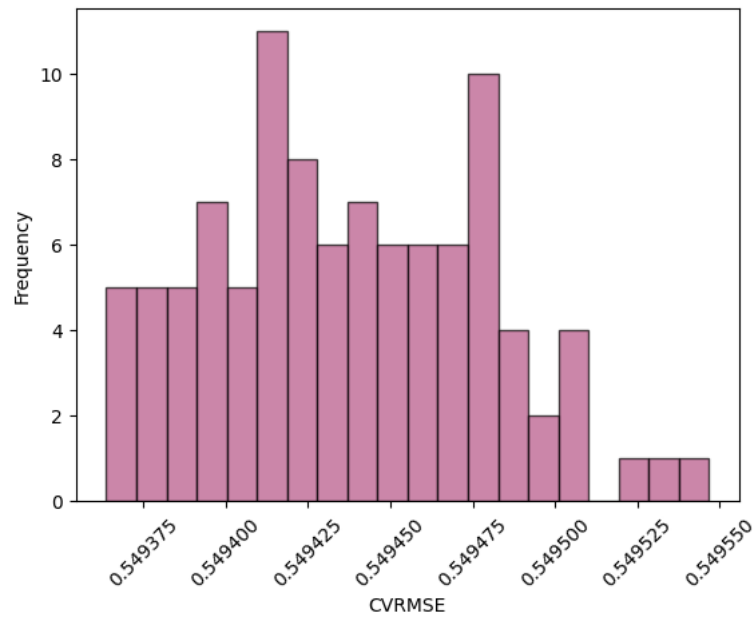


Fig 4.3 4th attempt: Monte-Carlo simulation to check the CV(RMSE) distributions.

Conclusions

Even before the calibration, the simpler model is close enough to the measured data. Some discrepancies exist because the input data and parameters are simplified and will not reflect the actual conditions. It is evidence that using lumped parameters in model V.3 also works, although it is very sensitive to the time-series inputs. However, there is still a large discrepancy between the summer calculation and the historical data; the calibration was meant to minimize that. The calibrations using derivative-based algorithms were not successful since the algorithms tended to look for local solutions and stopped when the objective did not change. The non-derivative algorithm was also unsuccessful, but it could explore more possibilities regarding the estimations. However, the Monte-Carlo simulation showed that the summer calculation could not be calibrated using parameter estimation. It is possible that the model is not sufficient because it considers the whole building as a single zone, while in reality, there are warmer areas due to the different amounts of sun radiation. These warmer areas might have different cooling behaviors, such as more mechanical or natural ventilation. The natural ventilation, which can be operated manually, is unpredictable and cannot be captured by this model as it only considers mechanical ventilation and infiltration. This ventilation problem does not occur in the winter calculation as the ventilation is only mechanical and more controlled. However, due to graduation time limitations, the RC-model cannot be calibrated further. Thus, the half-validated RC-model V.3 will be used to predict and analyze energy demand, for the MPC and retrofitting strategies, because of the validation scores and calculation time that outperforms other models. The parameters were kept the same as the initial guess as they had already been validated in winter.

4.2 Model Predictive Control

Some literature includes comfort aspects as objectives. However, in this study, comfort is solely utilized as constraints, allowing for violations if not satisfied. The results of both control algorithms for one loop can be observed in Fig 4.4. The loop only includes design days at peak winter and summer in January 2022 and June 2022. The simulation's length is chosen due to the graduation time limitation and the fact that the simulation took 4-hours just to loop through one design day. Details of the design days can be found in the appendix M.

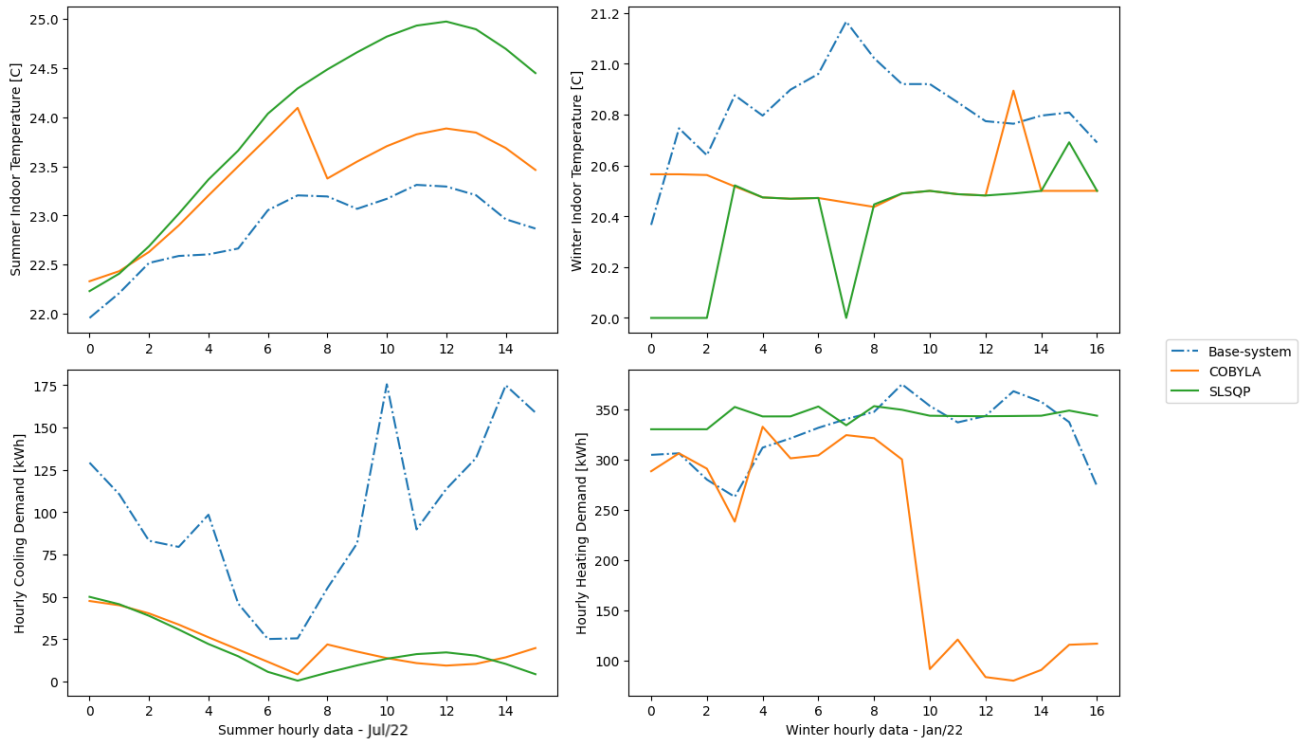


Fig 4.4 Energy demand and indoor temperature from both MPC algorithms.

The results from both MPC algorithms differ from the base-system because the base-system does not consider the comfort range and only uses non-adaptive setpoints. Both algorithms tend to start at around the same energy demand as the base-system in winter. COBYLA in winter experiences an extreme drop and reaches the lowest energy demand compared to the other two systems at the end of the timestep. When compared to SLSQP, COBYLA exhibits more aggressive and unstable energy changes. However, the indoor temperature produced by COBYLA tends to be more stable. For SLSQP, the indoor temperature fluctuates more than COBYLA, but these fluctuations are insignificant as they do not exceed 1°C. Additionally, SLSQP is the most stable of the two systems for energy demand.

Results for the summer design day are smoother compared to winter. Temperatures from SLSQP tend to be higher than COBYLA, which is the opposite of what was observed in winter. The starting energy demand in summer from both MPC systems is almost the same, with SLSQP slightly higher, similar to winter. With a lower initial

demand, about half that of the base-system, the energy demand from both MPC systems gradually decreases and allows the temperature to rise, unlike the trends of the base-system. Towards the end of the timestep, COBYLA exhibits a small spike, making it slightly more aggressive compared to SLSQP, but the energy values are not significantly different.

Overall, the base-system in summer has higher energy demand with an indoor temperature range of only 1 degree Celsius. However, both MPC systems strive to push the comfort and energy limits, resulting in lower energy demand with higher temperatures, but still within the acceptable threshold. For winter, the concept is similar to the energy produced by MPC, which is lower with lower temperatures compared to the base-system. SLSQP tends to push the indoor temperature as high and low as the comfort constraints allow, while COBYLA seems to prioritize pushing the energy limits.

Conclusions

MPC works as an optimizer. If there are no constraints, the algorithm will try to push the objective value to 0. However, with constraints, there are limitations. It is clear that MPC can reduce the energy demand and get as low as possible while also pushing the comfort boundaries. Optimization is about a trade-off or win-win solution, therefore it makes sense that MPC will sacrifice a bit of the comfort to get to a lower demand.

As seen in the energy results, COBYLA is more aggressive because of its handling nature. It works by approximating the feasible region with linear constraints and tends to aggressively move toward the feasible region's boundaries to find the optimal solution (Powell, 1994). SLSQP, on the other hand, tends to be smoother as it uses the exact gradient and quadratic programming for the estimation (Kraft, 1988).

Chapter 5

Retrofitting the Existing Glass

5.1 Identifying the Impact on Window's Resistance and Absorptance Value

Table 5.1 Thermal properties of the systems (1).

System	R strategy [m ² K/W]	R total [m ² K/W]	U -value total [W/m ² K]	SHGC total
Base	-	0.606	1.65	0.4
1	-	0.82	1.22	0.29
2	0.23	0.84	1.19	0.28
3	0.007	0.613	1.63	0.328
4	0.0004	0.6064	1.65	0.236

Table 5.2 Thermal properties of the systems (2).

System	Retrofitting Strategies			Window Glass		
	Thickness [m]	U -value [W/m ² K]	Absorption	R [m ² K/W]	U -value [W/m ² K]	SHGC
5	0.003	0.01	0.44	0.606	1.65	0.4
6	0.003	0.3	0.36	0.606	1.65	0.4
7	0.001	0.54	0.3	0.606	1.65	0.4
8	0.127	0.35	0.1	0.606	1.65	0.4

The incorporation of films directly influences the window's thermal properties, specifically its heat resistance R and solar heat gain coefficient (SHGC), owing to their attachment to the glass surface. Solar control films exhibit a negligible impact on the window's heat resistance R , resulting in a slight reduction compared to the base glass. However, the impacts of the SHGC depend on the positioning of the solar control film. When applied to the inside pane, the SHGC reduction is the lowest among all films, at approximately 18%. Conversely, when positioned on the outside pane, the same film demonstrates the lowest SHGC value, exhibiting a reduction of 41% compared to the original glass. Additionally, Low-E and insulating films yield notable reductions in both thermal transmission and heat gain. Specifically, thermal transmission is reduced by 26% and 28% for Low-E and insulating films, respectively.

On the other hand, the addition of curtains does not immediately enhance the properties of the glass itself. The solar absorption values vary depending on factors such as thickness, density, opening size, and fabric material of the curtain. System 5 exhibits the highest absorption due to its darker color, while transparent bubble wrap possesses the lowest absorption coefficient with its thin plastic surface. These material properties also impact the resistance of the curtains. Thermal curtains (system 5) exhibit the highest resistance, followed by system 6, which is also a thermal curtain but with a wider opening. The bubble wrap, containing air as insulation, follows, with the sheer curtain having the lowest resistance.

However, it is essential to note that the thermal network, presented in Fig 5.1, indicates that the curtain itself is not the sole contributor to increased resistance. While the fabric

blocks solar radiation from entering the indoor space, the heat transfer between indoor and outdoor spaces is also reduced due to the air between the glass and the curtain, thereby adding further resistance.

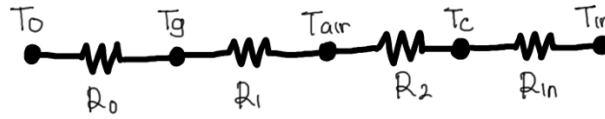


Fig 5.1 Thermal network of window, air in between, and curtain.

5.2 Impact on heat loss/gain for winter and summer through window

Merely examining thermal resistance is insufficient for assessing the behavior of a system, especially when the system involves glazing. This is because glazing also experiences heat gains from solar radiation. While in winter, it might suffice to assess only thermal transmission since solar radiation is less intense, the increased solar radiation significantly influences system performance in summer. Therefore, to evaluate how each system performs under different peak conditions (summer and winter), it is necessary to calculate total heat gain and heat loss through the system, including both transmission and solar gain.

Heat gains are calculated in June 2022, representing peak summer conditions, while heat loss is assessed in January 2022, representing peak winter conditions. Heat gain/loss in both seasons takes into account both $Q_{transmission}$ and Q_{solar} utilizing U_{value} and A_1 as the reciprocal of the system's resistance and absorptance coefficient, respectively (equations 22 and 23). In addition to those equations, the calculations also consider convection with the outdoor and indoor air with α_{conv-o} and α_{conv-i} at 25 and 2.5, respectively. These simulations are steady-state analyses during peak design hours, as detailed in Table 5.3, which are collected from building sensors and weather station data.

$$Q_{trans} = U_{system} \times A_{system} \times (T_{outdoor} - T_{indoor}) \quad (22)$$

$$Q_{sol} = A_{1,system} \times A_{system} \times q_{sol} \quad (23)$$

Table 5.3 Peak summer and winter design hours.

Season	$T_{outdoor}$ [C]	Solar irradiation	T_{indoor} [C]
Summer	37.7	634	23.053
Winter	0.5	25	20.52

As illustrated in Fig 5.2, in summer, without considering ventilation, the heat gain from thermal transmission for all films is nearly identical to that of the base glass, with minimal variations. In terms of reduction, films only marginally reduce thermal

transmission by approximately 0.07% to 1.73%. This suggests that while the films alter the resistance of the window, their impact is negligible. Similarly, in winter, systems with films exhibit similar thermal transmission reduction, with the insulating film having the lowest transmission due to its lower U-value compared to other films.

Conversely, solar gains exhibit more significant variation as the solar heat gain coefficients (SHGCs) fluctuate more. Similar to summer, the trends in solar absorption during winter varied the same. The lowest solar absorption is observed for the film with the lowest absorption coefficient, namely the solar control film placed on the outside pane. All films demonstrate a more substantial reduction in solar gain, ranging from around 18% to 41% for both summer and winter. This evidence shows that films can effectively reduce solar gain especially during summer months.

Conversely, Curtains experience higher total heat gain during summer peak due to additional solar gain on the fabrics, not only at the glass. The highest recorded gain is observed in system number 5, as it exhibits the highest solar absorption among the curtains. Bubble wrap, on the other hand, registers the lowest solar gain due to its transparent surface color. When compared to the use of films, curtains actually increase solar gain by approximately 29% to 180% when compared to the solar gain on the original glass, for both summer and winter conditions. However, regarding thermal transmission, curtains can reduce heat gain by approximately 40% to 55% during peak summer periods and heat loss by around 14%.

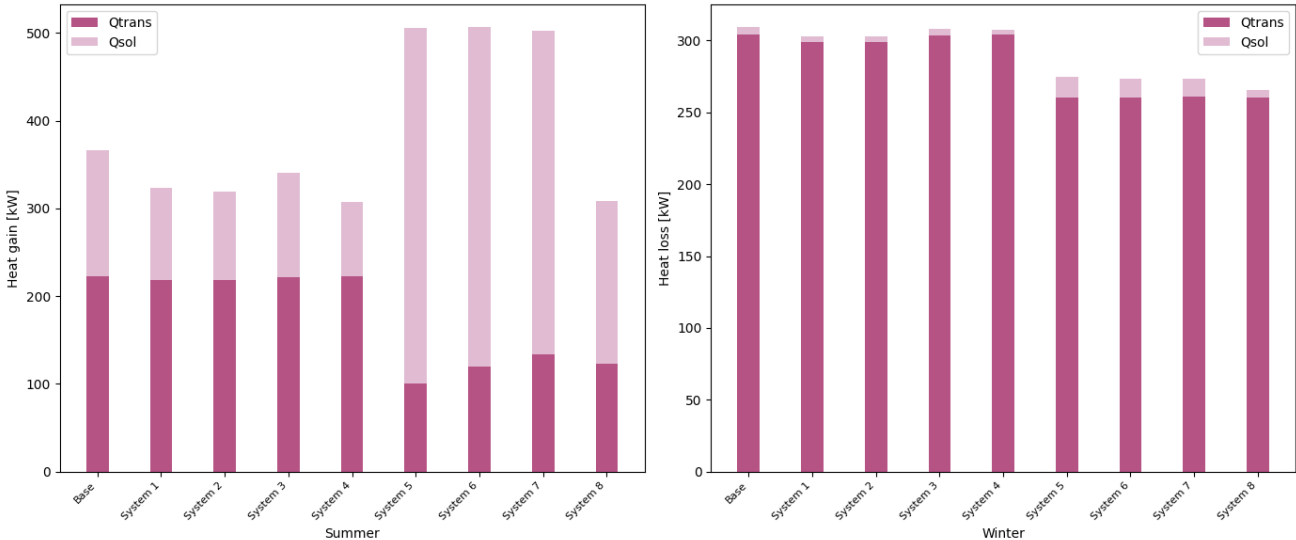


Fig 5.2 Q transmission and Q solar in summer and winter.

Comparing total gain for summer and winter is not as straightforward as adding $Q_{transmission}$ and Q_{solar} . For summer, the calculation simply involves adding $Q_{transmission}$ and Q_{solar} because both are positive (both of them represent gains). However, for winter, $Q_{transmission}$ is negative because the outside temperature is lower than the indoor temperature, resulting in heat loss, while Q_{solar} remains positive (heat

gain). Therefore, the total heat loss for winter is calculated as $Q_{solar} - Q_{transmission}$.

The results, which can be seen in Fig 5.3, show that curtains result in more total heat gain during summer compared to films because they absorb more solar radiation. Meanwhile, for winter, curtains perform better due to the additional solar absorption and acting as a barrier to heat transfer from the inside to the outside of the building. Films, on the other hand, perform almost the same as the base window during winter due to the minimal difference in resistance between the base glass and the filmed glass. However, their performance varies during summer, considering that films impact the solar heat gain coefficient.

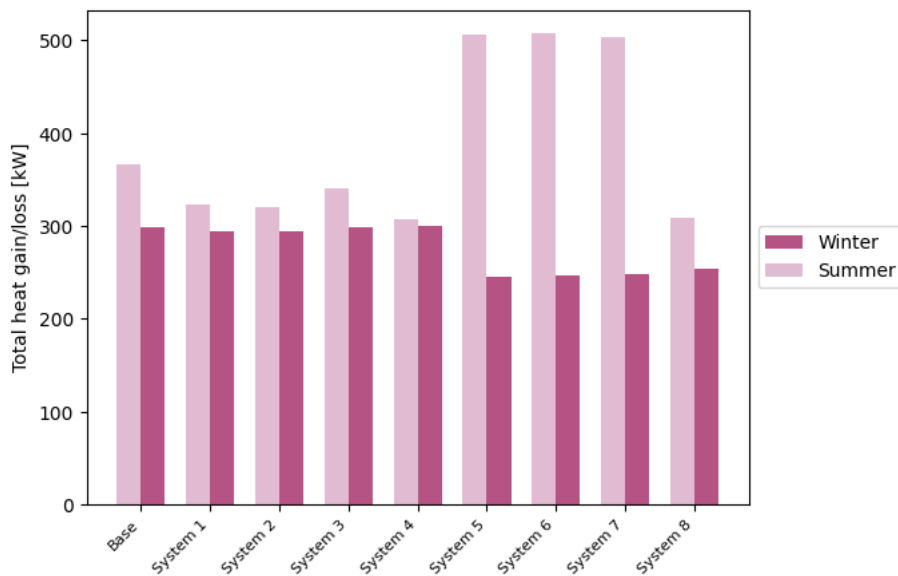


Fig 5.3 Comparison of total heat gain/loss through window in summer and winter.

Overall, for summer, the solar control film placed on the outside (system 4) performs the best at 307.67 kWh, which is only slightly different from bubble wrap (system 8) at 308.92 kWh. The system with the worst performance is the thermal curtain with 0% openness (system 5) at 505.78%. Meanwhile, for winter, the curtain system 5 actually performs the best at 246.11%, and the worst is system 4 at 300.58 kWh. From this, it can be observed that systems with low total heat gain will have high total heat loss, so systems that work well for summer may perform poorly for winter, and vice versa.

However, this initial calculation only considers thermal transfer and solar gain on the glass with films and curtains. In reality, there are more thermal transfers such as solar radiation absorbed by other surfaces, radiation between materials, advection involving ventilation, and internal heat gain from occupants. Therefore, further analysis is required for a more comprehensive understanding of thermal transfer. The thermal balance of the entire building is what constitutes the energy demand, which will be discussed in the next section.

5.3 Impact on energy demand and comfort in building

Calculating the energy demand and comfort requires the whole building calculation. This sub-section explores the impacts of each retrofitting system on both base-system and MPC in summer and winter. From the last sub-section, it is clear that some system performs better only in one of the seasons. However, it is also essential to check with the whole building.

Energy Demand

Base-system

The simulation is conducted using the validated RC-model V.3. For systems with films, the calculation matrix used is the same as the matrix used for baseline simulations. However, for systems with curtains, there is an addition to the calculation matrix, namely the presence of air between the curtains and glazing, as well as the curtains themselves. This simulation is run for the design months, namely January 2022 and July 2022, representing peak winter and summer. The results displayed in Table 5.4 represent the total energy demand for each design month.

Table 5.4 Total cooling and heating load [kWh] for peak months.

Season	Total cooling and heating load [kWh]								
	Base	1	2	3	4	5	6	7	8
Summer	64,620.49	64,589.56	64,586.73	64,641.19	64,656.46	50,931.45	60,857.74	68,688.25	48,146.61
Winter	226,173.85	225,850.08	225,826.94	226,166.92	226,186.77	168,866.71	180,485.15	211,142.93	137,911.12

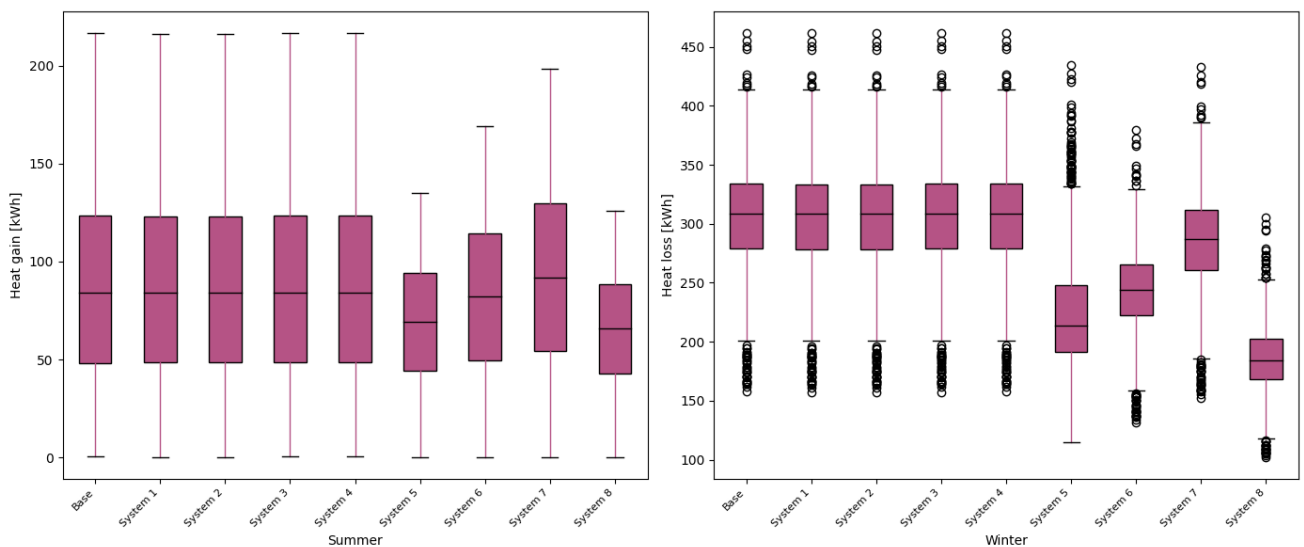


Fig 5.4 Cooling-load and heating-load comparison in existing control [kWh].

From the results, it can be observed that various types of films do not significantly impact the energy demand, both in summer and winter. Meanwhile, curtains perform better than films in both months. This is contrary to the initial calculations conducted earlier. The superior performance of curtains is attributed to their role as transmission and solar gain blockers for indoor air and other materials within the building. The performance of curtains varies depending on the type of material used. The larger the opening of the curtains, the greater the total heat gain/loss. System 5, with the tiniest opening, works better for both summer and winter compared to other fabric curtains. Bubble wrap outperforms system 5 because it acts as insulation due to its air pockets.

If sorted from the best performing for summer: system 8, 5, 6, 2, 1, base, 3, 4, 7. From this sequence, it can be seen that systems 3, 4, and 7 perform worse than the baseline, so they will not be considered for the next step. The reductions achieved using the remaining systems are 0.255%, 0.212%, 0.058%, 0.00052%, and 0.00048%, respectively. Systems 8 and 5 outperform the other systems regarding energy demand reduction, thus this study chooses these two systems for further analysis using the MPC system for the summer season. Additionally, the boxplot in Fig 5.4 indicates that both systems have a narrower quartile range compared to other systems. This suggests stability in energy demand at each timestep and peak, with peaks not significantly higher compared to other systems.

For winter, the performance sequence is system 8, 5, 6, 7, 2, 1, 3, base, 4. System 4 performs worse than the baseline again, so it will not be considered for the next step. The reductions achieved for the remaining systems are 0.39%, 0.253%, 0.202%, 0.066%, 0.0015%, 0.0014%, and 3.06E-05%, respectively. Once again, the reduction values of systems 8 and 5 outperform the other systems. System 6 also has a relatively high reduction value compared to the next-ranked systems. However, because the lowest heating demand of system 6 is still higher than that of system 5, only systems 8 and 5 will be further analyzed.

MPC-system

From the discussion on the base-system, it can be seen that systems 5 and 8, which are thermal curtain and bubble wrap, respectively, outperformed other systems in both summer and winter seasons. Therefore, it was decided that these two systems would be further analyzed using the MPC system. This simulation uses the validated RC-model V.3 and the MPC system with the previously outlined two algorithms. The matrix used was the one that included the curtain.

Similar to the previous MPC chapter, this simulation uses design days and only includes the opening hours of the Pulse building, from 8 AM to 12 midnight. This design day represents the peak winter and peak summer in 2022. Details for this design day can be found in appendix M.

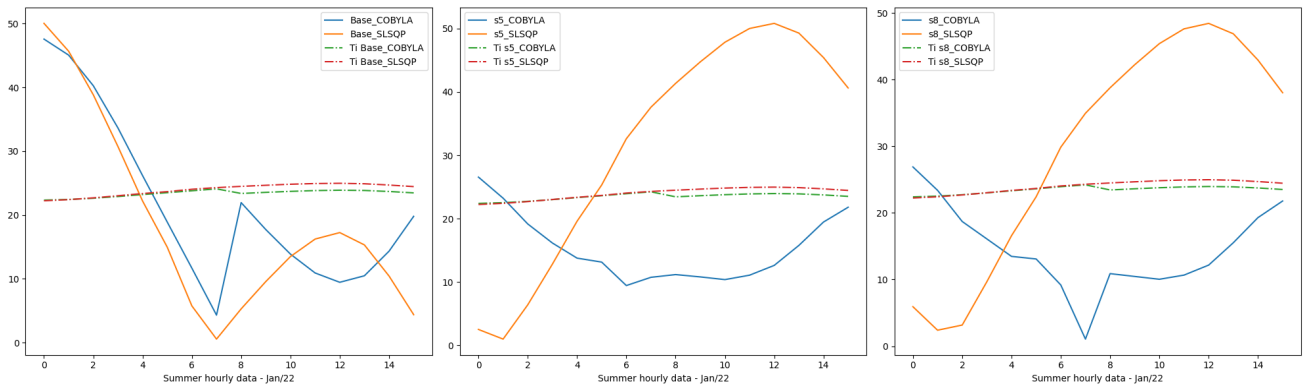


Fig 5.5 Summer energy demand with MPC.

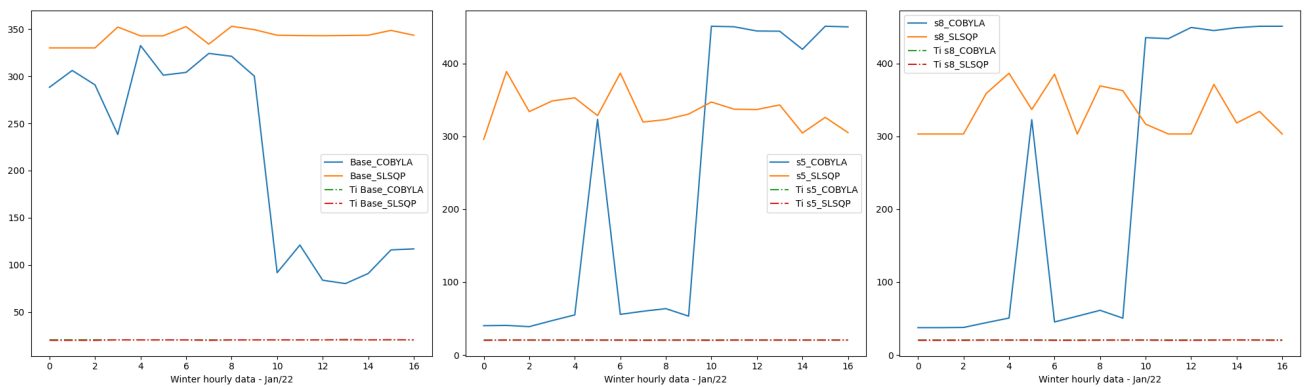


Fig 5.6 Winter energy demand with MPC.

Compared to the MPC for the base scenarios in summer, the two systems (systems 5 and 8) exhibit lower energy demand starts using both MPC algorithms. SLSQP, as experienced in the base scenario, tends to experience an increase at the end of the timestep. When observed, indoor temperatures for all systems indicate that COBYLA results in lower temperatures compared to using SLSQP. The temperature differences between all summer alternatives are almost negligible as seen in Fig 5.5. Compared with the base MPC, using COBYLA, the total energy reduction obtained is 29% and 33% for systems 5 and 8, respectively. Meanwhile, using SLSQP, the total energy demand generated is even greater than the base-MPC, with 69% and 58% increases for both systems, respectively.

As seen in Fig 5.6, COBYLA in all systems starts at a lower energy amount than SLSQP for winter. Unlike the base MPC, COBYLA in systems with curtains shows a tendency to increase its energy demand towards the end of the timestep with spikes near the beginning. Similar to the base MPC, COBYLA is more aggressive than SLSQP. As for SLSQP at systems 5 and 8, their performances are more stable than the base MPC with some fluctuation, yet still more stable compared to COBYLA, which exhibits significant increases and drops. Compared to the base MPC, the use of SLSQP in systems 5 and 8 actually increases by 2% and 2.8%, respectively. Meanwhile, with the use of COBYLA, the increases are larger, reaching 4.8% and 3.9%, respectively.

Base-system vs MPC-system

To examine the overall energy performance of all alternatives, the entire difference in total energy demand (compared to the baseline) on the design day can be viewed in Table 5.5. The detailed values for each alternative can be seen in appendix N. Alternatives ending with "C" indicate the use of MPC-COBYLA, while those ending with "S" indicate the use of MPC-SLSQP. If there is no suffix, it means the base-system was used.

Table 5.5 Energy demand reduction comparison for each alternative.

Seasons	Cooling and heating load reduction compared to baseline							
	B_C	B_S	sys5	sys5_C	sys5_S	sys8	sys8_C	sys8_S
Summer	82.87%	82.46%	49.72%	82.87%	82.49%	55.17%	82.87%	82.49%
Winter	39.57%	7.73%	15.95%	42.15%	9.08%	37.37%	42.71%	14.92%

For summer, the most effective alternatives are *B_C*, *sys5_C*, and *sys8_C*, which all have the same reduction value. They are followed by *sys5_S* and *sys8_S*, then *B_S*. The two lowest-performing alternatives are *sys8* and *sys5*. This indicates that for all systems, COBYLA is superior in reducing energy demand for winter. Following COBYLA, systems that use SLSQP perform slightly less efficiently. Meanwhile, system 5 and system 8 using the base-system can only reduce about 50% from the baseline.

For winter, the highest reduction is achieved by COBYLA systems, such as *B_C*, *sys5_C*, and *sys8_C*. In contrast to winter, systems using SLSQP have the lowest reduction values, reaching a maximum of only 15%. Finally, curtains (systems 5 and 8) are able to reduce energy demand by up to 37% from the baseline, better than SLSQP.

Comfort on Base-system and MPC-system

In addition to examining the energy demand from the baseline and the two strategies in the base-system and MPC-system, this study also considers thermal comfort, measured using the ATG metric. Surface temperature and indoor temperature information of the building are obtained from the calculations of the base-system and MPC-system. With this information, the mean radiant temperature and indoor operative temperature can be calculated. The results of each plotting of operative temperature at the day's running mean outdoor temperature according to the ATG graph can be found in Fig 5.7. The gray dashed lines on the graph represent the lower and upper bounds of the indoor operative temperature for the running mean outdoor temperature on the design days (22.8 degrees for design days in summer and 4.2 degrees for design days in winter).

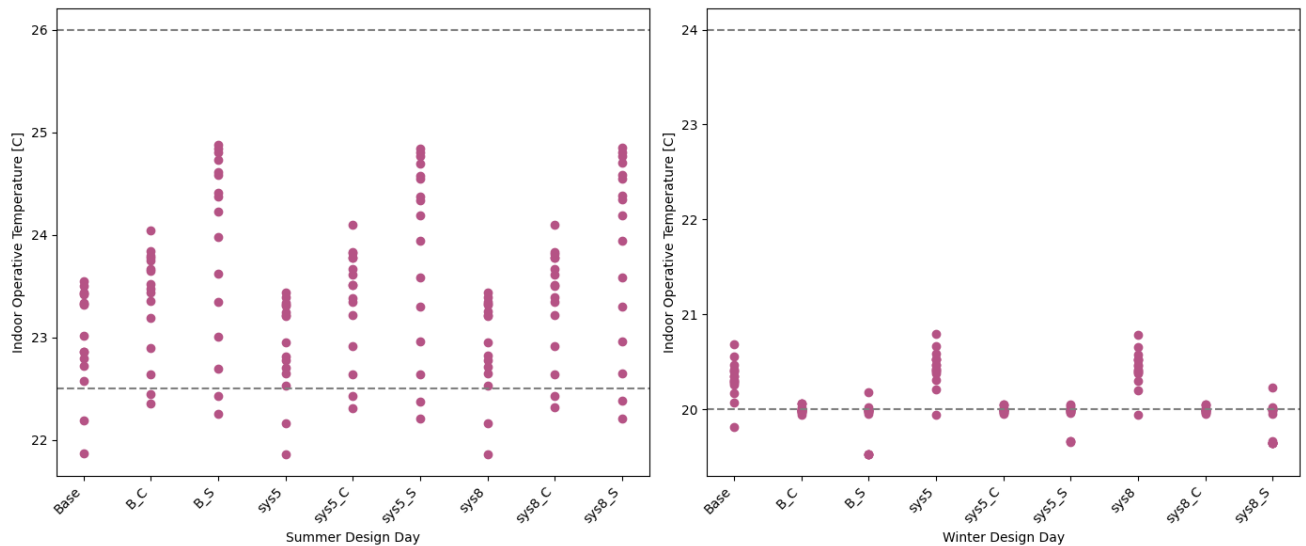


Fig 5.7 Comfort measures for every alternative.

On the summer design day, all alternatives have two hours of discomfort. These two hours occur during the night when the outdoor temperature drops, which naturally leads to a drop in the mean radiant temperature (MRT) as well. However, in alternatives using MPC, both in the base and curtain systems, the indoor operative temperature during discomfort tends to be higher. Systems with SLSQP have the highest peaks, followed by systems with COBYLA, and the lowest peaks are observed in systems with existing control. Looking at the temperature distribution, systems without MPC perform better in maintaining the stability of the operative temperature. Systems with curtains have a narrower temperature range compared to the baseline, as the MRT in both of these systems does not consider the glass temperature. For summer, occupants prefer cooler room temperatures (but not below the lower limit), so it can be said that systems with curtains perform better in terms of comfort, even though it is only a slight difference from the baseline.

As for the winter design day, occupants prefer warmer room temperatures, so systems with curtains perform better. Systems with MPC tend to push the comfort boundary, resulting in indoor operative temperatures approaching the lower bound. Systems with SLSQP have higher discomfort compared to the baseline, while COBYLA has the lowest discomfort. In terms of the stability of indoor operative temperature, COBYLA performs the best but is very close to the lower bound.

Conclusions

Considering the results of energy demand reduction and comfort metrics, for summer, systems with MPC indeed can significantly reduce energy demand, but this also means that indoor air temperatures are higher, leading to increased temperatures of indoor materials. For the 2022 case, the indoor operative temperatures have not yet exceeded the upper comfort limit, but there is a potential for overheating if a heatwave occurs.

Systems with curtains are better at maintaining stability and preventing indoor operative temperatures from getting too hot, but their energy reduction is not as impressive as MPC. This also applies to winter, where systems with curtains can better "warm up" the room while still experiencing discomfort hours. SLSQP performs less effectively at reducing energy demand than it does in summer. Due to this anomaly (different from summer), systems with curtains seem like a win-win solution because they provide the best comfort and can reduce energy consumption more effectively, especially system 8.

Chapter 6

Fixing Pulse

6.1 Smart System vs Retrofitting

From the previous chapter, it can be deduced that smart systems and retrofitting strategies can reduce energy demand and improve thermal comfort. However, smart systems tend to focus more on saving energy rather than enhancing comfort, whereas retrofitting strategies perform the opposite function. The decision between converting the current system into a smart one or implementing retrofitting should begin with assessing the building's conditions.

The Pulse Building is a net-zero building, meaning that it generates sufficient energy from renewable sources to meet its demand. Consequently, energy saving is not a critical concern for this building. If a smart system is to be chosen, its purpose should shift from reducing energy demand to maximizing the effectiveness and efficiency of the existing renewable energy sources. Therefore, the preferred option is to proceed with retrofitting.

6.2 Materiality

Several criteria are considered when selecting materials. These criteria relate to the material's tactility, lifecycle, and performance concerning daylight and visual aspects. Fig 6.1 visualizes the criteria that are used. Each criterion has two considerations, for example, for color, the options are warm and cold. Fig 6.2 illustrates the criteria, options, and the chosen options.

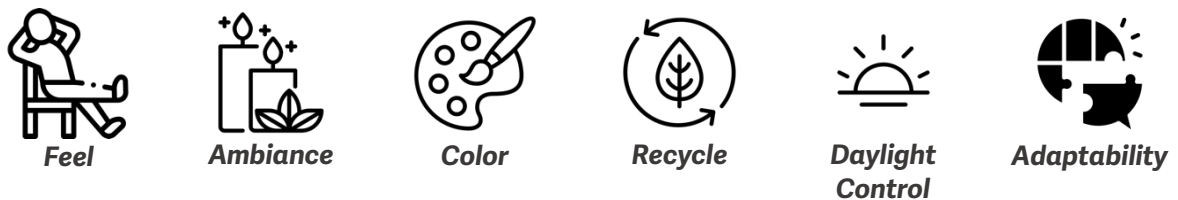


Fig 6.1 Criteria for material selection.

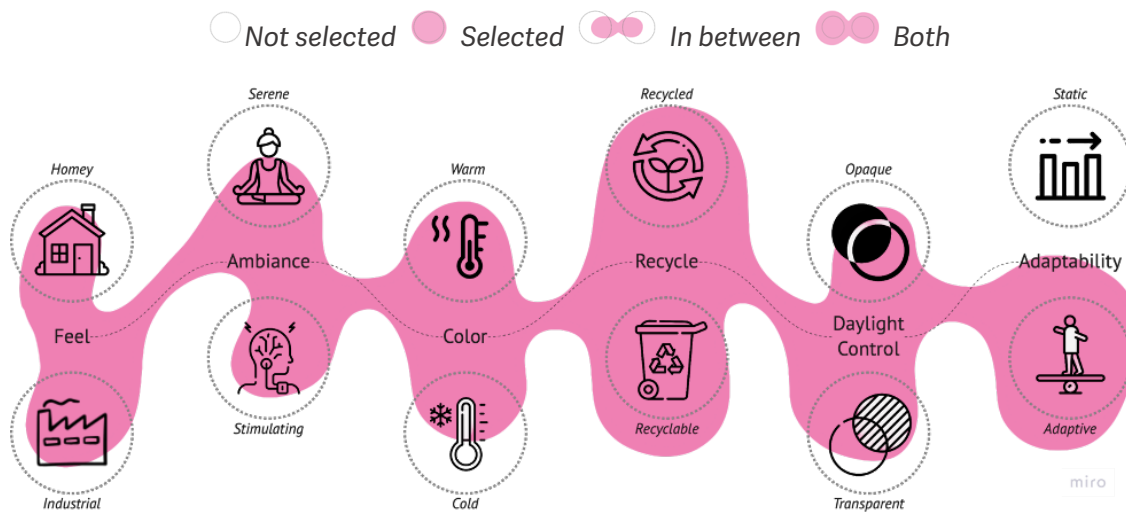


Fig 6.2 The criteria, options, and the chosen options for material selection.

Feel

Students choose to study and complete assignments on campus because they feel demotivated and too relaxed at home. However, a very formal space can also make them feel pressured. Therefore, the curtain design will incorporate both homey and industrial concepts. These two concepts are expected to help occupants feel comfortable as if they were at home while maintaining a level of formality to avoid becoming too relaxed. These concepts can be represented through the texture and pattern of the materials. Homey is associated with warmth and comfort, characterized by soft-textured natural fabrics. In contrast, the industrial concept conveys an edgy and modern feel, resembling materials like metal or plastic. Fig 6.3 illustrates the mood boards selected to combine these two concepts.

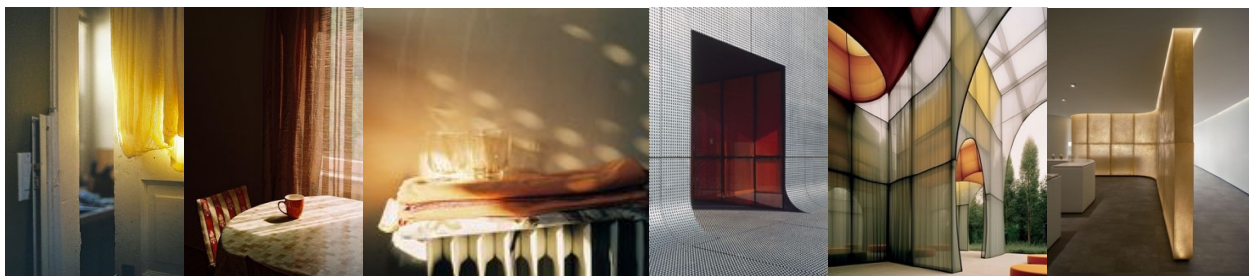


Fig 6.3 Feel concept mood boards. Source: Pinterest.com.

Ambiance

TU Delft's campus hosts various studies that require different learning environments. For instance, students from the Faculty of Architecture and the Built Environment need a study space that can stimulate creative thoughts, while students from the Faculty of Civil Engineering require a quiet and focused atmosphere. Considering that the Pulse Building is a shared space, its ambiance will combine serene and stimulating concepts to accommodate the needs of its occupants. The serene concept is characterized by neutral colors, calmness, and peace, whereas the stimulating concept is associated with varied textures, patterns, and focal points. Fig 6.4 presents the mood boards for both ambiance concepts.

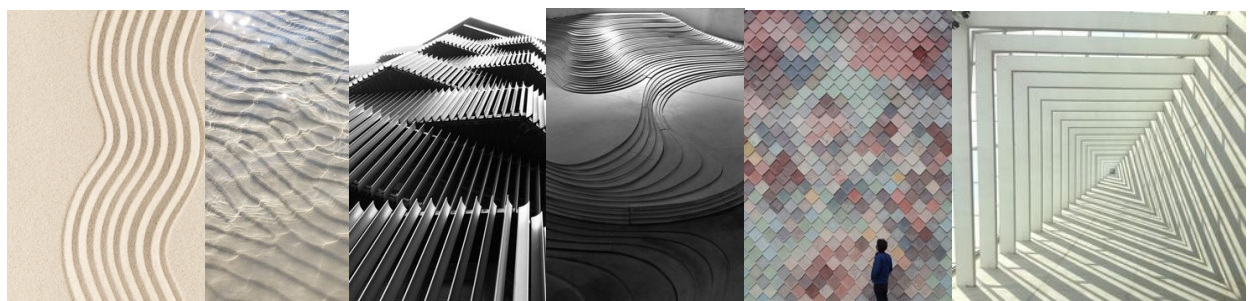


Fig 6.4 Ambiance concept mood boards. Source: Pinterest.com.

Color

The selection of colors, in addition to influencing solar absorption, can also affect a space's perceived warmth or coolness. The curtain design for the Pulse Building will use cool color tones during summer and warm color tones during winter. These choices will help ensure that the Pulse Building remains comfortable and conducive to various study needs throughout the year. Light shades will be chosen to support the previously explained ambiance concepts. Fig 6.5 illustrates the color mood board.

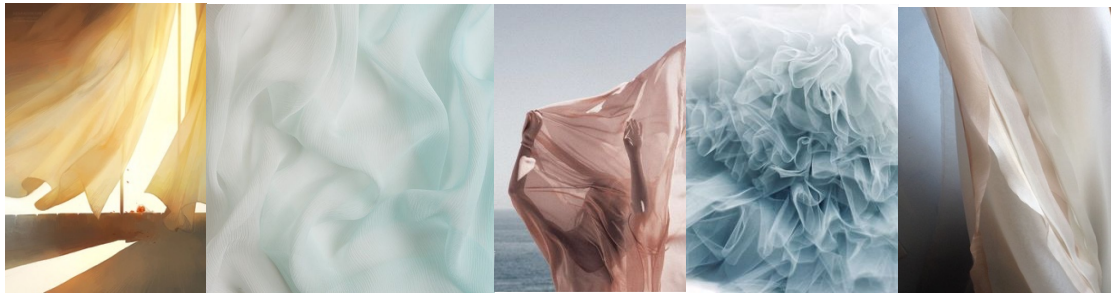


Fig 6.5 Color concept mood board. Source: Pinterest.com.

Recycle

To reduce the waste generated in the TU Delft environment daily, the curtain material will utilize recycled materials from this waste. Additionally, the curtain material can be recycled again, making it more beneficial and reducing further waste. Some potential waste materials that can be used for the curtains include vegetables or fruit peels, paper, plastic, and cans. This approach not only promotes sustainability by repurposing waste but also aligns with the principles of a circular economy, ensuring that materials are kept in use for as long as possible and minimizing environmental impact.

Daylight control

In addition to serving as a temperature barrier between indoor air and window glass, curtains are also used to control the amount of daylight entering a space. Excessive light and focused light can cause glare, while a lack of sunlight can be detrimental to the well-being of occupants. Therefore, the concept for the curtain material is to allow sunlight to enter gently (translucent). Using translucent materials, the curtains will balance the need for natural light with the need to reduce glare, creating a comfortable and healthy indoor environment. Fig 6.6 is a mood board for translucent materials.

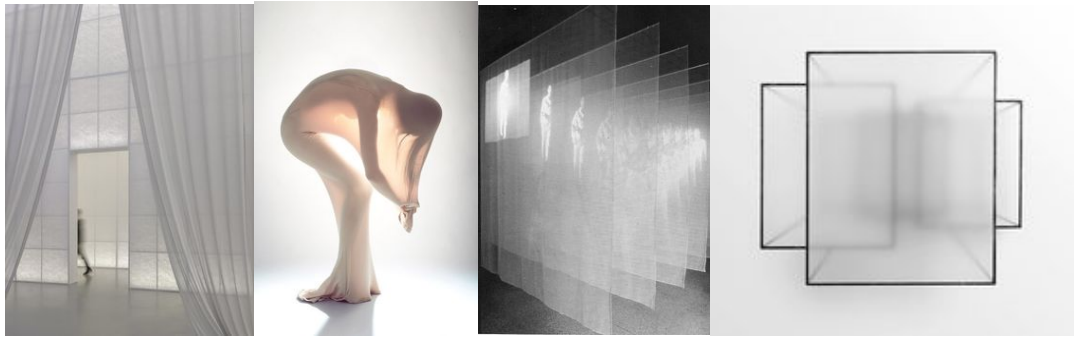


Fig 6.6 Translucent concept mood boards. Source: Pinterest.com.

Adaptability

Sunlight changes throughout the day, making static solutions either overkill or subject to trade-offs. Therefore, these curtains are designed to adapt to changing environmental conditions. Using adaptive concept, the curtains will provide a more effective and comfortable solution for managing daylight and temperature in the Pulse Building.

The Chosen Material: Recycled Paper

The chosen material is recycled paper, considering all the concepts, mood boards, and personal preferences. This material can create a homey feel with its texture and an industrial vibe with proper cutting and arrangement. The color of this paper can be made to follow the concepts of translucency, serenity, warmth, and coolness. The irregular pattern produced by recycled paper supports the stimulating concept. The drawback of this material is its lack of adaptability. This material's color, shape, and texture will remain constant regardless of the amount of sunlight or temperature differences. Therefore, the adaptive concept will be realized mechanically. Figure 9 illustrates the recycled paper.

In addition to the aforementioned reasons related to the concept, this material is chosen for its potential beyond design and performance aspects. Given that producing this material is not overly complex, there is potential to open a recycling paper workshop at X-TU Delft. This initiative can enhance environmental awareness and foster a sense of belonging among students, as the curtains used would be their own creations. Additionally, the colors and additional patterns on the recycled paper can be customized to match the events happening at TU Delft.

6.3 Position

The curtains made from recycled paper will be placed inside the glass façade of the Pulse Building. This glass façade area includes the *horeca* area on the ground floor, study areas from the first floor to the top floor, and classrooms.

One of the key concepts for the curtain design is daylight control and adaptability. As illustrated in Figure 6, sunlight changes throughout the seasons and times of day. During winter, daylight is needed because winter days tend to be dark, which is essential for warming the room. Therefore, the design of the curtain is based on the summer months, as sunlight in summer is harsher, although the curtain can still be used in winter to add resistance. These months are June, July, August, and September. According to (Moan et al., 2014), strong sunlight occurs between 10 am and 4 pm. During these months and times, the angles of sunlight incidence are 30, 40, 50, and 60 degrees, as shown in Fig 6.7.

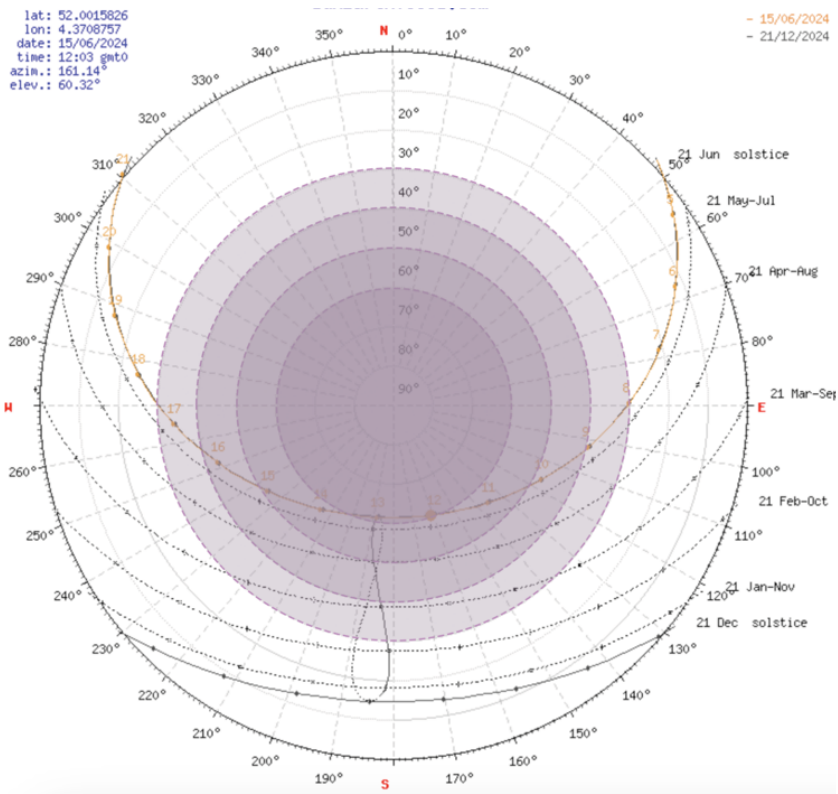


Fig 6.7 The angles of sunlight incidence between 10 am and 4 pm in summer.

The adaptability concept of these curtains is designed to address these angles, as shown in Figure 8. Instead of using a single curtain with adjustable height, this design employs three curtains of different heights. These curtains will automatically lower with the utilization of heat sensors and sun tracking sensors installed on the glass façade, as well as illuminance sensors placed on the desk surfaces near the glass façade. The heat sensor will detect the temperature of the glass façade, the sun tracking sensor will detect the angle of sunlight incidence, and the illuminance sensor will measure the amount of illuminance. The illuminance threshold for educational buildings is 300-400 lux (IESNA, 2000). These three sensors are integrated with the model that is used for MPC, a responsive control system, and simple actuators such as Arduino and servo motors.

The first curtain will descend when the heat sensor detects the glass temperature and checks the comfort using the building model, or when the amount of illuminance on the desks exceeds the threshold, regardless of the angle of sunlight incidence. This curtain will fully cover the window and serve as a heat transfer resistance between the window glass and indoor air. Its translucent color will allow sunlight to enter the room. The second curtain will descend based on two conditions: when the illuminance sensor detects that the amount of illuminance on the desks exceeds the threshold after the first curtain has descended, and when the angle of sunlight incidence is between 30-40 degrees. The third curtain will descend based on two conditions: when the illuminance sensor detects that the amount of illuminance on the desks exceeds the threshold after the second curtain has descended, and when the angle of sunlight incidence is between 50-60 degrees. Fig 6.8 illustrates the three curtains and their respective conditions.

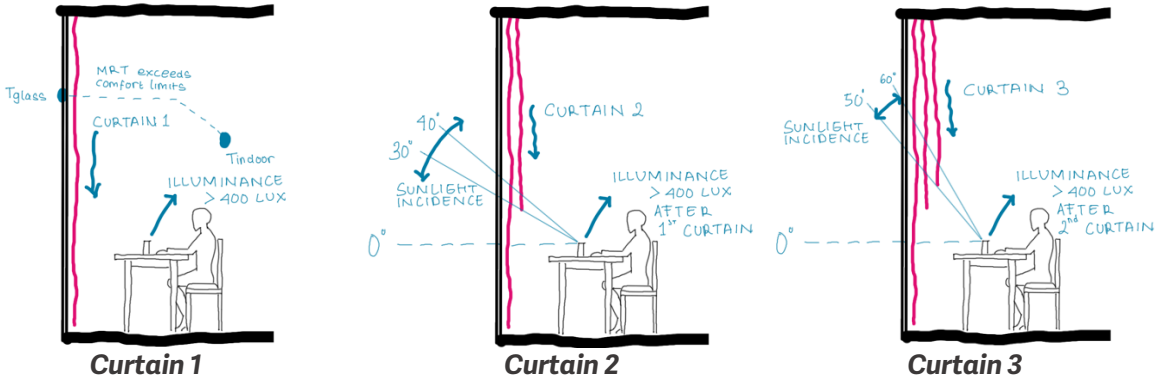


Fig 6.8 Curtains and their conditions.

6.4 Composition

One of the concepts of these curtains is about ambiance. A focused and distraction-free environment is created through the uniform vertical lines of the curtain modules. These vertical lines also signify that the building is a formal building. To stimulate creative thinking, the curtains feature horizontal lines arranged in a wave-like pattern to introduce an organic and flexible feel. To emphasize the vertical lines and add an artistic view to refresh the occupants' minds at night, the curtains are equipped with strip lights at the bottom weights. Fig 6.9 illustrates the design process of the curtain compositions, Fig 6.10 illustrates the different curtain layers, Fig 6.11 illustrates the different appearances in summer and winter, and Fig 6.12 illustrates the curtains from the exterior at night.

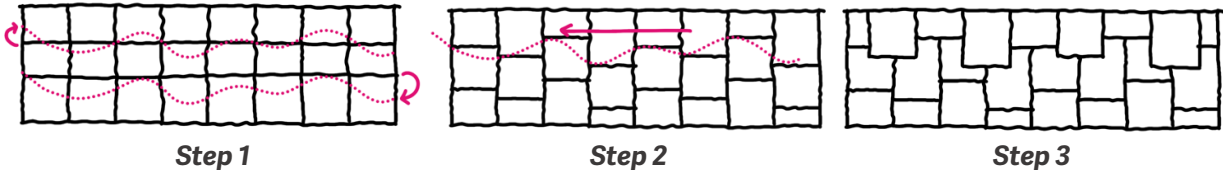


Fig 6.9 Schematic design process.

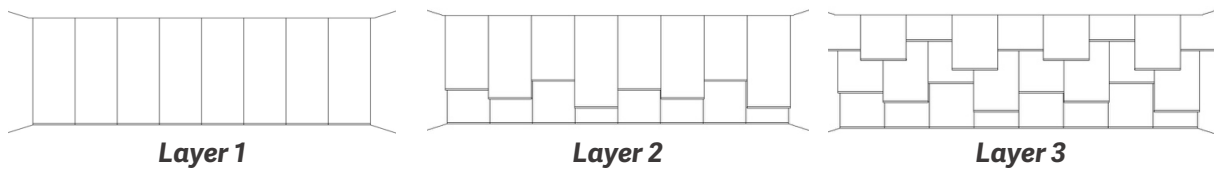


Fig 6.10 Different curtain layers.



Summer



Winter

Fig 6.11 Interior looks in summer and winter.

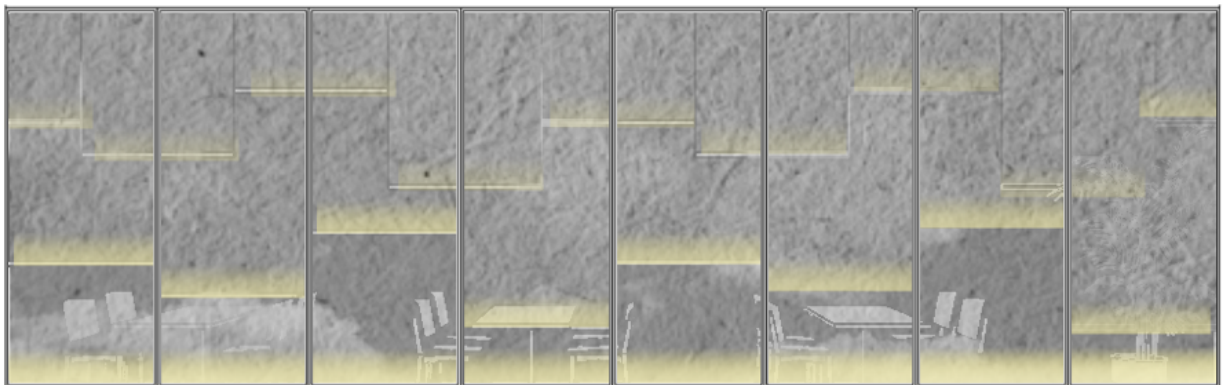


Fig 6.12 Exterior looks at night.

Chapter 7

Conclusions

Conclusions

The study kicks off with a basic question: Which approach yields better energy savings and comfort in glass facade buildings—upgrading the HVAC system or retrofitting? To contribute to answering that main question, this study experiments with a smart BMS, specifically MPC, along with several retrofitting strategies, including glass films and curtains.

From the experiments with three types of models, the results indicate that using a simpler model (V.3) is actually more accurate, although there are still discrepancies with measured data. This model also reduces computing time, allowing forecasts to work faster because the input and output time ranges to and from the actual building are only 1 hour. Of the two optimization algorithms tested, COBYLA proved to be more aggressive, while SLSQP was more stable, but both algorithms succeeded in reducing energy demand. A drawback of MPC in this study is that it can violate one or more constraints if disturbances are too high (convergence fails). This will likely occur if the formulated problem is too strict (especially regarding comfort) and the algorithm used does not allow for constraint priority.

Retrofitting strategies cannot be assessed solely based on transmission and solar gain because their behavior can differ with the presence of ventilation and occupants. Compared to MPC, curtains may not reduce energy demand as dramatically as smart systems, but they can provide indoor thermal comfort. For summer, solar blockage is indeed crucial for thermal comfort. This is evident in how curtains can lower and stabilize the operative temperature. The same concept applies in winter, where curtains act as a barrier to block heat from escaping indoors. MPC is more suitable if the building is not predominantly glass and reducing energy demand is the main concern. However, if comfort is equally important, adding building features to block solar radiation in summer and prevent heat loss in winter would be better.

As for the Pulse Building, energy demand is not a primary concern since it is already net-zero. Therefore, improvements can be made by retrofitting using recycled paper curtains with translucent colors to support sustainability. These curtains are not only used to improve thermal comfort but also to control sunlight. Additionally, the curtains are designed to support the well-being of the occupants.

Limitations

The case study utilized in this thesis involves a building with a glass façade containing multiple rooms, but only one thermal zone is considered. The single zone, combined with the lumped parameters, impacts the accuracy of the model especially for the summer calculation. Several aspects of this building can be controlled, but in this thesis, MPC only regulates the setpoints. The energy sources and delivery systems are not considered. The occupant schedule used is a representation of the academic

calendar and may not fully reflect real-world conditions. Only three optimization algorithms are analyzed for parameter optimization, and two optimization algorithms are used for control optimization. The investigated retrofitting strategies focus solely on indoor strategies, comprising films and curtains.

Future Research Directions

The study focuses on operational energy without considering its sources and delivery methods for heating and cooling. It would be interesting to differentiate between renewable and non-renewable energy sources and compare various heating and cooling methods like floor heating and climate ceilings. Exploring adaptive retrofitting strategies such as PCM, photochromic, and electrochromic materials would be intriguing if the modeling can accommodate them. The retrofitting strategies presented in this study also need validation for other building typologies. The optimization performance of this study still needs validation using other algorithms. Parameter estimation and smart building systems can employ various algorithms, including genetic algorithms, so future research could include them and compare them with retrofitting strategies. Faster algorithms also need to be explored. More variables to be included in MPC, such as CO₂, wind pressure, and rain, are also desired to gain more accuracy. It would also be nice to validate the MPC loop using a real disturbance and assess the whole summer/winter month or even a year. Robustness and embodied energy should also be checked to make the selected alternatives more concrete. These considerations are aimed at achieving bigger sustainability goals for future research.

Reflections

This thesis combines building physics, design informatics, and retrofitting strategies for glass buildings to understand how smart systems and retrofitting strategies affect energy consumption and indoor thermal comfort in glass façade buildings. So far, the outcomes provide a good depiction of how both factors behave, but they also raise new "what if" questions that have the potential to deepen or broaden this research.

Research and Design

A broader inquiry drives the main question of this study: how can existing buildings be improved to achieve energy efficiency and occupant comfort? This research aims to influence the direction of building improvements, whether by transitioning to smart systems or implementing retrofitting measures. Furthermore, this study can provide guidance for future building projects, aiding in the selection of suitable strategies to optimize energy efficiency and enhance occupant comfort.

Ethics

In the context of energy reduction, it is clear that the more savings, the better. However, when comfort comes into play and optimization is necessary, the question "how comfortable is uncomfortable?" always arises, especially when the optimizer treats both objectives equally and tends to push towards the very end of comfort thresholds. The building chosen as the case study is a public and international campus facility, which means its users could come from various backgrounds and experience different climates, possibly even more extreme than those in the Netherlands. The question is, do the comfort boundaries used still apply to all users, including those from diverse environments? Additionally, internal heat gain calculations often overlook differences in heat production between individuals, such as between men and women or young and older people, which can also affect their thermal comfort levels. How can smart systems and retrofitting strategies address these issues? While humans can adapt, can buildings also be part of the solution? This would require sophisticated sensor and algorithm use, which ultimately can enhance control system performance. However, excessive building monitoring can also make occupants feel monitored or intimidated. All these considerations need to be taken into account when developing holistic and integrated solutions.

Societal Impact

The chosen case study for this research is a university building where occupants, mostly students, often spend extended hours, sometimes even into the night. Improving comfort in this building can significantly enhance the productivity of its occupants. Apart from boosting the performance of the university's students, a more comfortable building environment can bridge the gap between those with higher education and those who simply need a place to work briefly. This inclusivity is further enhanced as the building is open to the public and designed to make everyone feel welcome by

the thermal comfort. The indirect improvement in building performance, leading to enhanced student productivity, also fosters a brighter future, as these students will become the next generation of leaders. Imagine if they could not concentrate due to uncomfortable temperatures while studying in this building and then had to apply their knowledge later in life.

Despite Pulse being an energy-efficient building, the aim of this study is to further reduce energy demand by implementing smart systems and retrofitting. This directly contributes to lowering primary energy consumption and can benefit the planet. Pulse is already a sustainable building equipped with numerous active sensors, so transitioning to an MPC system, which can enhance the sustainability, does not require extensive effort as it would in low performance buildings. The chosen retrofitting strategies are also selected to minimize additional structures or special treatments to keep costs down, enabling a shorter payback time and allowing more focus on enhancing building performance rather than just recovering investments. Many aspects are simplified in this study, so direct adoption into the building may not be straightforward. Future research should further validate how MPC and retrofitting strategies behave in real-world scenarios, where various disturbances occur, and human intervention is possible.

References

- Afroz, Z., Shafiullah, G., Urmee, T., & Higgins, G. (2018). Modeling techniques used in building HVAC control systems: A review. *Renewable and Sustainable Energy Reviews*, 83, 64-84. <https://doi.org/10.1016/j.rser.2017.10.044>
- Alnuaimi, A., Natarajan, S., & Kershaw, T. (2022). The comfort and energy impact of overcooled buildings in warm climates. *Energy and Buildings*, 260, 111938. <https://doi.org/10.1016/j.enbuild.2022.111938>
- ANSI/ASHRAE Standard. (2017). *Thermal Environmental Conditions for Human Occupancy*.
- Ardente, F., Beccali, M., Cellura, M., & Mistretta, M. (2011). Energy and environmental benefits in public buildings as a result of retrofit actions. *Renewable and Sustainable Energy Reviews*, 15(1), 460-470. <https://doi.org/10.1016/j.rser.2010.09.022>
- ASHRAE. (1992). Thermal Environmental Conditions for Human Occupancy. *ANSI/ASHRAE*, 55, 5. <https://cir.nii.ac.jp/crid/1574231875437564672>
- Balali, Y., Chong, A., Busch, A., & O'Keefe, S. (2023). Energy modelling and control of building heating and cooling systems with data-driven and hybrid models—A review. *Renewable and Sustainable Energy Reviews*, 183, 113496. <https://doi.org/10.1016/j.rser.2023.113496>
- Barbosa, R., Barták, M., L.M Hensen, J., & G.L.C Loomans, M. (2015, December 7). *Ventilative Cooling Control Strategies Applied to Passive House in*

Order to Avoid Indoor Overheating. 2015 Building Simulation Conference. <https://doi.org/10.26868/25222708.2015.2637>

Beltrán, M., Schibille, N., Brock, F., Gratuze, B., Vallcorba, O., & Pradell, T. (2020).

Modernist enamels: Composition, microstructure and stability. *Journal of the European Ceramic Society*, 40(4), 1753-1766.

<https://doi.org/10.1016/j.jeurceramsoc.2019.11.038>

Bendapudi, S. (2002). *A Review of Literature on Dynamic Models of Vapor Compression Equipment*.

Berthou, T., Stabat, P., Salvazet, R., & Marchio, D. (2014). Development and

validation of a gray box model to predict thermal behavior of occupied office buildings. *Energy and Buildings*, 74, 91-100.

<https://doi.org/10.1016/j.enbuild.2014.01.038>

BIS. (2013). *Bubble Wrap Window Insulation*.

<https://www.builditsolar.com/Projects/Conservation/bubblewrap.htm>

Boerstra, A. C., van Hoof, J., & van Weele, A. M. (2015). A new hybrid thermal comfort guideline for the Netherlands: Background and development.

Architectural Science Review, 58(1), 24-34.

<https://doi.org/10.1080/00038628.2014.971702>

Boodi, A., Beddiar, K., Amirat, Y., & Benbouzid, M. (2022). Building Thermal-

Network Models: A Comparative Analysis, Recommendations, and Perspectives. *Energies*, 15(4), 1328.

<https://doi.org/10.3390/en15041328>

Chaiyapinunt, S., & Khamporn, N. (2021). Effect of solar radiation on human thermal comfort in a tropical climate. *Indoor and Built Environment*, 30(3), 391-410. <https://doi.org/10.1177/1420326X19891761>

Chaiyapinunt, S., Phueakphongsuriya, B., Mongkornsaksit, K., & Khomporn, N. (2005). Performance rating of glass windows and glass windows with films in aspect of thermal comfort and heat transmission. *Energy and Buildings*, 37(7), 725-738. <https://doi.org/10.1016/j.enbuild.2004.10.008>

Charles, K. E. (2003). Fanger's thermal comfort and draught models. *National Research Council of Canada*. <https://doi.org/10.4224/20378865>

Chvatal, K. M. S., & Corvacho, H. (2009). The impact of increasing the building envelope insulation upon the risk of overheating in summer and an increased energy consumption. *Journal of Building Performance Simulation*, 2(4), 267-282. <https://doi.org/10.1080/19401490903095865>

Chwieduk, D. (2014). Chapter 6–Energy Balance of a Building with Regard to Solar Radiation Exposure. In D. Chwieduk (Ed.), *Solar Energy in Buildings* (pp. 173-288). Academic Press. <https://doi.org/10.1016/B978-0-12-410514-0.00006-2>

Delcroix, B., Ny, J. L., Bernier, M., Azam, M., Qu, B., & Venne, J.-S. (2021). Autoregressive neural networks with exogenous variables for indoor temperature prediction in buildings. *Building Simulation*, 14(1), 165-178.

<https://doi.org/10.1007/s12273-019-0597-2>

Djongyang, N., Tchinda, R., & Njomo, D. (2010). Thermal comfort: A review paper. *Renewable and Sustainable Energy Reviews*, 14(9), 2626–2640.

<https://doi.org/10.1016/j.rser.2010.07.040>

Doherty, T., & Arens, E. A. (1988). *Evaluation of the physiological bases of thermal comfort models*. <https://escholarship.org/uc/item/6pq3r5pr>

Drgoňa, J., Arroyo, J., Cupeiro Figueroa, I., Blum, D., Arendt, K., Kim, D., Ollé, E.

P., Oravec, J., Wetter, M., Vrabie, D. L., & Helsen, L. (2020). All you need to know about model predictive control for buildings. *Annual Reviews in Control*, 50, 190–232. <https://doi.org/10.1016/j.arcontrol.2020.09.001>

EPD. (2022). *Commercial Insulating Window Film | 3M Energy Efficiency Solutions*. EPD. <https://epdwindowfilm.com/3m-commercial-insulating-window-film/>

EPD. (2024). *Do you install window film on the inside or outside of a building?*

EPD. <https://epdwindowfilm.com/faq/do-you-install-window-film-on-the-inside-or-outside-of-a-building/>

Faílde, D., Viqueira, J. D., Mussa Juane, M., & Gómez, A. (2023). Using

Differential Evolution to avoid local minima in Variational Quantum Algorithms. *Scientific Reports*, 13(1), 16230.

<https://doi.org/10.1038/s41598-023-43404-3>

Farag, A. A., Ali, Z. M., Zaki, A. M., H.Rizk, F., Eid, M. M., & EL-Kenawy, E.-S. M.

- (2024). Exploring Optimization Algorithms: A Review of Methods and Applications. *Full Length Article, Volume 7*(Issue 2), 08-17.
<https://doi.org/10.54216/JAIM.070201>
- Gupta, R., & Gregg, M. (2018). Assessing energy use and overheating risk in net zero energy dwellings in UK. *Energy and Buildings, 158*, 897-905.
<https://doi.org/10.1016/j.enbuild.2017.10.061>
- Hensen, J. J. (1991). *On the thermal interaction of building structure and heating and ventilating system.* <https://doi.org/10.6100/IR353263>
- Hensen, J. L. M., & Centnerova, L. (2001). *Energy simulation of traditional vs. Adaptive thermal comfort for two moderate climate regions.*
- Hollenbeck, C., & Naumann, I. (2023, December 5). *Key contributions of MEP in the life cycle assessment of buildings.* LINEAR.
<https://www.linear.eu/en/blog/key-contributions-of-mep-in-the-life-cycle-assessment-of-buildings/>
- Holst, J., Holst, U., Madsen, H., & Melgaard, H. (1992). Validation of Grey Box Models. *IFAC Proceedings Volumes, 25*(14), 53-60.
[https://doi.org/10.1016/S1474-6670\(17\)50712-0](https://doi.org/10.1016/S1474-6670(17)50712-0)
- Humphreys, M. (1976). Field studies of thermal comfort compared and applied. *Applied Ergonomics, 7*(4), 230. [https://doi.org/10.1016/0003-6870\(76\)90104-6](https://doi.org/10.1016/0003-6870(76)90104-6)
- Humphreys, M. (1978). Outdoor temperatures and comfort indoors. *Batiment*

International, Building Research and Practice, 6(2), 92-92.
<https://doi.org/10.1080/09613217808550656>

Humphreys, M. A., Rijal, H. B., & Nicol, J. F. (2013). Updating the adaptive relation between climate and comfort indoors; new insights and an extended database. *Building and Environment*, 63, 40-55.
<https://doi.org/10.1016/j.buildenv.2013.01.024>

IEA. (2023, October 24). *World Energy Outlook 2023*. IEA.
<https://www.iea.org/reports/world-energy-outlook-2023>

Jansen, S. C. (2020). *Overview of theory on Energy Systems for Buildings and Neighbourhoods*.
<https://brightspace.tudelft.nl/d2l/le/content/502866/viewContent/3097198/View>

Joseph, J. (2018). Chapter 45–Facility Design and Process Utilities. In G. Jagschies, E. Lindskog, K. Łącki, & P. Galliher (Eds.), *Biopharmaceutical Processing* (pp. 933-986). Elsevier. <https://doi.org/10.1016/B978-0-08-100623-8.00045-1>

Kazanci, O. B., & Olesen, B. W. (2016). Beyond nearly zero-energy buildings: Experimental investigation of the thermal indoor environment and energy performance of a single-family house designed for plus-energy targets. *Science and Technology for the Built Environment*, 22(7), 1024-1038. <https://doi.org/10.1080/23744731.2016.1208001>

- Khamporn, N., & Chaiyapinunt, S. (2014). An Investigation on the Human Thermal Comfort from a Glass Window. *Engineering Journal*, 18(1), 25-44. <https://doi.org/10.4186/ej.2014.18.1.25>
- Kim, D., Lee, J., Do, S., Mago, P. J., Lee, K. H., & Cho, H. (2022). Energy Modeling and Model Predictive Control for HVAC in Buildings: A Review of Current Research Trends. *Energies*, 15(19), Article 19. <https://doi.org/10.3390/en15197231>
- Kontes, G. D., Giannakis, G. I., Horn, P., Steiger, S., & Rovas, D. V. (2017). Using Thermostats for Indoor Climate Control in Office Buildings: The Effect on Thermal Comfort. *Energies*, 10(9), Article 9. <https://doi.org/10.3390/en10091368>
- Kraft, D. (1988). *A Software Package for Sequential Quadratic Programming*.
- Kristensen, N. R., Madsen, H., & Jørgensen, S. B. (2004). Parameter estimation in stochastic grey-box models. *Automatica*, 40(2), 225-237. <https://doi.org/10.1016/j.automatica.2003.10.001>
- Kwok, A. G., & Rajkovich, N. B. (2010). Addressing climate change in comfort standards. *Building and Environment*, 45(1), 18-22. <https://doi.org/10.1016/j.buildenv.2009.02.005>
- Leitão, A. (2017). *Building performance evaluation: A dutch perspective in thermal comfort and energy consumption*. <https://www.semanticscholar.org/paper/Building-performance->

evaluation%3A-a-dutch-in-thermal-

Leit%C3%A3o/b6c025ddc16159a55e9b10959c602f61853fccac

Li, P., Qiao, H., Li, Y., Seem, J. E., Winkler, J., & Li, X. (2014). Recent advances in dynamic modeling of HVAC equipment. Part 1: Equipment modeling. *HVAC and R Research*, 20(1), 136-149. Scopus. <https://doi.org/10.1080/10789669.2013.836877>

Li, Y., O'Neill, Z., Zhang, L., Chen, J., Im, P., & DeGraw, J. (2021). Grey-box modeling and application for building energy simulations—A critical review. *Renewable and Sustainable Energy Reviews*, 146, 111174. <https://doi.org/10.1016/j.rser.2021.111174>

Lin, S., Wang, H., Zhang, X., Wang, D., Zu, D., Song, J., Liu, Z., Huang, Y., Huang, K., Tao, N., Li, Z., Bai, X., Li, B., Lei, M., Yu, Z., & Wu, H. (2019). Direct spray-coating of highly robust and transparent Ag nanowires for energy saving windows. *Nano Energy*, 62, 111-116. <https://doi.org/10.1016/j.nanoen.2019.04.071>

Lin, Z., & Deng, S. (2008). A study on the thermal comfort in sleeping environments in the subtropics-Developing a thermal comfort model for sleeping environments. *Building and Environment*, 43(1), 70-81. Scopus. <https://doi.org/10.1016/j.buildenv.2006.11.026>

Liu, Z., Zhang, X., Sun, Y., & Zhou, Y. (2023). Advanced controls on energy reliability, flexibility and occupant-centric control for smart and energy-

efficient buildings. *Energy and Buildings*, 297, 113436.
<https://doi.org/10.1016/j.enbuild.2023.113436>

Ljung, L. (2001). Black-box models from input-output measurements. *IMTC 2001. Proceedings of the 18th IEEE Instrumentation and Measurement Technology Conference. Rediscovering Measurement in the Age of Informatics (Cat. No.01CH 37188)*, 1, 138-146 vol.1.
<https://doi.org/10.1109/IMTC.2001.928802>

Lu, C., Li, S., & Lu, Z. (2022). Building energy prediction using artificial neural networks: A literature survey. *Energy and Buildings*, 262, 111718.
<https://doi.org/10.1016/j.enbuild.2021.111718>

Maciejowski, J. M., & Huzmezan, M. (1997). Predictive control. In J.-F. Magni, S. Bennani, & J. Terlouw (Eds.), *Robust Flight Control* (pp. 125-134). Springer. <https://doi.org/10.1007/BFb0113856>

Mărginean, C. (2019). *Optimized Facade Design towards Nearly Zero-Energy Residential High-Rises: Facade Design Assessment Criteria for Residential High-Rise Buildings in the NL*.
<https://repository.tudelft.nl/islandora/object/uuid%3Abfa000ca-ca95-4ebb-ae38-fa20365d4725>

Moan, J., Grigalavicius, M., Dahlback, A., Baturaite, Z., & Juzeniene, A. (2014). Ultraviolet-radiation and health: optimal time for sun exposure. *Advances in experimental medicine and biology*, 810, 423-428.

- Mousavi, S., Gheibi, M., Wacławek, S., Smith, N. R., Hajiaghahi-Keshteli, M., & Behzadian, K. (2023). Low-energy residential building optimisation for energy and comfort enhancement in semi-arid climate conditions. *Energy Conversion and Management*, 291, 117264. <https://doi.org/10.1016/j.enconman.2023.117264>
- Mtibaa, F., Nguyen, K.-K., Dermardiros, V., & Cheriet, M. (2021). *Online Genetic-Algorithm-based Model Predictive Control Framework for Multi-Zone Buildings*. <https://doi.org/10.23919/ECC54610.2021.9654929>
- NEN-EN. (2005). *NEN-EN-ISO 7730*. <https://www.nen.nl/nen-en-iso-7730-2005-en-104787>
- NEN-EN. (2007). *NEN-EN 15251*. <https://www.nen.nl/nen-en-15251-2007-en-114091>
- Nicol, F., Humphreys, M., & Roaf, S. (2012). *Adaptive Thermal Comfort: Principles and Practice*. Routledge. <https://doi.org/10.4324/9780203123010>
- Powell, M. J. D. (1994). A Direct Search Optimization Method That Models the Objective and Constraint Functions by Linear Interpolation. In S. Gomez & J.-P. Hennart (Eds.), *Advances in Optimization and Numerical Analysis* (pp. 51-67). Springer Netherlands. https://doi.org/10.1007/978-94-015-8330-5_4
- Rea, M. S., & Illuminating Engineering Society of North America. (2000). *The iesna lighting handbook: reference & application* (9th ed.). Illuminating

Engineering Society of North America.

Roaf, S., Nicol, F., Humphreys, M., Tuohy, P., & Boerstra, A. (2010). Twentieth century standards for thermal comfort: Promoting high energy buildings. *Architectural Science Review*, 53(1), 65-77.
<https://doi.org/10.3763/asre.2009.0111>

Ruiz, G. R., & Bandera, C. F. (2017). Validation of Calibrated Energy Models: Common Errors. *Energies*, 10(10), Article 10.
<https://doi.org/10.3390/en10101587>

Salcan-Reyes, G., Cajo, R., Aguirre, A., Espinoza, V., Plaza, D., & Martín, C. (2024, February 5). *Comparison of Control Strategies for Temperature Control of Buildings*. ASME 2023 International Mechanical Engineering Congress and Exposition. <https://doi.org/10.1115/IMECE2023-113573>

Sarihi, S., Mehdizadeh Saradj, F., & Faizi, M. (2021). A Critical Review of Façade Retrofit Measures for Minimizing Heating and Cooling Demand in Existing Buildings. *Sustainable Cities and Society*, 64, 102525.
<https://doi.org/10.1016/j.scs.2020.102525>

Shamsi, M. H., Ali, U., Mangina, E., & O'Donnell, J. (2021). Feature assessment frameworks to evaluate reduced-order grey-box building energy models. *Applied Energy*, 298, 117174.
<https://doi.org/10.1016/j.apenergy.2021.117174>

Simion, M., Socaciu, L., & Unguresan, P. (2016). Factors which Influence the

- Thermal Comfort Inside of Vehicles. *Energy Procedia*, 85, 472-480.
<https://doi.org/10.1016/j.egypro.2015.12.229>
- Solano, J. C., Caamaño-Martín, E., Olivieri, L., & Almeida-Galárraga, D. (2021). HVAC systems and thermal comfort in buildings climate control: An experimental case study. *Energy Reports*, 7, 269-277.
<https://doi.org/10.1016/j.egypro.2021.06.045>
- Sotex. (2024). *Tissuthèque* by Sotexpro.
<https://tissutheque.sotexpro.fr/en?isfabric=1&q=&act=0&acmin=0&acmax=1>
- SS. (2024). *Window Insulation Film Solar 80 C*.
<https://solarscreen.eu/en/products/solar-80-c>
- Stephens, B. (2019, November). *Building Energy Balances*. CAE 331/513 Building Science.
- Taufiqoh, A.F. (n.d.). *mood board thesis*. Pinterest. Retrieved June 17, 2023, from <https://pin.it/28hTPE3yc>
- Trier, F., & Ranke, U. (2007). The Glass Surface and Ways of Its Modification. *Glassman Europe 2007 Conference*.
- Van Den Bergh, S., Hart, R., Jelle, B. P., & Gustavsen, A. (2013). Window spacers and edge seals in insulating glass units: A state-of-the-art review and future perspectives. *Energy and Buildings*, 58, 263-280.
<https://doi.org/10.1016/j.enbuild.2012.10.006>

- Vaughn, M. (2014). 2013-2014: ASHRAE research report. *ASHRAE Journal*, 56(10), 89-99.
- Wahi, P. (2020). *Robustness of Building Envelope: Investigating robust design solutions for energy efficient educational buildings*.
<https://repository.tudelft.nl/islandora/object/uuid%3Af7743926-86dd-46be-9c08-6f00debb9a3c>
- Wang, D., Liu, Y., Wang, Y., Zhang, Q., & Liu, J. (2015). Theoretical and experimental research on the additional thermal resistance of a built-in curtain on a glazed window. *Energy and Buildings*, 88, 68-77.
<https://doi.org/10.1016/j.enbuild.2014.11.047>
- Wang, S., & Xu, X. (2006). Simplified building model for transient thermal performance estimation using GA-based parameter identification. *International Journal of Thermal Sciences*, 45(4), 419-432.
<https://doi.org/10.1016/j.ijthermalsci.2005.06.009>
- Wang, Z., Chen, Y., & Li, Y. (2019). Development of RC model for thermal dynamic analysis of buildings through model structure simplification. *Energy and Buildings*, 195, 51-67.
<https://doi.org/10.1016/j.enbuild.2019.04.042>
- Wright, J. L., Kotey, N. A., Barnaby, C. S., & Collins, M. R. (2009). *Solar Gain through Windows with Shading Devices: Simulation Versus Measurement*.
<https://uwspace.uwaterloo.ca/handle/10012/11596>

- Yin, R., Xu, P., & Shen, P. (2012). Case study: Energy savings from solar window film in two commercial buildings in Shanghai. *Energy and Buildings*, 45, 132-140. <https://doi.org/10.1016/j.enbuild.2011.10.062>
- Zhang, S., Chen, Y., Zhang, W., & Feng, R. (2021). A novel ensemble deep learning model with dynamic error correction and multi-objective ensemble pruning for time series forecasting. *Information Sciences*, 544, 427-445. <https://doi.org/10.1016/j.ins.2020.08.053>
- Zhang, X., Pipattanasomporn, M., Chen, T., & Rahman, S. (2020). An IoT-Based Thermal Model Learning Framework for Smart Buildings. *IEEE Internet of Things Journal*, 7(1), 518-527. <https://doi.org/10.1109/JIOT.2019.2951106>

Appendices

Appendix A

Pulse materials (source: Wahi, 2020; Pulse's manager; and Ector Hoogstad)

External Wall A (Facade Opaque elements)			External Wall B (Facade Opaque elements) and Skylights		
Category	Walls		Category	Walls	
Region	Netherlands		Region	Netherlands	
Definition Method : Layers			Definition Method : Layers		
Outer Layer			Outer Layer		
1	Material	Soda Lime Glass	1	Material	Metal-aluminium cladding
	Thk. (m)	.0060		Thk. (m)	.0010
2	Material	Air Gap	2	Material	Foam Phenol
	Thk. (m)	.01		Thk. (m)	.148
3	Material	Foam -Phenol	3	Material	Metal-aluminium cladding
	Thk. (m)	.250		Thk. (m)	.0010
4	Material	Plasterboard	4	Material	NCM-Unventilated Cavity
	Thk. (m)	.0125		Thk. (m)	.290
Inner Layer			5	Material	Plasterboard
Avg. Thickness (m)				Thk. (m)	.00125
R-Value (calculated)			6	Material	Mineral Fibre (wool)
R-Value (specified)				Thk. (m)	.100
			7	Material	Plasterboard
				Thk. (m)	.00125
Inner Layer			Inner Layer		
Thickness (m)			Thickness (m)		
R-Value (calculated)			R-Value (calculated)		
R-Value (specified)			R-Value (specified)		

Partition Wall C			Internal Floors		
Category	Partitions		Category	Slabs	
Region	Netherlands		Region	Netherlands	
Definition Method : Layers			Definition Method : Layers		
Outer Layer			Outer Layer		
1	Material	Plasterboard (CIBSE)	1	Material	Cement Screed
	Thk. (m)	.0250		Thk. (m)	.080
2	Material	Mineral Fibre (wool)	2	Material	Cast Concrete
	Thk. (m)	.100		Thk. (m)	.395
3	Material	Plasterboard (CIBSE)	Inner Layer		
	Thk. (m)	.0250	Thickness (m)		
Inner Layer			R-Value (calculated)		
Thickness (m)			R-Value (calculated)		
R-Value (calculated)			R-Value (calculated)		
R-Value (specified)			R-Value (calculated)		

Roof			External Glazing A (Facade Transparent elements)	
Category	Roof		Category	Double Glazing
Region	Netherlands		Region	Netherlands
Definition Method : Layers			Definition Method : Simple	
Outer Layer			G-Value	0.4
1	Material	Prefab (roofing)	Light Transmission	.7
	Thk. (m)	.075	U-Value	1.0 W/m ² K
2	Material	Foam Polyisocyanate	U-Value (specified)	≤ 1.65 W/m ² K
	Thk. (m)	.165	Solar Shading	
3	Material	Concrete Cast-Cellular	Internal Blinds	Shading Roll-Medium Translucent
	Thk. (m)	.320	Position	Internal
Inner Layer			Control	Solar (according to ISSO 32)
Avg. Thickness (m)			Setpoint : 250 W/m ²	
R-Value (calculated)			Operation	8:00 - 18:00
R-Value (calculated)				
R-Value (specified)				

	type	type omschrijving	materiaal	leverancier	type	kleur code	kleur	afmetingen	bijzonderheden	hoofdzakelijke toepassingsgebied
Gevel	GA1		gecoat metaal	ODG		ral 9006	glansgraad (50%)	conform tekening	onderregel, profielen, incl taatsdeuren. Scheerplaatige hoelen. Dikte profiel te bepalen a.h.v. definitieve berekening.	stijlen incl draaiende delen plangevel en achtergevel begane grond
		beglazing		Saint Gobain	climatop XN plug in		transparant	conform tekening en eisen	beglazing dient binnen het gewel: volledig gelijk uitstraling te hebben. Zvarte afstandhouder. Dooral- en lateraliteit conform eisen. Geen delijsten of oplingende bevestigingen. Bemontering in definitieve opbouw en ditte ter goedkeuring aan architect	
		kit en rubbers folie vervallen							zivarte kit en rubbers	
	GA2	Toumiquet	samengesteld	Boon Edam		ral 9006	glansgraad (50%)	conform tekening	Leidingen en bekabeling toumiquet en toegangscontrole installaties in weg zelfwerk opmerken. aansluitend gevelwand zetwerk gevel en MVA deur. Glazen toumiquet met interne roideuren. RVG plafond met LED spots. Geheel veevstandsklasse 2. Vrije doorloophoogte 2800mm. blanke beglazing	toumiquet begane grond
	GA3	beglazing		Saint Gobain	climatop XN plug in	RAL 7043	verkeersgrjs B	conform tekening en eisen	beglazing dient binnen het gewel: volledig gelijk uitstraling te hebben. Zvarte afstandhouder. zivarte kit. Dooral- en lateraliteit conform eisen. Geen delijsten of oplingende bevestigingen. Bemontering in definitieve opbouw en ditte ter goedkeuring aan architect	venster plangevel verdiepingen
	GA4	vliegevelstelsel zonder stjeen (NO en ZW gevel)	egels: stjeen, PAF rramen en aansluitend zetwerk			RAL 7025	lichtgrjs		by aansluiting binnenvanden en rondom PAF rramen veel stjeen voortzet. Inclusief taatsdeuren in kleur frame.	zjgevels
		beglazing		Saint Gobain	Climatop Cool-Lite ST			conform tekening en eisen	beglazing dient binnen het gewel: volledig gelijk uitstraling te hebben. grize afstandhouder. Dooral- en lateraliteit conform eisen. Geen delijsten of oplingende bevestigingen. Bemontering in definitieve opbouw en ditte ter goedkeuring aan architect	
			shadowbox		SGG Climaplus Coolite ST, PLUS IN Shadowbox	RAL 7043	RAL 7043	conform tekening en eisen	beglazing dient binnen het gewel: volledig gelijk uitstraling te hebben. grize afstandhouder ter goedkeuring architect. Dooral- en lateraliteit conform eisen. Geen delijsten of oplingende bevestigingen. Bemontering in definitieve opbouw en ditte ter goedkeuring aan architect	
		gewelhousters vervallen								
			kit en rubbers				grjs		ter goedkeuring aan architect	
		spanconstructie 3d amorf gevel	gecoat nis				n.tb			
	GB1	metaalveefsel				RV5 316			inclusief alle bevestigingsmiddelen, zie code	kopgevel, anterieurplafond
		hulpconstructie metaalveefsel (gevel en plafond)							Alle gevelconstructievoorzieningen t.b.v. gewelmech incl bevestigingsmiddelen en afstandhouders in n/a 316	gevel en bevestigingsmiddelen (incl spoorbus) plafond, incl onlopend kader sporing meech kopgevel verdieping
			rs verzinkt staal			rs verzinkt staal	rs verzinkt staal			heeklijnen spanvoorzieningen gevel en plafond
			gecoat staal			RAL 9007	glansgraad (50%)		incl bevestigingsmiddelen hulpconstructie	hulpconstructie boven plafond exterieur en interieur
	GB2	3D amorf gevel t.b.v. zonwering (directielevring)					translucent wit			
	GB3	profielplaat, sandwichplaat				RAL 7021	zivertgrjs		inclusief sandwichpanelen, alle bevestigingsmiddelen, laders, lamellen met achterconstructie en noodoverstorten. Plaatswijziging inclusief uitgelijnde bevestiging ter goedkeuring aan architect	achtergevel begane grond
	GC1	aluminium sandwichplaat				RAL 9007	glansgraad (50%)	conform tekening en eisen	inclusief kopse kanten en eindkap. Uitgelijnd op gebouwgrnd. Ongevelde hoogte	kopgevel verdiepingen
	GD	beglazing		Saint Gobain	Climatop Cool-Lite ST	RAL 7043	verkeersgrjs B	conform tekening en eisen	beglazing dient binnen het gewel: volledig gelijk uitstraling te hebben. Zvarte afstandhouder. Dooral- en lateraliteit conform eisen. Geen delijsten of oplingende bevestigingen. Bemontering in definitieve opbouw en ditte ter goedkeuring aan architect, zonder stjeen.	spiekraam zuidoostloep
			kit en rubbers				zivertgrjs		ter goedkeuring aan architect	

Appendix B

Academic calendar

TU Delft Calendar, Academic Year 2021-2022

1st SEMESTER

Week no.	35	36	37	38	39	40	41	42	43	44	45	46	47	48	49	50	51	52	1	2	3	4
Week type	C	C	C	C	CT	C	C	CW	CWT	T	C	C	C	C	CT	C	V	V	C	CW	CWT	T
Teaching week	1.1	1.2	1.3	1.4	1.5	1.6	1.7	1.8	1.9	1.10	2.1	2.2	2.3	2.4	2.5	2.6	2.7	X-mas Holidays		2.8	2.9	2.10
Monday	Start Acad. year	Open. Acad. year	13	20	27	4	11	18	25	1	8	15	22	29	6	13	20	27	3	10	17	24
Tuesday	31	7	14	21	28	5	12	19	26	2	9	16	23	30	7	14	21	28	4	11	18	25
Wednesday	1	8	15	22	29	6	13	20	27	3	10	17	24	1	8	15	22	29	5	12	19	26
Thursday	2	9	16	23	30	7	14	21	28	4	11	18	25	2	9	16	23	30	6	13	20	27
Friday	3	10	17	24	1	8	15	22	29	5	12	19	26	3	10	17	24	31	7	14	21	28
Saturday	4	11	18	25	2	9	16	23	30	6	13	20	27	4	11	18	25	1	8	15	22	29
Sunday	5	12	19	26	3	10	17	24	31	7	14	21	28	5	12	19	26	2	9	16	23	30
	September				October				November				December				January					

2nd SEMESTER

Week no.	5	6	7	8	9	10	11	12	13	14	15	16	17	18	19	20	21	22	23	24	25
Week type	V	C	C	C	C	CT	C	C	CW	CWT	T	C	C	C	C	C	C	C	CW	CWT	T
Teaching week	Spring break	3.1	3.2	3.3	3.4	3.5	3.6	3.7	3.8	3.9	3.10	4.1	4.2	4.3	4.4	4.5	4.6	4.7	4.8	4.9	4.10
Monday	31	7	14	21	28	7	14	21	28	4	11	Easter Monday	25	2	9	16	23	30	Whit Monday	13	20
Tuesday	1	8	15	22	1	8	15	22	29	5	12	19	26	3	10	17	24	31	7	14	21
Wednesday	2	9	16	23	2	9	16	23	30	6	13	20	Kings day	4	11	18	25	1	8	15	22
Thursday	3	10	17	24	3	10	17	24	31	7	14	21	28	Liberation day	12	19	Ascension Day	2	9	16	23
Friday	4	11	18	25	4	11	18	25	1	8	Good Friday	22	29	6	13	20	27	3	10	17	24
Saturday	5	12	19	26	5	12	19	26	2	9	16	23	30	7	14	21	28	4	11	18	25
Sunday	6	13	20	27	6	13	20	27	3	10	17	24	1	8	15	22	29	5	12	19	26
	February			March			April			May			June								

SUMMER PERIOD 2022

Week no.	26	27	28	29	30	31	32	33	34
Week type	W/V	W/V	T	V	V	V	V	V	V
Summer period week	5.1	5.2	5.3	5.4	5.5	5.6	5.7	5.8	5.9
Monday	27	4	11	18	25	1	8	15	22
Tuesday	28	5	12	19	26	2	9	16	23
Wednesday	29	6	13	20	27	3	10	17	24
Thursday	30	7	14	21	28	4	11	18	25
Friday	1	8	15	22	29	5	12	19	26
Saturday	2	9	16	23	30	6	13	20	27
Sunday	3	10	17	24	31	7	14	21	28
	July				August				

Week 5.1 and 5.2: free weeks only for resits, no regular teaching.

LEGENDA

C	=	Lectures and other teaching activities
CT	=	Lectures and examinations BSc-programmes
CW	=	Lectures / free week; varies per study programme
CWT	=	Lectures/free week/examinations/resits; varies per study programme
T	=	Examinations / Resits
V	=	No Teaching, Vacation or public holiday

29 August 2022: start academic year 2022-2023, week 35 (to be confirmed)
5 September 2022: Opening Academic Year

Appendix C

Occupant assumption based on rooms capacitance

Rooms capacitance can be found at <https://spacefinder.tudelft.nl/en/spaces/>

Descriptions	Occupant Count Assumptions
Class (full)	1020
Study (only the study area)	400
Close	0

Descriptions	Hourly Occupant Count Assumptions
Weekdays	$[\text{close}] * 7 + [\text{class} + \text{study}] * 5 + [\text{study}] * 1 + [\text{class} + \text{study}] * 4 + [\text{study} * 0.5] * 7$
Weekends (summer)	$[\text{close}] * 7 + [\text{study} * 0.3] * 10 + [0] * 7$
Weekends (winter)	$[\text{close}] * 7 + [\text{study} * 0.3] * 10 + [\text{study} * 0.5] * 7$
Exam weekdays	$[\text{close}] * 7 + [\text{class} + \text{study}] * 5 + [\text{study}] * 1 + [\text{class} + \text{study}] * 4 + [\text{study}] * 7$
Exam weekends	$[\text{close}] * 7 + [\text{study}] * 17$

Appendix D

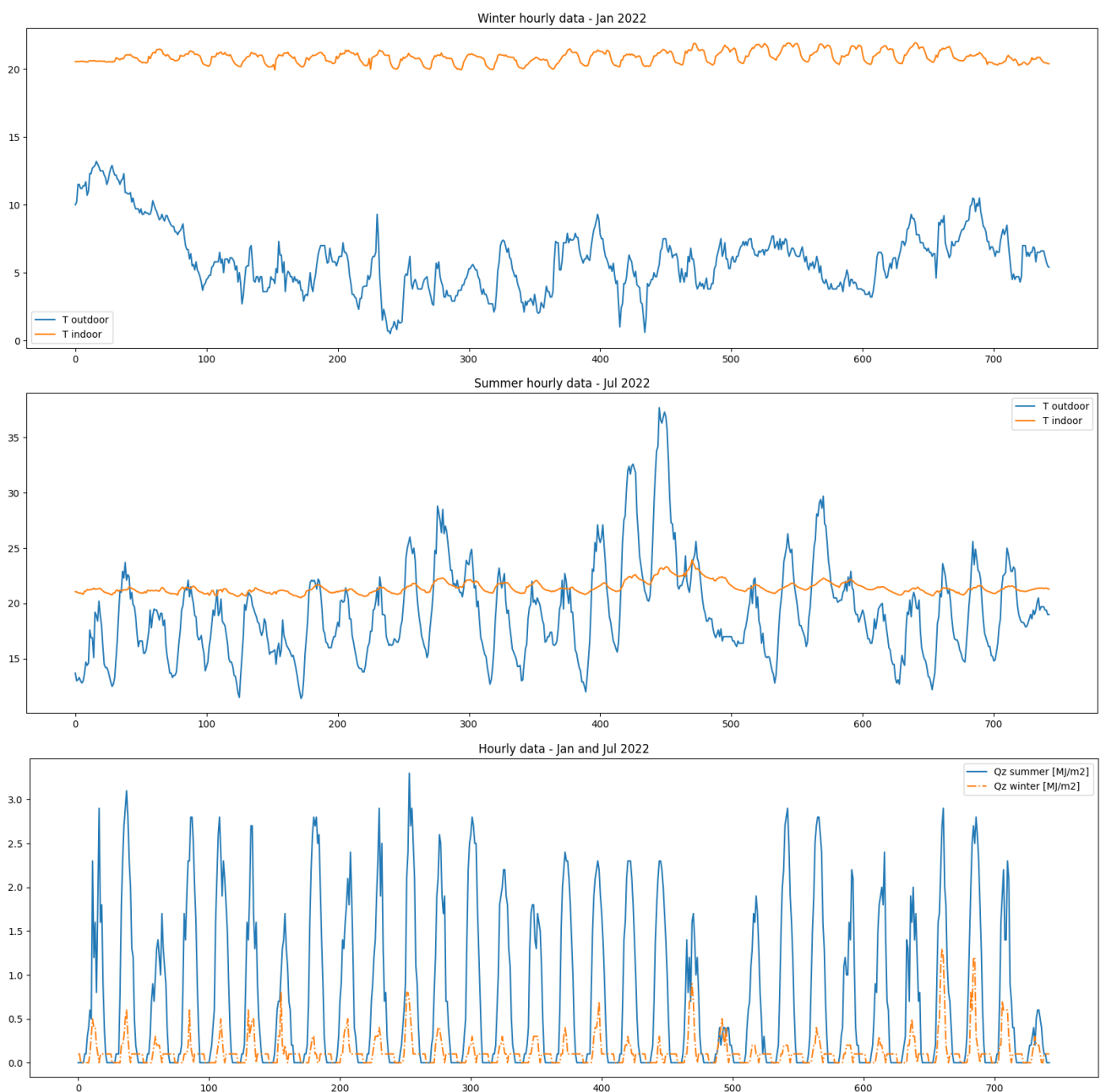
Static parameters

Parameters	Values	Units
T_o	Appendix E	°C
T_i	Appendix E	°C
$A_{gl-lump}$	6266.48	m ²
$A_{opaque\ envelope-lump}$	1448.3	m ²
$A_{inner\ walls-lump}$	1960	m ²
$A_{inner\ floors-lump}$	1775.2	m ²
U-value Glass-lump	1.65	W/m ² K
A_1	0.4	-
F	0-1	-
α_{conv_o}	25	W/m ² K
α_{conv_i}	2.5	W/m ² K
α_{rad}	5.1	W/m ² K
U-value Opaque-lump	0.14	W/m ² K
D_1	0.25	-
$d_{all\ response\ factor}$	0.08	m
$R_{inner\ envelope\ RF}$	0.512	m ² K/W
$R_{inner\ floors\ RF}$	0.1	m ² K/W
$R_{inner\ walls\ RF}$	0.512	m ² K/W
k	d/R	W/mK
$\rho_{inner\ envelope\ RF}$	800	Kg/m ²
$\rho_{inner\ floors\ RF}$	1600	Kg/m ²
$\rho_{inner\ walls\ RF}$	800	Kg/m ²

$C_{pinner\ envelope\ RF}$	1090	J/kgK
$C_{pinner\ floors\ F}$	840	J/kgK
$C_{pinner\ walls\ RF}$	1090	J/kgK
Q_z	Appendix E	MJ/m ²
Vent	36/3600	m ³ /s/person
ρ_{air}	1.2	Kg/m ³
$C_{p\ air}$	1000	J/kgK
Q_{int}	100	W/m ² /person

Appendix E

Timeseries parameters



window f1		wall g1		overhang floor h1		indoor air		wall j1	
NODE f1	0	NODE g1	$Ag1*(Xcor_g1*Tpast)$	NODE h1	0	NODE i	0	NODE j1	0
solar from section 1		solar from section 1		solar from section 1		ventilation	vent*person*rho_air*Cp_air*(To-Ti)	solar from section 1	
SOLAR	Af1*A1*Qz	SOLAR_wb1	Ab1*D1*Qz*Fb1g1	SOLAR_wb1	Ab1*D1*Qz*Fb1h1	ADVECTION		SOLAR_wb1	
SOLAR_wb1	Ab1*A1*Qz*Fb1f1	SOLAR_wd1	Ad1*D1*Qz*Fd1g1	SOLAR_wk1	Ak1*D1*Qz*Fk1h1	convection with section 1		SOLAR_wd1	
SOLAR_wd1	Ad1*A1*Qz*Fd1f1	SOLAR	Ag1*D1*Qz	SOLAR_wd1	Ad1*D1*Qz*Fd1h1	CONVECTION_a1	alfaconv_a1*Ah1*(Ta1-Ti)	SOLAR	
solar from section 2		solar from section 2		solar from section 2		CONVECTION_b1	alfaconv_b1*Ab1*(Tb1-Ti)	solar from section 2	
SOLAR_wa2	Aa2*A1*Qz*Fa2f1	SOLAR_wa2	Aa2*D1*Qz*Fa2g1	SOLAR	Ah1*D1*Qz	CONVECTION_c1	alfaconv_c1*Ac1*(Tc1-Ti)	SOLAR_wa2	
SOLAR_wj2	Aj2*A1*Qz*Fj2f1	SOLAR_wj2	Aj2*D1*Qz*Fj2g1	SOLAR_wa2	Aa2*D1*Qz*Fa2h1	CONVECTION_d1	alfaconv_d1*Ad1*(Td1-Ti)	SOLAR_wj2	
convection and conduction		convection and conduction		convection and conduction		CONVECTION_f1	alfaconv_f1*Af1*(Tf1-Ti)	convection and conduction	
CONVECTION_o	alfaconv_o1*Af1*(To-Tf1)	CONVECTION_o	alfaconv_o1*Ag1*(To-Tg1)	convection and conduction		CONVECTION_g1	alfaconv_g1*Ag1*(Tg1-Ti)	CONVECTION_o	
CONVECTION_i	alfaconv_i1*Af1*(Ti-Tf1)	CONVECTION_i	alfaconv_i1*Ag1*(Ti-Tg1)	CONVECTION_o	alfaconv_o1*Ah1*(To-Th1)	CONVECTION_h1	alfaconv_h1*Ah1*(Th1-Ti)	CONVECTION_i	
radiation to section 1		CONDUCTION	$(1/((1/alfao_g1)+Rc_g1))*Ag1*(To-Tg1)$	CONVECTION_i	alfaconv_i1*Ah1*(Ti-Th1)	CONVECTION_j1	alfaconv_j1*Aj1*(Tj1-Ti)	CONDUCTION	
RADIATION_a1	alfarad_f1*Af1*Ff1a1*(Ta1-Tf1)	ABSORPTION	$Ag1*X0_g1*Tg1$	convection with section 2		CONVECTION_k1	alfaconv_k1*Ak1*(Tk1-Ti)	ABSORPTION	
RADIATION_b1	alfarad_f1*Af1*Ff1b1*(Tb1-Tf1)	ABSORPTION_n	Ag1*(Xcor_g1*Tpast)					ABSORPTION_n	
RADIATION_d1	alfarad_f1*Af1*Ff1d1*(Td1-Tf1)	radiation to section 1						radiation to section 1	
radiation to section 2		RADIATION_a1	alfarad_g1*Ag1*Fg1a1*(Ta1-Tg1)	radiation to section 1		CONVECTION_a2	alfaconv_a2*Aa2*(Ta2-Ti)	RADIATION_a1	
RADIATION_a2	alfarad_f1*Af1*Ff1a2*(Ta2-Tf1)	RADIATION_b1	alfarad_g1*Ag1*Fg1b1*(Tb1-Tg1)	RADIATION_a1	alfarad_h1*Ah1*Fh1a1*(Ta1-Th1)	CONVECTION_b2	alfaconv_b2*Ab2*(Tb2-Ti)	RADIATION_b1	
RADIATION_b2	alfarad_f1*Af1*Ff1b2*(Tb2-Tf1)	RADIATION_d1	alfarad_g1*Ag1*Fg1d1*(Td1-Tg1)	RADIATION_b1	alfarad_h1*Ah1*Fh1b1*(Tb1-Th1)	CONVECTION_c2	alfaconv_c2*Ac2*(Tc2-Ti)	RADIATION_c1	
RADIATION_c2	alfarad_f1*Af1*Ff1c2*(Tc2-Tf1)	radiation to section 2		RADIATION_d1	alfarad_h1*Ah1*Fh1d1*(Td1-Th1)	CONVECTION_d2	alfaconv_d2*Ad2*(Td2-Ti)	RADIATION_d1	
RADIATION_d2	alfarad_f1*Af1*Ff1d2*(Td2-Tf1)	RADIATION_a2	alfarad_g1*Ag1*Fg1a2*(Ta2-Tg1)	RADIATION_j1	alfarad_h1*Ah1*Fh1j1*(Tj1-Th1)	CONVECTION_g2	alfaconv_g2*Ag2*(Tg2-Ti)	RADIATION_h1	
RADIATION_f2	alfarad_f1*Af1*Ff1f2*(Tf2-Tf1)	RADIATION_b2	alfarad_g1*Ag1*Fg1b2*(Tb2-Tg1)	RADIATION_k1	alfarad_h1*Ah1*Fh1k1*(Tk1-Th1)	CONVECTION_h2	alfaconv_h2*Ah2*(Th2-Ti)	radiation to section 2	
RADIATION_g2	alfarad_f1*Af1*Ff1g2*(Tg2-Tf1)	RADIATION_c2	alfarad_g1*Ag1*Fg1c2*(Tc2-Tg1)	RADIATION_m1	alfarad_h1*Ah1*Fh1m1*(Tm1-Th1)	CONVECTION_j2	alfaconv_j2*Aj2*(Tj2-Ti)	RADIATION_a2	
RADIATION_h2	alfarad_f1*Af1*Ff1h2*(Th2-Tf1)	RADIATION_d2	alfarad_g1*Ag1*Fg1d2*(Td2-Tg1)	radiation to section 2		convection with roof l and floor e		RADIATION_b2	
RADIATION_j2	alfarad_f1*Af1*Ff1j2*(Tj2-Tf1)	RADIATION_f2	alfarad_g1*Ag1*Fg1f2*(Tf2-Tg1)	RADIATION_a2	alfarad_h1*Ah1*Fh1a2*(Ta2-Th1)	CONVECTION_e	alfaconv_e1* Ae*(Te-Ti)	RADIATION_c2	
radiation to roof l and floor e		RADIATION_g2	alfarad_g1*Ag1*Fg1g2*(Tg2-Tg1)	RADIATION_b2	alfarad_h1*Ah1*Fh1b2*(Tb2-Th1)	CONVECTION_l	alfaconv_l1*Al*(Ti-Tl)	RADIATION_f2	
RADIATION_e	alfarad_f1*Af1*Ff1e*(Te-Tf1)	RADIATION_h2	alfarad_g1*Ag1*Fg1h2*(Th2-Tg1)	RADIATION_c2	alfarad_h1*Ah1*Fh1c2*(Tc2-Th1)	heat load		RADIATION_h2	
RADIATION_j	alfarad_f1*Af1*Ff1j*(Tj-Tf1)	RADIATION_j2	alfarad_g1*Ag1*Fg1j2*(Tj2-Tg1)	RADIATION_g2	alfarad_h1*Ah1*Fh1g2*(Tg2-Th1)	INTERNAL LOAD	Qint	RADIATION_j2	
		radiation to roof l and floor e		RADIATION_h2	alfarad_h1*Ah1*Fh1h2*(Th2-Th1)	RADIATION_h2	Qheat	radiation to roof l and floor e	
		RADIATION_e	alfarad_g1*Ag1*Fg1e*(Te-Tg1)	RADIATION_j2	alfarad_h1*Ah1*Fh1j2*(Tj2-Th1)			RADIATION_e	
		RADIATION_j	alfarad_g1*Ag1*Fg1j*(Tj-Tg1)	radiation to roof l				RADIATION_j	
				RADIATION_j	alfarad_h1*Ah1*Fh1j*(Tj-Th1)				

right equation	$Af1*A1*Qz+Ab1*A1*Qz*Fb1f1+Ad1*A1*Qz*Fd1f1+Aa2*A1*Qz*Fa2f1+Aj2*A1*Qz*Fj2f1+alfaconv_f1o*Af1*(To-Tf1)+alfaconv_f1i*Af1*(Ti-Tf1)+alfarad_f1*Af1*Ff1a1*(Ta1-Tf1)+alfarad_f1*Af1*Ff1b1*(Tb1-Tf1)+alfarad_f1*Af1*Ff1d1*(Td1-Tf1)+alfarad_f1*Af1*Ff1a2*(Ta2-Tf1)+alfarad_f1*Af1*Ff1b2*(Tb2-Tf1)+alfarad_f1*Af1*Ff1c2*(Tc2-Tf1)+alfarad_f1*Af1*Ff1f2*(Tf2-Tf1)+alfarad_f1*Af1*Ff1g2*(Tg2-Tf1)+alfarad_f1*Af1*Ff1h2*(Th2-Tf1)+alfarad_f1*Af1*Ff1j2*(Tj2-Tf1)+alfarad_f1*Af1*Ff1e*(Te-Tf1)+alfarad_f1*Af1*Ff1j*(Tj-Tf1)$	right equation	$Ab1*D1*Qz*Fb1g1+Ad1*D1*Qz*Fd1g1+Ag1*D1*Qz+Aj2*D1*Qz*Fj2g1+alfaconv_g1o*Ag1*(To-Tg1)+alfaconv_g1i*Ag1*(Ti-Tg1)+1/((1/alfao_g1)+Rc_g1))*Ag1*(To-Tg1)+Ag1*X0_g1*Tg1+alfarad_g1*Ag1*Fg1a1*(Ta1-Tg1)+alfarad_g1*Ag1*Fg1b1*(Tb1-Tg1)+alfarad_g1*Ag1*Fg1d1*(Td1-Tg1)+alfarad_g1*Ag1*Fg1a2*(Ta2-Tg1)+alfarad_g1*Ag1*Fg1b2*(Tb2-Tg1)+alfarad_g1*Ag1*Fg1c2*(Tc2-Tg1)+alfarad_g1*Ag1*Fg1f2*(Tf2-Tg1)+alfarad_g1*Ag1*Fg1g2*(Tg2-Tg1)+alfarad_g1*Ag1*Fg1h2*(Th2-Tg1)+alfarad_g1*Ag1*Fg1j2*(Tj2-Tg1)+alfarad_g1*Ag1*Fg1e*(Te-Tg1)+alfarad_g1*Ag1*Fg1j*(Tj-Tg1)$	right equation	$Ab1*D1*Qz*Fb1h1+Ak1*D1*Qz*Fk1h1+Ad1*D1*Qz*Fd1h1+Ah1*D1*Qz+Aa2*D1*Qz*Fa2h1+Aj2*D1*Qz*Fj2h1+alfaconv_h1o*Ah1*(To-Th1)+alfaconv_h1i*Ah1*(Ti-Th1)+alfarad_h1*Ah1*Fh1a1*(Ta1-Th1)+alfarad_h1*Ah1*Fh1b1*(Tb1-Th1)+alfarad_h1*Ah1*Fh1d1*(Td1-Th1)+alfarad_h1*Ah1*Fh1j1*(Tj1-Th1)+alfarad_h1*Ah1*Fh1k1*(Tk1-Th1)+alfarad_h1*Ah1*Fh1m1*(Tm1-Th1)+alfarad_h1*Ah1*Fh1a2*(Ta2-Th1)+alfarad_h1*Ah1*Fh1b2*(Tb2-Th1)+alfarad_h1*Ah1*Fh1c2*(Tc2-Th1)+alfarad_h1*Ah1*Fh1g2*(Tg2-Th1)+alfarad_h1*Ah1*Fh1h2*(Th2-Th1)+alfarad_h1*Ah1*Fh1j2*(Tj2-Th1)+alfarad_h1*Ah1*Fh1e*(Te-Th1)+alfarad_h1*Ah1*Fh1j*(Tj-Th1)$	right equation	vent*person*rho_air*Cp_air*(To-Ti)+alfaconv_a1*Aa1*(Ta1-Ti)+alfaconv_b1*Ab1*(Tb1-Ti)+alfaconv_c1*Ac1*(Tc1-Ti)+alfaconv_d1*Ad1*(Td1-Ti)+alfaconv_f1*Af1*(Tf1-Ti)+alfaconv_g1*Ag1*(Tg1-Ti)+alfaconv_h1*Ah1*(Th1-Ti)+alfaconv_j1*Aj1*(Tj1-Ti)+alfaconv_k1*Ak1*(Tk1-Ti)+alfaconv_v_a2*Aa2*(Ta2-Ti)+alfaconv_b2*Ab2*(Tb2-Ti)+alfaconv_c2*Ac2*(Tc2-Ti)+alfaconv_d2*Ad2*(Td2-Ti)+alfaconv_f2*Af2*(Tf2-Ti)+alfaconv_g2*Ag2*(Tg2-Ti)+alfaconv_h2*Ah2*(Th2-Ti)+alfaconv_j2*Aj2*(Tj2-Ti)+alfaconv_ei*Ae*(Te-Ti)+alfaconv_li*Al*(Ti-Tl)+Qint+Qheat	right equation	$Ag1*(Xcor_g1*Tpast)$
left equation	0	left equation	$Ag1*(Xcor_g1*Tpast)$	left equation	0	left equation	0	left equation	0

window k1	common roof l			adiabatic m1	window a2	wall b2
node k1	0	node l	Al*(Xcor_j)*Tpast	node m1	Am1*(Xcor_m1)*Tpast	node b2
solar from section 1	solar from section 1	solar from section 1	solar from section 1	solar from section 1	solar from section 1	solar from section 1
Ab1*D1*Qz*Fb1j1 Ad1*D1*Qz*Fd1j1 Aj1*D1*Qz	SOLAR SOLAR_wb1 SOLAR_wd1 solar from section 2	Ak1*A1*Qz Ab1*A1*Qz*Fb1k1 Ad1*A1*Qz*Fd1k1 SOLAR	SOLAR_wb1 SOLAR_wd1 SOLAR_wf1 SOLAR_wk1 SOLAR	Ab1*D1*Qz*Fb1l Ad1*D1*Qz*Fd1l Af1*D1*Qz*Ff1l Ak1*D1*Qz*Fk1l SOLAR	SOLAR_wb1 SOLAR_wd1 SOLAR_wf1 SOLAR_wk1 solar from section 2	Ab1*A1*Qz*Fb1a2 Ad1*A1*Qz*Fd1a2 Af1*A1*Qz*Ff1a2 Ak1*A1*Qz*Fk1a2 SOLAR
Aa2*D1*Qz*Fa2j1 Aj2*D1*Qz*Fj2j1	SOLAR_wa2 SOLAR_wj2 convection and conduction	Aa2*A1*Qz*Fa2k1 Aj2*A1*Qz*Fj2k1 convection and conduction	SOLAR_wa2 SOLAR_wj2 convection and conduction	Aa2*D1*Qz*Fa2m1 Aj2*D1*Qz*Fj2m1 convection and conduction	Aa2*A1*Qz Aj2*A1*Qz*Fj2a2 convection and conduction	Aa2*A1*Qz Aj2*A1*Qz*Fj2a2 convection and conduction
alfaconv_lo*Aj1*(To-Tj1) alfaconv_ji*Aj1*(Ti-Tj1) CONVECTION_i (1/(1/alfao_j1)+Rc_j1))*Aj1*(To-Tj1) Aj1*-X0_j1*Tj1 Aj1*(Xcor_j1)*Tpast	CONVECTION_o CONVECTION_i radiation to section 1	alfaconv_klo*Ak1*(To-Tk1) alfaconv_ki*Ak1*(Ti-Tk1) convection and conduction	CONVECTION_o CONVECTION_i CONDUCTION ABSORPTION ABSORPTION_n radiation to section 1	alfaconv_mlo*Am1*(Ti-Tm1) Aj2*D1*Qz*Fj2l ABSORPTION AM1*-X0_m1*Tm1 Am1*(Xcor_m1)*Tpast	CONVECTION_o CONVECTION_i radiation to section 1	alfaconv_a2o*Aa2*(To-Ta2) alfaconv_a2i*Aa2*(Ti-Ta2) CONDUCTION ABSORPTION CONVECTION_n radiation to section 1
alfarad_j1*Aj1*Fj1a1*(Ta1-Tj1) alfarad_j1*Aj1*Fj1b1*(Tb1-Tj1) alfarad_j1*Aj1*Fj1c1*(Tc1-Tj1) alfarad_j1*Aj1*Fj1d1*(Td1-Tj1) alfarad_j1*Aj1*Fj1h1*(Th1-Tj1)	RADIATION_a1 RADIATION_b1 RADIATION_c1 RADIATION_d1 RADIATION_h1 radiation to section 2	alfarad_k1*Ak1*Fk1a1*(Ta1-Tk1) alfarad_k1*Ak1*Fk1b1*(Tb1-Tk1) alfarad_k1*Ak1*Fk1c1*(Tc1-Tk1) alfarad_k1*Ak1*Fk1d1*(Td1-Tk1) alfarad_k1*Ak1*Fk1h1*(Th1-Tk1) alfarad_k1*Ak1*Fk1a2*(Ta2-Tk1) alfarad_k1*Ak1*Fk1b2*(Tb2-Tk1) alfarad_k1*Ak1*Fk1c2*(Tc2-Tk1) alfarad_k1*Ak1*Fk1d2*(Td2-Tk1) alfarad_k1*Ak1*Fk1h2*(Th2-Tk1)	RADIATION_a1 RADIATION_b1 RADIATION_c1 RADIATION_d1 RADIATION_n radiation to section 1	alfarad_j1*Aj1*Fj1a1*(Ta1-Tj1) alfarad_j1*Aj1*Fj1b1*(Tb1-Tj1) alfarad_j1*Aj1*Fj1c1*(Tc1-Tj1) alfarad_j1*Aj1*Fj1d1*(Td1-Tj1) alfarad_j1*Aj1*Fj1h1*(Th1-Tj1) alfarad_j1*Aj1*Fj1a2*(Ta2-Tj1) alfarad_j1*Aj1*Fj1b2*(Tb2-Tj1) alfarad_j1*Aj1*Fj1c2*(Tc2-Tj1) alfarad_j1*Aj1*Fj1d2*(Td2-Tj1) alfarad_j1*Aj1*Fj1h2*(Th2-Tj1)	RADIATION_a1 RADIATION_b1 RADIATION_c1 RADIATION_d1 RADIATION_n radiation to section 2	alfarad_a2*Aa2*Fa2a1*(Ta1-Ta2) alfarad_a2*Aa2*Fa2b1*(Tb1-Ta2) alfarad_a2*Aa2*Fa2c1*(Tc1-Ta2) alfarad_a2*Aa2*Fa2d1*(Td1-Ta2) alfarad_a2*Aa2*Fa2h1*(Th1-Ta2) alfarad_a2*Aa2*Fa2g1*(Tg1-Ta2) alfarad_a2*Aa2*Fa2h1*(Th1-Ta2) alfarad_a2*Aa2*Fa2j1*(Tj1-Ta2) alfarad_a2*Aa2*Fa2k1*(Tk1-Ta2) alfarad_a2*Aa2*Fa2m1*(Tm1-Ta2)
alfarad_j1*Aj1*Fj1e*(Te-Tj1) alfarad_j1*Aj1*Fj1j*(Tj-Tj1)	RADIATION_e RADIATION_j radiation to roof l and floor e	alfarad_k1*Ak1*Fk1e*(Te-Tk1) alfarad_k1*Ak1*Fk1j*(Tj-Tk1) radiation to section 2	RADIATION_k1 RADIATION_l radiation to section 2	alfarad_j1*Aj1*Fj1e*(Te-Tj1) alfarad_j1*Aj1*Fj1j*(Tj-Tj1) alfarad_j1*Aj1*Fj1a1*(Ta1-Tj1) alfarad_j1*Aj1*Fj1b1*(Tb1-Tj1) alfarad_j1*Aj1*Fj1c1*(Tc1-Tj1) alfarad_j1*Aj1*Fj1d1*(Td1-Tj1) alfarad_j1*Aj1*Fj1h1*(Th1-Tj1) alfarad_j1*Aj1*Fj1a2*(Ta2-Tj1) alfarad_j1*Aj1*Fj1b2*(Tb2-Tj1) alfarad_j1*Aj1*Fj1c2*(Tc2-Tj1) alfarad_j1*Aj1*Fj1d2*(Td2-Tj1) alfarad_j1*Aj1*Fj1h2*(Th2-Tj1) alfarad_j1*Aj1*Fj1e*(Te-Tj1) alfarad_j1*Aj1*Fj1j*(Tj-Tj1)	RADIATION_a1 RADIATION_b1 RADIATION_c1 RADIATION_d1 RADIATION_n radiation to section 2	alfarad_a2*Aa2*Fa2f1*(Tf1-Ta2) alfarad_a2*Aa2*Fa2g1*(Tg1-Ta2) alfarad_a2*Aa2*Fa2h1*(Th1-Ta2) alfarad_a2*Aa2*Fa2j1*(Tj1-Ta2) alfarad_a2*Aa2*Fa2k1*(Tk1-Ta2) alfarad_a2*Aa2*Fa2m1*(Tm1-Ta2)

Ab1*D1*Qz*Fb1j1+Ad1*D1*Qz*Fd1j1+Aj1*D1*Qz*Fa2j1+Aj2*D1*Qz*Fj2j1+alfaconv_lo*Aj1*(To-Tj1)+alfaconv_ji*Aj1*(Ti-Tj1)+(1/(1/alfao_j1)+Rc_j1))*Aj1*(To-Tj1)+Aj1*-X0_j1*Tj1+alfarad_j1*Aj1*Fj1a1*(Ta1-Tj1)+alfarad_j1*Aj1*Fj1b1*(Tb1-Tj1)+alfarad_j1*Aj1*Fj1c1*(Tc1-Tj1)+alfarad_j1*Aj1*Fj1d1*(Td1-Tj1)+alfarad_j1*Aj1*Fj1h1*(Th1-Tj1)+alfarad_j1*Aj1*Fj1a2*(Ta2-Tj1)+alfarad_j1*Aj1*Fj1b2*(Tb2-Tj1)+alfarad_j1*Aj1*Fj1c2*(Tc2-Tj1)+alfarad_j1*Aj1*Fj1d2*(Td2-Tj1)+alfarad_j1*Aj1*Fj1h2*(Th2-Tj1)+alfarad_j1*Aj1*Fj1e*(Te-Tj1)+alfarad_j1*Aj1*Fj1j*(Tj-Tj1)

right equation

left equation

Ab1*D1*Qz*Fb1l+Ad1*D1*Qz*Fd1l+Af1*D1*Qz*Ff1l+Ak1*D1*Qz*Fk1l+Al*D1*Qz+AA2*D1*Qz*Fa2l+A2*D1*Qz*Fj2l+alfaconv_lo*Al*(To-Tl)+alfaconv_lj*Al*(Ti-Tl)+(1/(1/alfao_l1)+Rc_l1))*Al*(To-Tl)+Al*-X0_l1*Tl+alfarad_l1*Al*Fla1*(Ta1-Tl)+alfarad_l1*Al*Flb1*(Tb1-Tl)+alfarad_l1*Al*Flc1*(Tc1-Tl)+alfarad_l1*Al*Fld1*(Td1-Tl)+alfarad_l1*Al*Flh1*(Th1-Tl)+alfarad_l1*Al*Fla2*(Ta2-Tl)+alfarad_l1*Al*Flb2*(Tb2-Tl)+alfarad_l1*Al*Flc2*(Tc2-Tl)+alfarad_l1*Al*Fld2*(Td2-Tl)+alfarad_l1*Al*Flh2*(Th2-Tl)+alfarad_l1*Al*Fle*(Te-Tl)+alfarad_l1*Al*Flj*(Tj-Tl)

right equation

left equation

Ab1*D1*Qz*Fb1m1+Ad1*D1*Qz*Fd1m1+Aa2*D1*Qz*Fa2m1+Aj2*D1*Qz*Fj2m1+alfaconv_lo*Am1*(To-Tm1)+alfaconv_lm1*Am1*(Ti-Tm1)+(1/(1/alfao_m1)+Rc_m1))*Am1*(To-Tm1)+Am1*-X0_m1*Tm1+alfarad_m1*Am1*Fm1a1*(Ta1-Tm1)+alfarad_m1*Am1*Fm1b1*(Tb1-Tm1)+alfarad_m1*Am1*Fm1c1*(Tc1-Tm1)+alfarad_m1*Am1*Fm1d1*(Td1-Tm1)+alfarad_m1*Am1*Fm1h1*(Th1-Tm1)+alfarad_m1*Am1*Fm1a2*(Ta2-Tm1)+alfarad_m1*Am1*Fm1b2*(Tb2-Tm1)+alfarad_m1*Am1*Fm1c2*(Tc2-Tm1)+alfarad_m1*Am1*Fm1d2*(Td2-Tm1)+alfarad_m1*Am1*Fm1h2*(Th2-Tm1)+alfarad_m1*Am1*Fm1e*(Te-Tm1)+alfarad_m1*Am1*Fm1j*(Tj-Tm1)

right equation

left equation

Ab1*A1*Qz*Fb1a2+Ad1*A1*Qz*Fd1a2+Af1*A1*Qz*Ff1a2+Ak1*A1*Qz*Fk1a2+Al*A1*Qz+AA2*A1*Qz*Fa2a2+A2*A1*Qz*Fj2a2+alfaconv_lo*Aa2*(To-Ta2)+alfaconv_la2*Aa2*(Ti-Ta2)+alfaconv_a2o*Aa2*(To-Ta2)+alfaconv_a2i*Aa2*(Ti-Ta2)+alfarad_a2*Aa2*Fa2a1*(Ta1-Ta2)+alfarad_a2*Aa2*Fa2b1*(Tb1-Ta2)+alfarad_a2*Aa2*Fa2c1*(Tc1-Ta2)+alfarad_a2*Aa2*Fa2d1*(Td1-Ta2)+alfarad_a2*Aa2*Fa2h1*(Th1-Ta2)+alfarad_a2*Aa2*Fa2g1*(Tg1-Ta2)+alfarad_a2*Aa2*Fa2j1*(Tj1-Ta2)+alfarad_a2*Aa2*Fa2k1*(Tk1-Ta2)+alfarad_a2*Aa2*Fa2m1*(Tm1-Ta2)

right equation

left equation

wall h2		window j2	
NODE h2	$Ah2*(Xcor_h2*Tpast)$	NODE j2	0
solar from section 1		solar from section 1	
SOLAR_wb1	$Ab1*D1*Qz*Fb1h2$	SOLAR_wb1	$Ab1*A1*Qz*Fb1j2$
SOLAR_wd1	$Ad1*D1*Qz*Fd1h2$	SOLAR_wd1	$Ad1*A1*Qz*Fd1j2$
SOLAR_wf1	$Af1*D1*Qz*Ff1h2$	SOLAR_wf1	$Af1*A1*Qz*Ff1j2$
SOLAR_wk1	$Ak1*D1*Qz*Fk1h2$	SOLAR_wk1	$Ak1*A1*Qz*Fk1j2$
solar from section 2		solar from section 2	
SOLAR_wa2	$Aa2*D1*Qz*Fa2h2$	SOLAR	$Aj2*A1*Qz$
convection and conduction		SOLAR_wa2	$Aa2*A1*Qz*Fa2j2$
CONVECTION_o	$alfaconv_h2o*Ah2*(To-Th2)$	convection and conduction	
CONVECTION_i	$alfaconv_h2i*Ah2*(Ti-Th2)$	CONVECTION_o	$alfaconv_j2o*Aj2*(To-Tj2)$
CONDUCTION	$(1/((1/alfao_h2)+Rc_h2))*Ah2*(To-Th2)$	CONVECTION_i	$alfaconv_j2i*Aj2*(Ti-Tj2)$
ABSORPTION	$Ah2*-X0_h2*Th2$	radiation to section 1	
ABSORPTION_n	$Ah2*(Xcor_h2*Tpast)$	RADIATION_a1	$alfarad_j2*Aj2*Fj2a1*(Ta1-Tj2)$
radiation to section 1		RADIATION_b1	$alfarad_j2*Aj2*Fj2b1*(Tb1-Tj2)$
RADIATION_a1	$alfarad_h2*Ah2*Fh2a1*(Ta1-Th2)$	RADIATION_c1	$alfarad_j2*Aj2*Fj2c1*(Tc1-Tj2)$
RADIATION_b1	$alfarad_h2*Ah2*Fh2b1*(Tb1-Th2)$	RADIATION_d1	$alfarad_j2*Aj2*Fj2d1*(Td1-Tj2)$
RADIATION_c1	$alfarad_h2*Ah2*Fh2c1*(Tc1-Th2)$	RADIATION_f1	$alfarad_j2*Aj2*Fj2f1*(Tf1-Tj2)$
RADIATION_d1	$alfarad_h2*Ah2*Fh2d1*(Td1-Th2)$	RADIATION_g1	$alfarad_j2*Aj2*Fj2g1*(Tg1-Tj2)$
RADIATION_f1	$alfarad_h2*Ah2*Fh2f1*(Tf1-Th2)$	RADIATION_h1	$alfarad_j2*Aj2*Fj2h1*(Th1-Tj2)$
RADIATION_g1	$alfarad_h2*Ah2*Fh2g1*(Tg1-Th2)$	RADIATION_j1	$alfarad_j2*Aj2*Fj2j1*(Tj1-Tj2)$
RADIATION_h1	$alfarad_h2*Ah2*Fh2h1*(Th1-Th2)$	RADIATION_k1	$alfarad_j2*Aj2*Fj2k1*(Tk1-Tj2)$
RADIATION_j1	$alfarad_h2*Ah2*Fh2j1*(Tj1-Th2)$	RADIATION_m1	$alfarad_j2*Aj2*Fj2m1*(Tm1-Tj2)$
RADIATION_k1	$alfarad_h2*Ah2*Fh2k1*(Tk1-Th2)$	radiation to section 2	
RADIATION_m1	$alfarad_h2*Ah2*Fh2m1*(Tm1-Th2)$	RADIATION_a2	$alfarad_j2*Aj2*Fj2a2*(Ta2-Tj2)$
radiation to section 2		RADIATION_b2	$alfarad_j2*Aj2*Fj2b2*(Tb2-Tj2)$
RADIATION_a2	$alfarad_h2*Ah2*Fh2a2*(Ta2-Th2)$	RADIATION_c2	$alfarad_j2*Aj2*Fj2c2*(Tc2-Tj2)$
RADIATION_b2	$alfarad_h2*Ah2*Fh2b2*(Tb2-Th2)$	RADIATION_d2	$alfarad_j2*Aj2*Fj2d2*(Td2-Tj2)$
RADIATION_c2	$alfarad_h2*Ah2*Fh2c2*(Tc2-Th2)$	radiation to roof l and floor e	
RADIATION_d2	$alfarad_h2*Ah2*Fh2d2*(Td2-Th2)$	RADIATION_e	$alfarad_j2*Aj2*Fj2e*(Te-Tj2)$
radiation to roof l and floor e		RADIATION_l	$alfarad_j2*Aj2*Fj2l*(Tl-Tj2)$
RADIATION_e	$alfarad_h2*Ah2*Fh2e*(Te-Th2)$		
RADIATION_l	$alfarad_h2*Ah2*Fh2l*(Tl-Th2)$		

right equation	$Ab1*D1*Qz*Fb1h2+Ad1*D1*Qz*Fd1h2+Af1*D1*Qz*Ff1h2+Ak1*D1*Qz*Fk1h2+Aa2*D1*Qz*Fa2h2+alfaconv_h2o*Ah2*(To-Th2)+alfaconv_h2i*Ah2*(Ti-Th2)+(1/((1/alfao_h2)+Rc_h2))*Ah2*(To-Th2)+Ah2*-X0_h2*Th2+alfarad_h2*Ah2*Fh2a1*(Ta1-Th2)+alfarad_h2*Ah2*Fh2b1*(Tb1-Th2)+alfarad_h2*Ah2*Fh2c1*(Tc1-Th2)+alfarad_h2*Ah2*Fh2d1*(Td1-Th2)+alfarad_h2*Ah2*Fh2f1*(Tf1-Th2)+alfarad_h2*Ah2*Fh2g1*(Tg1-Th2)+alfarad_h2*Ah2*Fh2h1*(Th1-Th2)+alfarad_h2*Ah2*Fh2j1*(Tj1-Th2)+alfarad_h2*Ah2*Fh2k1*(Tk1-Th2)+alfarad_h2*Ah2*Fh2m1*(Tm1-Th2)+alfarad_h2*Ah2*Fh2a2*(Ta2-Th2)+alfarad_h2*Ah2*Fh2b2*(Tb2-Th2)+alfarad_h2*Ah2*Fh2c2*(Tc2-Th2)+alfarad_h2*Ah2*Fh2d2*(Td2-Th2)+alfarad_h2*Ah2*Fh2e*(Te-Th2)+alfarad_h2*Ah2*Fh2l*(Tl-Th2)$	right equation	$Ab1*A1*Qz*Fb1j2+Ad1*A1*Qz*Fd1j2+Af1*A1*Qz*Ff1j2+Ak1*A1*Qz*Fk1j2+Aa2*A1*Qz*Fa2j2+alfaconv_j2o*Aj2*(To-Tj2)+alfaconv_j2i*Aj2*(Ti-Tj2)+alfarad_j2*Aj2*Fj2a1*(Ta1-Tj2)+alfarad_j2*Aj2*Fj2b1*(Tb1-Tj2)+alfarad_j2*Aj2*Fj2c1*(Tc1-Tj2)+alfarad_j2*Aj2*Fj2d1*(Td1-Tj2)+alfarad_j2*Aj2*Fj2f1*(Tf1-Tj2)+alfarad_j2*Aj2*Fj2g1*(Tg1-Tj2)+alfarad_j2*Aj2*Fj2h1*(Th1-Tj2)+alfarad_j2*Aj2*Fj2j1*(Tj1-Tj2)+alfarad_j2*Aj2*Fj2k1*(Tk1-Tj2)+alfarad_j2*Aj2*Fj2m1*(Tm1-Tj2)+alfarad_j2*Aj2*Fj2a2*(Ta2-Tj2)+alfarad_j2*Aj2*Fj2b2*(Tb2-Tj2)+alfarad_j2*Aj2*Fj2c2*(Tc2-Tj2)+alfarad_j2*Aj2*Fj2d2*(Td2-Tj2)+alfarad_j2*Aj2*Fj2e*(Te-Tj2)+alfarad_j2*Aj2*Fj2l*(Tl-Tj2)$
left equation	$Ah2*(Xcor_h2*Tpast)$	left equation	0

window f1		wall g1		overhang floor h1		indoor air		wall j1
NODE f1	0	NODE g1	$Ag1*(Xcor_g1*Tpast)$	NODE h1	0	NODE i	0	NODE j1
solar from section 1		solar from section 1		solar from section 1		ventilation		solar from section 1
SOLAR	$Af1*A1*Qz$	SOLAR_wb1	$Ab1*D1*Qz*Fb1g1$	SOLAR_wb1	$Ab1*D1*Qz*Fb1h1$	ADVECTION	$vent*person*rho_air* Cp_air*(To-Ti)$	SOLAR_wb1
SOLAR_wb1	$Ab1*A1*Qz*Fb1f1$	SOLAR_wd1	$Ad1*D1*Qz*Fd1g1$	SOLAR_wk1	$Ak1*D1*Qz*Fk1h1$	convection with section 1		SOLAR_wd1
SOLAR_wd1	$Ad1*A1*Qz*Fd1f1$	SOLAR	$Ag1*D1*Qz$	SOLAR_wd1	$Ad1*D1*Qz*Fd1h1$	CONVECTION_a1	$alfaconv_a1*Aa1*(Ta1-Ti)$	SOLAR
solar from section 2		solar from section 2		solar from section 2		CONVECTION_b1	$alfaconv_b1*Ab1*(Tb1-Ti)$	solar from section 2
SOLAR_wa2	$Aa2*A1*Qz*Fa2f1$	SOLAR_wa2	$Aa2*D1*Qz*Fa2g1$	SOLAR	$Ah1*D1*Qz$	CONVECTION_c1	$alfaconv_c1*Ac1*(Tc1-Ti)$	SOLAR_wa2
SOLAR_wj2	$Aj2*A1*Qz*Fj2f1$	SOLAR_wj2	$Aj2*D1*Qz*Fj2g1$	SOLAR_wa2	$Aa2*D1*Qz*Fa2h1$	CONVECTION_d1	$alfaconv_d1*Ad1*(Td1-Ti)$	SOLAR_wj2
convection and conduction		convection and conduction		convection and conduction		CONVECTION_f1	$alfaconv_f1*Af1*(Tf1-Ti)$	convection and conduction
CONVECTION_o	$alfaconv_f1o*Af1*(To-Tf1)$	CONVECTION_o	$alfaconv_g1o*Ag1*(To-Tg1)$	CONVECTION_o	$alfaconv_h1o*Ah1*(To-Th1)$	CONVECTION_g1	$alfaconv_g1*Ag1*(Tg1-Ti)$	CONVECTION_o
CONVECTION_i	$alfaconv_f1i*Af1*(Ti-Tf1)$	CONVECTION_i	$alfaconv_g1i*Ag1*(Ti-Tg1)$	CONVECTION_i	$alfaconv_h1i*Ah1*(Ti-Th1)$	CONVECTION_h1	$alfaconv_h1*Ah1*(Th1-Ti)$	CONVECTION_i
radiation to section 1		CONDUCTION	$(1/(1/alfaconv_g1)+Rc_g1))*Ag1*(To-Tg1)$	CONVECTION_j1		CONVECTION_j1	$alfaconv_j1*Aj1*(Tj1-Ti)$	CONDUCTION
RADIATION_a1	$alfarad_f1*Af1*Ff1a1*(Ta1-Tf1)$	ABSORPTION	$Ag1*X0_g1*Tg1$	CONVECTION_k1		CONVECTION_k1	$alfaconv_k1*Ak1*(Tk1-Ti)$	ABSORPTION
RADIATION_b1	$alfarad_f1*Af1*Ff1b1*(Tb1-Tf1)$	ABSORPTION_n	$Ag1*(Xcor_g1*Tpast)$	convection with section 2		CONVECTION_a2	$alfaconv_a2*Aa2*(Ta2-Ti)$	ABSORPTION_n
RADIATION_d1	$alfarad_f1*Af1*Ff1d1*(Td1-Tf1)$	radiation to section 1		CONVECTION_b2		CONVECTION_b2	$alfaconv_b2*Ab2*(Tb2-Ti)$	radiation to section 1
radiation to section 2		RADIATION_a1	$alfarad_g1*Ag1*Fg1a1*(Ta1-Tg1)$	CONVECTION_c2		CONVECTION_c2	$alfaconv_c2*Ac2*(Tc2-Ti)$	RADIATION_a1
RADIATION_a2	$alfarad_f1*Af1*Ff1a2*(Ta2-Tf1)$	RADIATION_b1	$alfarad_g1*Ag1*Fg1b1*(Tb1-Tg1)$	CONVECTION_d2		CONVECTION_d2	$alfaconv_d2*Ad2*(Td2-Ti)$	RADIATION_b1
RADIATION_b2	$alfarad_f1*Af1*Ff1b2*(Tb2-Tf1)$	RADIATION_d1	$alfarad_g1*Ag1*Fg1d1*(Td1-Tg1)$	RADIATION_d1	$alfarad_h1*Ah1*Fh1d1*(Td1-Th1)$	CONVECTION_f2	$alfaconv_f2*Af2*(Tf2-Ti)$	RADIATION_c1
RADIATION_c2	$alfarad_f1*Af1*Ff1c2*(Tc2-Tf1)$	radiation to section 2		RADIATION_j1	$alfarad_h1*Ah1*Fh1j1*(Tj1-Th1)$	CONVECTION_g2	$alfaconv_g2*Ag2*(Tg2-Ti)$	RADIATION_d1
RADIATION_d2	$alfarad_f1*Af1*Ff1d2*(Td2-Tf1)$	RADIATION_a2	$alfarad_g1*Ag1*Fg1a2*(Ta2-Tg1)$	RADIATION_k1	$alfarad_h1*Ah1*Fh1k1*(Tk1-Th1)$	CONVECTION_h2	$alfaconv_h2*Ah2*(Th2-Ti)$	RADIATION_h1
RADIATION_f2	$alfarad_f1*Af1*Ff1f2*(Tf2-Tf1)$	RADIATION_b2	$alfarad_g1*Ag1*Fg1b2*(Tb2-Tg1)$	RADIATION_m1	$alfarad_h1*Ah1*Fh1m1*(Tm1-Th1)$	CONVECTION_j2	$alfaconv_j2*Aj2*(Tj2-Ti)$	radiation to section 2
RADIATION_g2	$alfarad_f1*Af1*Ff1g2*(Tg2-Tf1)$	RADIATION_c2	$alfarad_g1*Ag1*Fg1c2*(Tc2-Tg1)$	radiation to section 2		convection with roof l and floor e		RADIATION_a2
RADIATION_h2	$alfarad_f1*Af1*Ff1h2*(Th2-Tf1)$	RADIATION_d2	$alfarad_g1*Ag1*Fg1d2*(Td2-Tg1)$	RADIATION_a2	$alfarad_h1*Ah1*Fh1a2*(Ta2-Th1)$	CONVECTION_e	$alfaconv_ei*Ae*(Te-Ti)$	RADIATION_b2
RADIATION_j2	$alfarad_f1*Af1*Ff1j2*(Tj2-Tf1)$	RADIATION_f2	$alfarad_g1*Ag1*Fg1f2*(Tf2-Tg1)$	RADIATION_b2	$alfarad_h1*Ah1*Fh1b2*(Tb2-Th1)$	CONVECTION_i	$alfaconv_ii*Ai*(Ti-Ti)$	RADIATION_d2
radiation to roof l and floor e		RADIATION_g2	$alfarad_g1*Ag1*Fg1g2*(Tg2-Tg1)$	RADIATION_h2	$alfarad_h1*Ah1*Fh1h2*(Th2-Th1)$	heat load		RADIATION_f2
RADIATION_e	$alfarad_f1*Af1*Ff1e*(Te-Tf1)$	RADIATION_j2	$alfarad_g1*Ag1*Fg1j2*(Tj2-Tg1)$	RADIATION_g2	$alfarad_h1*Ah1*Fh1g2*(Tg2-Th1)$	INTERNAL LOAD	Qint	RADIATION_j2
RADIATION_j	$alfarad_f1*Af1*Ff1j*(Tj-Tf1)$	radiation to roof l and floor e		RADIATION_h2	$alfarad_h1*Ah1*Fh1h2*(Th2-Th1)$	H/C LOAD	Qheat	radiation to roof l and floor e
		RADIATION_e	$alfarad_g1*Ag1*Fg1e*(Te-Tg1)$	RADIATION_j2	$alfarad_h1*Ah1*Fh1j2*(Tj2-Th1)$	convection with inner wall and floor		RADIATION_e
		RADIATION_j	$alfarad_g1*Ag1*Fg1j*(Tj-Tg1)$	radiation to roof l		CONVECTION_n	$alfaconv_ni*An*(Tn-Ti)$	RADIATION_j
				RADIATION_j	$alfarad_h1*Ah1*Fh1j*(Tj-Th1)$	CONVECTION_p	$alfaconv_pi*Ap*(Tp-Ti)$	

right equation

$$Af1*A1*Qz+Ab1*A1*Qz*Fb1f1+Ad1*A1*Qz*Fd1f1+Aa2*A1*Qz*Fa2f1+Aj2*A1*Qz*Fj2f1+alfaconv_f1o*Af1*(To-Tf1)+alfarad_f1*Af1*Ff1a1*(Ta1-Tf1)+alfarad_f1*Af1*Ff1b1*(Tb1-Tf1)+alfarad_f1*Af1*Ff1d1*(Td1-Tf1)+alfarad_f1*Af1*Ff1a2*(Ta2-Tf1)+alfarad_f1*Af1*Ff1b2*(Tb2-Tf1)+alfarad_f1*Af1*Ff1c2*(Tc2-Tf1)+alfarad_f1*Af1*Ff1d2*(Td2-Tf1)+alfarad_f1*Af1*Ff1f2*(Tf2-Tf1)+alfarad_f1*Af1*Ff1g2*(Tg2-Tf1)+alfarad_f1*Af1*Ff1h2*(Th2-Tf1)+alfarad_f1*Af1*Ff1j2*(Tj2-Tf1)+alfarad_f1*Af1*Ff1e*(Te-Tf1)+alfarad_f1*Af1*Ff1j*(Tj-Tf1)$$

left equation

$$0$$

right equation

$$Ab1*D1*Qz*Fb1g1+Ad1*D1*Qz*Fd1g1+Ag1*D1*Qz+Aj2*D1*Qz*Fj2g1+alfaconv_g1o*Ag1*(To-Tg1)+alfarad_g1*Ag1*(Ti-Tg1)+alfarad_g1*Ag1*Fg1a1*(Ta1-Tg1)+alfarad_g1*Ag1*Fg1b1*(Tb1-Tg1)+alfarad_g1*Ag1*Fg1d1*(Td1-Tg1)+alfarad_g1*Ag1*Fg1a2*(Ta2-Tg1)+alfarad_g1*Ag1*Fg1b2*(Tb2-Tg1)+alfarad_g1*Ag1*Fg1c2*(Tc2-Tg1)+alfarad_g1*Ag1*Fg1d2*(Td2-Tg1)+alfarad_g1*Ag1*Fg1f2*(Tf2-Tg1)+alfarad_g1*Ag1*Fg1g2*(Tg2-Tg1)+alfarad_g1*Ag1*Fg1j2*(Tj2-Tg1)+alfarad_g1*Ag1*Fg1e*(Te-Tg1)+alfarad_g1*Ag1*Fg1j*(Tj-Tg1)$$

left equation

$$Ag1*(Xcor_g1*Tpast)$$

right equation

$$Ab1*D1*Qz*Fb1h1+Ak1*D1*Qz*Fk1h1+Ah1*D1*Qz+Aj2*D1*Qz*Fj2h1+alfaconv_h1o*Ah1*(To-Th1)+alfarad_h1*Ah1*Fh1a1*(Ta1-Th1)+alfarad_h1*Ah1*Fh1b1*(Tb1-Th1)+alfarad_h1*Ah1*Fh1d1*(Td1-Th1)+alfarad_h1*Ah1*Fh1a2*(Ta2-Th1)+alfarad_h1*Ah1*Fh1b2*(Tb2-Th1)+alfarad_h1*Ah1*Fh1c2*(Tc2-Th1)+alfarad_h1*Ah1*Fh1d2*(Td2-Th1)+alfarad_h1*Ah1*Fh1f2*(Tf2-Th1)+alfarad_h1*Ah1*Fh1g2*(Tg2-Th1)+alfarad_h1*Ah1*Fh1h2*(Th2-Th1)+alfarad_h1*Ah1*Fh1j2*(Tj2-Th1)+alfarad_h1*Ah1*Fh1e*(Te-Th1)+alfarad_h1*Ah1*Fh1j*(Tj-Th1)$$

left equation

$$0$$

right equation

$$vent*person*rho_air* Cp_air*(To-Ti)+alfaconv_a1*Aa1*(Ta1-Ti)+alfaconv_b1*Ab1*(Tb1-Ti)+alfaconv_c1*Ac1*(Tc1-Ti)+alfaconv_d1*Ad1*(Td1-Ti)+alfaconv_f1*Af1*(Tf1-Ti)+alfaconv_g1*Ag1*(Tg1-Ti)+alfaconv_h1*Ah1*(Th1-Ti)+alfaconv_j1*Aj1*(Tj1-Ti)+alfaconv_k1*Ak1*(Tk1-Ti)+alfaconv_a2*Aa2*(Ta2-Ti)+alfaconv_b2*Ab2*(Tb2-Ti)+alfaconv_c2*Ac2*(Tc2-Ti)+alfaconv_d2*Ad2*(Td2-Ti)+alfaconv_f2*Af2*(Tf2-Ti)+alfaconv_g2*Ag2*(Tg2-Ti)+alfaconv_h2*Ah2*(Th2-Ti)+alfaconv_j2*Aj2*(Tj2-Ti)+alfaconv_ei*Ae*(Te-Ti)+alfaconv_ii*Ai*(Ti-Ti)+Qint+Qheat+alfaconv_ni*An*(Tn-Ti)+alfaconv_pi*Ap*(Tp-Ti)$$

left equation

$$0$$

right equation

$$0$$

left equation

$$0$$

	roof c2		adiabatic d2		adiabatic f2		roof g2	
Ab2*(Xcor_b2*Tpast)	NODE c2	Ac2*(Xcor_c2*Tpast)	NODE d2	Ad2*(Xcor_d2*Tpast)	NODE f2	Af2*(Xcor_f2*Tpast)	NODE g2	Ag2*(Xcor_g2*Tpast)
Ab1*D1*Qz*Fb1b2	solar from section 1		solar from section 1		solar from section 1		solar from section 1	
Ad1*D1*Qz*Fd1b2	SOLAR_wd1	Ad1*D1*Qz*Ffd1c2	SOLAR_wb1	Ab1*D1*Qz*Fb1d2	SOLAR_wb1	Ab1*D1*Qz*Fb1f2	SOLAR_wd1	Ad1*D1*Qz*Fd1g2
Af1*D1*Qz*Ff1b2	SOLAR_wf1	Af1*D1*Qz*Ff1c2	SOLAR_wd1	Ad1*D1*Qz*Ffd1d2	SOLAR_wd1	Ad1*D1*Qz*Ffd1f2	SOLAR_wf1	Af1*D1*Qz*Ff1g2
Ak1*D1*Qz*Fk1b2	solar from section 2		SOLAR_wf1	Af1*D1*Qz*Ffd1d2	SOLAR_wf1	Af1*D1*Qz*Ffd1f2	solar from section 2	
	SOLAR	Ac2*D1*Qz	SOLAR_wk1	Ak1*D1*Qz*Fk1d2	SOLAR_wk1	Ak1*D1*Qz*Fk1f2	SOLAR_wa	Aa2*D1*Qz*Fa2g2
	SOLAR_wj2	Aj2*D1*Qz*Fj2c2					convection and conduction	
Ab2*D1*Qz	convection and conduction		SOLAR_wj2	Aj2*D1*Qz*Fj2d2	SOLAR_wj2	Aa2*D1*Qz*Fa2f2	CONVECTION_o	alfaconv_g20*Ag2*(To-Tg2)
Aj2*D1*Qz*Fj2b2	CONVECTION_o	alfaconv_c20*Ac2*(To-Tc2)	convection and conduction		CONVECTION_o		CONVECTION_i	alfaconv_g21*Ag2*(Ti-Tg2)
	CONVECTION_i	alfaconv_c21*Ac2*(Ti-Tc2)	CONVECTION_i	alfaconv_d21*Ad2*(Ti-Td2)	CONVECTION_i	alfaconv_f21*Af2*(Ti-Tf2)	CONDUCTION	(1/((1/alfa_g2)+Rc_g2))*Ag2*(To-Tg2)
alfaconv_b20*Ab2*(To-Tb2)	CONDUCTION	(1/((1/alfa_c2)+Rc_c2))*Ac2*(To-Tc2)	CONDUCTION	Ad2*X0_d2*Td2	ABSORPTION	Af2*X0_d2*Ff2	ABSORPTION	Ag2*X0_g2*Tg2
alfaconv_b21*Ab2*(Ti-Tb2)	ABSORPTION	Ac2*X0_c2*Tc2	ABSORPTION_n	Ad2*(Xcor_d2*Tpast)	ABSORPTION_n	Af2*(Xcor_f2*Tpast)	ABSORPTION_n	Ag2*(Xcor_g2*Tpast)
(1/((1/alfa_b2)+Rc_b2))*Ab2*(To-Tb2)	ABSORPTION_o	Ac2*(Xcor_c2*Tpast)	radiation to section 1		radiation to section 1		radiation to section 1	
Ab2*X0_b2*Tb2	radiation to section 1		RADIATION_a1	alfarad_d2*Ad2*Fd2a1*(Ta1-Td2)	RADIATION_a1	alfarad_f2*Af2*Ff2a1*(Ta1-Tf2)	RADIATION_d1	alfarad_g2*Ag2*Fg2d1*(Td1-Tg2)
Ab2*(Xcor_b2*Tpast)	RADIATION_d1	alfarad_c2*Ac2*Fc2d1*(Td1-Tc2)	RADIATION_b1	alfarad_d2*Ad2*Fd2b1*(Tb1-Td2)	RADIATION_b1	alfarad_f2*Af2*Ff2b1*(Tb1-Tf2)	RADIATION_f1	alfarad_g2*Ag2*Fg2f1*(Tf1-Tg2)
	RADIATION_f1	alfarad_c2*Ac2*Fc2f1*(Tf1-Tc2)	RADIATION_d1	alfarad_d2*Ad2*Fd2d1*(Td1-Td2)	RADIATION_d1	alfarad_f2*Af2*Ff2d1*(Td1-Tf2)	RADIATION_g1	alfarad_g2*Ag2*Fg2g1*(Tg1-Tg2)
alfarad_b2*Ab2*Fb2a1*(Ta1-Tb2)	RADIATION_g1	alfarad_c2*Ac2*Fc2g1*(Tg1-Tc2)	RADIATION_f1	alfarad_d2*Ad2*Fd2f1*(Tf1-Td2)	RADIATION_f1	alfarad_f2*Af2*Ff2f1*(Tf1-Tf2)	RADIATION_h1	alfarad_g2*Ag2*Fg2h1*(Th1-Tg2)
alfarad_b2*Ab2*Fb2b1*(Tb1-Tb2)	RADIATION_h1	alfarad_c2*Ac2*Fc2h1*(Th1-Tc2)	RADIATION_g1	alfarad_d2*Ad2*Fd2g1*(Tg1-Td2)	RADIATION_g1	alfarad_f2*Af2*Ff2g1*(Tg1-Tf2)	RADIATION_j1	alfarad_g2*Ag2*Fg2j1*(Tj1-Tg2)
alfarad_b2*Ab2*Fb2c1*(Tc1-Tb2)	RADIATION_j1	alfarad_c2*Ac2*Fc2j1*(Tj1-Tc2)	RADIATION_i1	alfarad_d2*Ad2*Fd2i1*(Ti1-Td2)	RADIATION_i1	alfarad_f2*Af2*Ff2i1*(Ti1-Tf2)	RADIATION_m1	alfarad_g2*Ag2*Fg2m1*(Tm1-Tg2)
alfarad_b2*Ab2*Fb2d1*(Td1-Tb2)	RADIATION_m1	alfarad_c2*Ac2*Fc2m1*(Tm1-Tc2)	RADIATION_k1	alfarad_d2*Ad2*Fd2k1*(Tk1-Td2)	RADIATION_k1	alfarad_f2*Af2*Ff2k1*(Tk1-Tf2)	radiation to section 2	
alfarad_b2*Ab2*Fb2f1*(Tf1-Tb2)	radiation to section 2		RADIATION_m1	alfarad_d2*Ad2*Fd2m1*(Tm1-Td2)	RADIATION_m1	alfarad_f2*Af2*Ff2m1*(Tm1-Tf2)	RADIATION_d2	alfarad_g2*Ag2*Fg2d2*(Td2-Tg2)
alfarad_b2*Ab2*Fb2g1*(Tg1-Tb2)	RADIATION_d2	alfarad_c2*Ac2*Fc2d2*(Td2-Tc2)	radiation to section 2		radiation to section 2		RADIATION_f2	alfarad_g2*Ag2*Fg2f2*(Tf2-Tg2)
alfarad_b2*Ab2*Fb2h1*(Th1-Tb2)	RADIATION_f2	alfarad_c2*Ac2*Fc2f2*(Tf2-Tc2)	RADIATION_c2	alfarad_d2*Ad2*Fd2c2*(Tc2-Td2)	RADIATION_a2	alfarad_f2*Af2*Ff2a2*(Ta2-Tf2)	radiation to floor e	
alfarad_b2*Ab2*Fb2j1*(Tj1-Tb2)	radiation to floor e		RADIATION_o2	alfarad_d2*Ad2*Fd2o2*(To2-Td2)	RADIATION_b2	alfarad_f2*Af2*Ff2b2*(Tb2-Tf2)	RADIATION_e	alfarad_g2*Ag2*Fg2e*(Te-Tg2)
alfarad_b2*Ab2*Fb2k1*(Tk1-Tb2)	RADIATION_e	alfarad_c2*Ac2*Fc2e*(Te-Tc2)	RADIATION_g2	alfarad_d2*Ad2*Fd2g2*(Tg2-Td2)	RADIATION_c2	alfarad_f2*Af2*Ff2c2*(Tc2-Tf2)		
alfarad_b2*Ab2*Fb2m1*(Tm1-Tb2)			RADIATION_h2	alfarad_d2*Ad2*Fd2h2*(Th2-Td2)	RADIATION_d2	alfarad_f2*Af2*Ff2d2*(Td2-Tf2)		
			RADIATION_j2	alfarad_d2*Ad2*Fd2j2*(Tj2-Td2)	RADIATION_g2	alfarad_f2*Af2*Ff2g2*(Tg2-Tf2)		
alfarad_b2*Ab2*Fb2f2*(Tf2-Tb2)			radiation to floor e		radiation to floor e			
alfarad_b2*Ab2*Fb2g2*(Tg2-Tb2)			RADIATION_e	alfarad_d2*Ad2*Fd2e*(Te-Td2)	RADIATION_e	alfarad_f2*Af2*Ff2e*(Te-Tf2)		
alfarad_b2*Ab2*Fb2h2*(Th2-Tb2)			RADIATION_j	alfarad_d2*Ad2*Fd2j*(Tj-Td2)	RADIATION_j	alfarad_f2*Af2*Ff2j*(Tj-Tf2)		
alfarad_b2*Ab2*Fb2j2*(Tj2-Tb2)								
alfarad_b2*Ab2*Fb2e*(Te-Tb2)								
alfarad_b2*Ab2*Fb2i*(Ti-Tb2)								
Ab1*D1*Qz*Fb1b2+Ad1*D1*Qz*Fd1b2+Af1*D1*Qz*Ff1b2+Ak1*D1*Qz*Fk1b2+Aj2*D1*Qz*Fj2b2+alfaconv_b20*Ab2*(To-Tb2)+alfaconv_b21*Ab2*(Ti-Tb2)+(1/((1/alfa_b2)+Rc_b2))*Ab2*(To-Tb2)+alfarad_b20*Ab2*Fb2a1*(Ta1-Tb2)+alfarad_b21*Ab2*Fb2b1*(Tb1-Tb2)+alfarad_b22*Ab2*Fb2c1*(Tc1-Tb2)+alfarad_b23*Ab2*Fb2d1*(Td1-Tb2)+alfarad_b24*Ab2*Fb2e*(Te-Tb2)+alfarad_b25*Ab2*Fb2f1*(Tf1-Tb2)+alfarad_b26*Ab2*Fb2g1*(Tg1-Tb2)+alfarad_b27*Ab2*Fb2h1*(Th1-Tb2)+alfarad_b28*Ab2*Fb2i*(Ti1-Tb2)+alfarad_b29*Ab2*Fb2j1*(Tj1-Tb2)+alfarad_b2a*Ab2*Fb2k1*(Tk1-Tb2)+alfarad_b2b*Ab2*Fb2l*(Tl1-Tb2)+alfarad_b2c*Ab2*Fb2m1*(Tm1-Tb2)+alfarad_b2d*Ab2*Fb2n1*(Tn1-Tb2)+alfarad_b2e*Ab2*Fb2o1*(To-Tb2)+alfarad_b2f*Ab2*Fb2p1*(Tp1-Tb2)+alfarad_b2g*Ab2*Fb2q1*(Tq1-Tb2)+alfarad_b2h*Ab2*Fb2r1*(Tr1-Tb2)+alfarad_b2i*Ab2*Fb2s1*(Ts1-Tb2)+alfarad_b2j*Ab2*Fb2t1*(Tt1-Tb2)+alfarad_b2k*Ab2*Fb2u1*(Tu1-Tb2)+alfarad_b2l*Ab2*Fb2v1*(Tv1-Tb2)+alfarad_b2m*Ab2*Fb2w1*(Tw1-Tb2)+alfarad_b2n*Ab2*Fb2x1*(Tx1-Tb2)+alfarad_b2o*Ab2*Fb2y1*(Ty1-Tb2)+alfarad_b2p*Ab2*Fb2z1*(Tz1-Tb2)+alfarad_b2q*Ab2*Fb2aa1*(Taa1-Tb2)+alfarad_b2r*Ab2*Fb2ab1*(Tab1-Tb2)+alfarad_b2s*Ab2*Fb2ac1*(Tbc1-Tb2)+alfarad_b2t*Ab2*Fb2ad1*(Tbd1-Tb2)+alfarad_b2u*Ab2*Fb2ae1*(Tbe1-Tb2)+alfarad_b2v*Ab2*Fb2af1*(Tbf1-Tb2)+alfarad_b2w*Ab2*Fb2ag1*(Tbg1-Tb2)+alfarad_b2x*Ab2*Fb2ah1*(Tbh1-Tb2)+alfarad_b2y*Ab2*Fb2ai1*(Tbi1-Tb2)+alfarad_b2z*Ab2*Fb2aj1*(Tbj1-Tb2)+alfarad_b2aa*Ab2*Fb2ak1*(Tbk1-Tb2)+alfarad_b2ab*Ab2*Fb2al1*(Tbl1-Tb2)+alfarad_b2ac*Ab2*Fb2am1*(Tbm1-Tb2)+alfarad_b2ad*Ab2*Fb2an1*(Tbn1-Tb2)+alfarad_b2ae*Ab2*Fb2ao1*(Tbo1-Tb2)+alfarad_b2af*Ab2*Fb2ap1*(Tbp1-Tb2)+alfarad_b2ag*Ab2*Fb2aq1*(Tbq1-Tb2)+alfarad_b2ah*Ab2*Fb2ar1*(Tbr1-Tb2)+alfarad_b2ai*Ab2*Fb2as1*(Tbs1-Tb2)+alfarad_b2aj*Ab2*Fb2at1*(Tbt1-Tb2)+alfarad_b2ak*Ab2*Fb2au1*(Tbu1-Tb2)+alfarad_b2al*Ab2*Fb2av1*(Tbv1-Tb2)+alfarad_b2am*Ab2*Fb2aw1*(Tbw1-Tb2)+alfarad_b2an*Ab2*Fb2ax1*(Tbx1-Tb2)+alfarad_b2ao*Ab2*Fb2ay1*(Tby1-Tb2)+alfarad_b2ap*Ab2*Fb2az1*(Tbz1-Tb2)+alfarad_b2aq*Ab2*Fb2ba1*(Tba1-Tb2)+alfarad_b2ar*Ab2*Fb2bb1*(Tbb1-Tb2)+alfarad_b2as*Ab2*Fb2bc1*(Tbc1-Tb2)+alfarad_b2at*Ab2*Fb2bd1*(Tbd1-Tb2)+alfarad_b2au*Ab2*Fb2be1*(Tbe1-Tb2)+alfarad_b2av*Ab2*Fb2bf1*(Tbf1-Tb2)+alfarad_b2aw*Ab2*Fb2bg1*(Tbg1-Tb2)+alfarad_b2ax*Ab2*Fb2bh1*(Tbh1-Tb2)+alfarad_b2ay*Ab2*Fb2bi1*(Tbi1-Tb2)+alfarad_b2az*Ab2*Fb2bj1*(Tbj1-Tb2)+alfarad_b2ba*Ab2*Fb2bk1*(Tbk1-Tb2)+alfarad_b2bb*Ab2*Fb2bl1*(Tbl1-Tb2)+alfarad_b2bc*Ab2*Fb2bm1*(Tbm1-Tb2)+alfarad_b2bd*Ab2*Fb2bn1*(Tbn1-Tb2)+alfarad_b2be*Ab2*Fb2bo1*(Tbo1-Tb2)+alfarad_b2bf*Ab2*Fb2bp1*(Tbp1-Tb2)+alfarad_b2bg*Ab2*Fb2bq1*(Tbq1-Tb2)+alfarad_b2bh*Ab2*Fb2br1*(Tbr1-Tb2)+alfarad_b2bi*Ab2*Fb2bs1*(Tbs1-Tb2)+alfarad_b2bj*Ab2*Fb2bt1*(Tbt1-Tb2)+alfarad_b2bk*Ab2*Fb2bu1*(Tbu1-Tb2)+alfarad_b2bl*Ab2*Fb2bv1*(Tbv1-Tb2)+alfarad_b2bm*Ab2*Fb2bw1*(Tbw1-Tb2)+alfarad_b2bn*Ab2*Fb2bx1*(Tbx1-Tb2)+alfarad_b2bo*Ab2*Fb2by1*(Tby1-Tb2)+alfarad_b2bp*Ab2*Fb2bz1*(Tbz1-Tb2)+alfarad_b2bq*Ab2*Fb2ca1*(Tca1-Tb2)+alfarad_b2br*Ab2*Fb2cb1*(Tcb1-Tb2)+alfarad_b2bs*Ab2*Fb2cc1*(Tcc1-Tb2)+alfarad_b2bt*Ab2*Fb2cd1*(Tcd1-Tb2)+alfarad_b2bu*Ab2*Fb2ce1*(Tce1-Tb2)+alfarad_b2bv*Ab2*Fb2cf1*(Tcf1-Tb2)+alfarad_b2bw*Ab2*Fb2cg1*(Tcg1-Tb2)+alfarad_b2bx*Ab2*Fb2ch1*(Tch1-Tb2)+alfarad_b2by*Ab2*Fb2ci1*(Tci1-Tb2)+alfarad_b2bz*Ab2*Fb2cj1*(Tcj1-Tb2)+alfarad_b2ca*Ab2*Fb2ck1*(Tck1-Tb2)+alfarad_b2cb*Ab2*Fb2cl1*(Tcl1-Tb2)+alfarad_b2cc*Ab2*Fb2cm1*(Tcm1-Tb2)+alfarad_b2cd*Ab2*Fb2cn1*(Tcn1-Tb2)+alfarad_b2ce*Ab2*Fb2co1*(Tco1-Tb2)+alfarad_b2cf*Ab2*Fb2cp1*(Tcp1-Tb2)+alfarad_b2cg*Ab2*Fb2cq1*(Tcq1-Tb2)+alfarad_b2ch*Ab2*Fb2cr1*(Tcr1-Tb2)+alfarad_b2ci*Ab2*Fb2cs1*(Tcs1-Tb2)+alfarad_b2cj*Ab2*Fb2ct1*(Tct1-Tb2)+alfarad_b2ck*Ab2*Fb2cu1*(Tcu1-Tb2)+alfarad_b2cl*Ab2*Fb2cv1*(Tcv1-Tb2)+alfarad_b2cm*Ab2*Fb2cw1*(Tcw1-Tb2)+alfarad_b2cn*Ab2*Fb2cx1*(Tcx1-Tb2)+alfarad_b2co*Ab2*Fb2cy1*(Tcy1-Tb2)+alfarad_b2cp*Ab2*Fb2cz1*(Tcz1-Tb2)+alfarad_b2cq*Ab2*Fb2da1*(Tda1-Tb2)+alfarad_b2cr*Ab2*Fb2db1*(Tdb1-Tb2)+alfarad_b2cs*Ab2*Fb2dc1*(Tdc1-Tb2)+alfarad_b2ct*Ab2*Fb2dd1*(Tdd1-Tb2)+alfarad_b2cu*Ab2*Fb2de1*(Tde1-Tb2)+alfarad_b2cv*Ab2*Fb2df1*(Tdf1-Tb2)+alfarad_b2cw*Ab2*Fb2dg1*(Tdg1-Tb2)+alfarad_b2cx*Ab2*Fb2dh1*(Tdh1-Tb2)+alfarad_b2cy*Ab2*Fb2di1*(Tdi1-Tb2)+alfarad_b2cz*Ab2*Fb2dj1*(Tdj1-Tb2)+alfarad_b2da*Ab2*Fb2dk1*(Tdk1-Tb2)+alfarad_b2db*Ab2*Fb2dl1*(Tdl1-Tb2)+alfarad_b2dc*Ab2*Fb2dm1*(Tdm1-Tb2)+alfarad_b2dd*Ab2*Fb2dn1*(Tdn1-Tb2)+alfarad_b2de*Ab2*Fb2do1*(Tdo1-Tb2)+alfarad_b2df*Ab2*Fb2dp1*(Tdp1-Tb2)+alfarad_b2dg*Ab2*Fb2dq1*(Tdq1-Tb2)+alfarad_b2dh*Ab2*Fb2dr1*(Tdr1-Tb2)+alfarad_b2di*Ab2*Fb2ds1*(Tds1-Tb2)+alfarad_b2dj*Ab2*Fb2dt1*(Tdt1-Tb2)+alfarad_b2dk*Ab2*Fb2du1*(Tdu1-Tb2)+alfarad_b2dl*Ab2*Fb2dv1*(Tdv1-Tb2)+alfarad_b2dm*Ab2*Fb2dw1*(Tdw1-Tb2)+alfarad_b2dn*Ab2*Fb2dx1*(Tdx1-Tb2)+alfarad_b2do*Ab2*Fb2dy1*(Tdy1-Tb2)+alfarad_b2dp*Ab2*Fb2dz1*(Tdz1-Tb2)+alfarad_b2dq*Ab2*Fb2ea1*(Tea1-Tb2)+alfarad_b2dr*Ab2*Fb2eb1*(Teb1-Tb2)+alfarad_b2ds*Ab2*Fb2ec1*(Tec1-Tb2)+alfarad_b2dt*Ab2*Fb2ed1*(Ted1-Tb2)+alfarad_b2du*Ab2*Fb2ef1*(Tef1-Tb2)+alfarad_b2dv*Ab2*Fb2eg1*(Teg1-Tb2)+alfarad_b2dw*Ab2*Fb2eh1*(Teh1-Tb2)+alfarad_b2dx*Ab2*Fb2ei1*(Tei1-Tb2)+alfarad_b2dy*Ab2*Fb2ej1*(Tej1-Tb2)+alfarad_b2dz*Ab2*Fb2ek1*(Tek1-Tb2)+alfarad_b2ea*Ab2*Fb2el1*(Tel1-Tb2)+alfarad_b2eb*Ab2*Fb2em1*(Tem1-Tb2)+alfarad_b2ec*Ab2*Fb2en1*(Ten1-Tb2)+alfarad_b2ed*Ab2*Fb2eo1*(Teo1-Tb2)+alfarad_b2ef*Ab2*Fb2ep1*(Tep1-Tb2)+alfarad_b2eg*Ab2*Fb2eq1*(Teq1-Tb2)+alfarad_b2eh*Ab2*Fb2er1*(Ter1-Tb2)+alfarad_b2ei*Ab2*Fb2es1*(Tes1-Tb2)+alfarad_b2ej*Ab2*Fb2et1*(Tet1-Tb2)+alfarad_b2ek*Ab2*Fb2eu1*(Teu1-Tb2)+alfarad_b2el*Ab2*Fb2ev1*(Tev1-Tb2)+alfarad_b2em*Ab2*Fb2ew1*(Tew1-Tb2)+alfarad_b2en*Ab2*Fb2ex1*(Tex1-Tb2)+alfarad_b2eo*Ab2*Fb2ey1*(Tey1-Tb2)+alfarad_b2ep*Ab2*Fb2ez1*(Tez1-Tb2)+alfarad_b2eq*Ab2*Fb2fa1*(Tfa1-Tb2)+alfarad_b2er*Ab2*Fb2fb1*(Tfb1-Tb2)+alfarad_b2es*Ab2*Fb2fc1*(Tfc1-Tb2)+alfarad_b2et*Ab2*Fb2fd1*(Tfd1-Tb2)+alfarad_b2eu*Ab2*Fb2fe1*(Tfe1-Tb2)+alfarad_b2ev*Ab2*Fb2fg1*(Tfg1-Tb2)+alfarad_b2ew*Ab2*Fb2fh1*(Tfh1-Tb2)+alfarad_b2ex*Ab2*Fb2fi1*(Tfi1-Tb2)+alfarad_b2ey*Ab2*Fb2fj1*(Tfj1-Tb2)+alfarad_b2ez*Ab2*Fb2fk1*(Tfk1-Tb2)+alfarad_b2fa*Ab2*Fb2fl1*(Tfl1-Tb2)+alfarad_b2fb*Ab2*Fb2fm1*(Tfm1-Tb2)+alfarad_b2fc*Ab2*Fb2fn1*(Tfn1-Tb2)+alfarad_b2fd*Ab2*Fb2fo1*(Tfo1-Tb2)+alfarad_b2fe*Ab2*Fb2fp1*(Tfp1-Tb2)+alfarad_b2fg*Ab2*Fb2fq1*(Tfq1-Tb2)+alfarad_b2fh*Ab2*Fb2fr1*(Tfr1-Tb2)+alfarad_b2fi*Ab2*Fb2fs1*(Tfs1-Tb2)+alfarad_b2fj*Ab2*Fb2ft1*(Tft1-Tb2)+alfarad_b2fk*Ab2*Fb2fu1*(Tfu1-Tb2)+alfarad_b2fl*Ab2*Fb2fv1*(Tfv1-Tb2)+alfarad_b2fm*Ab2*Fb2fw1*(Tfw1-Tb2)+alfarad_b2fn*Ab2*Fb2fx1*(Tfx1-Tb2)+alfarad_b2fo*Ab2*Fb2fy1*(Tfy1-Tb2)+alfarad_b2fp*Ab2*Fb2fz1*(Tfz1-Tb2)+alfarad_b2fq*Ab2*Fb2ga1*(Tga1-Tb2)+alfarad_b2fr*Ab2*Fb2gb1*(Tgb1-Tb2)+alfarad_b2fs*Ab2*Fb2gc1*(Tgc1-Tb2)+alfarad_b2ft*Ab2*Fb2gd1*(Tgd1-Tb2)+alfarad_b2fu*Ab2*Fb2ge1*(Tge1-Tb2)+alfarad_b2fv*Ab2*Fb2gf1*(Tgf1-Tb2)+alfarad_b2fw*Ab2*Fb2gh1*(Tgh1-Tb2)+alfarad_b2fx*Ab2*Fb2gi1*(Tgi1-Tb2)+alfarad_b2fy*Ab2*Fb2gj1*(Tgj1-Tb2)+alfarad_b2fz*Ab2*Fb2hk1*(Thk1-Tb2)+alfarad_b2ga*Ab2*Fb2hl1*(Thl1-Tb2)+alfarad_b2gb*Ab2*Fb2hm1*(Thm1-Tb2)+alfarad_b2gc*Ab2*Fb2hn1*(Thn1-Tb2)+alfarad_b2gd*Ab2*Fb2ho1*(Tho1-Tb2)+alfarad_b2ge*Ab2*Fb2hp1*(Thp1-Tb2)+alfarad_b2gf*Ab2*Fb2hq1*(Thq1-Tb2)+alfarad_b2gh*Ab2*Fb2hr1*(Thr1-Tb2)+alfarad_b2gi*Ab2*Fb2hs1*(Ths1-Tb2)+alfarad_b2gj*Ab2*Fb2ht1*(Tht1-Tb2)+alfarad_b2hk*Ab2*Fb2hu1*(Thu1-Tb2)+alfarad_b2hl*Ab2*Fb2hv1*(Thv1-Tb2)+alfarad_b2hm*Ab2*Fb2hw1*(Thw1-Tb2)+alfarad_b2hn*Ab2*Fb2hx1*(Thx1-Tb2)+alfarad_b2ho*Ab2*Fb2hy1*(Thy1-Tb2)+alfarad_b2hp*Ab2*Fb2hz1*(Thz1-Tb2)+alfarad_b2hq*Ab2*Fb2ia1*(Tia1-Tb2)+alfarad_b2hr*Ab2*Fb2ib1*(Tib1-Tb2)+alfarad_b2hs*Ab2*Fb2ic1*(Tic1-Tb2)+alfarad_b2ht*Ab2*Fb2id1*(Tid1-Tb2)+alfarad_b2hu*Ab2*Fb2ie1*(Tie1-Tb2)+alfarad_b2hv*Ab2*Fb2if1*(Tif1-Tb2)+alfarad_b2hw*Ab2*Fb2ig1*(Tig1-Tb2)+alfarad_b2hx*Ab2*Fb2ih1*(Tih1-Tb2)+alfarad_b2hy*Ab2*Fb2ij1*(Tij1-Tb2)+alfarad_b2hz*Ab2*Fb2ik1*(Tik1-Tb2)+alfarad_b2ia*Ab2*Fb2il1*(Til1-Tb2)+alfarad_b2ib*Ab2*Fb2im1*(Tim1-Tb2)+alfarad_b2ic*Ab2*Fb2in1*(Tin1-Tb2)+alfarad_b2id*Ab2*Fb2io1*(Tio1-Tb2)+alfarad_b2ie*Ab2*Fb2ip1*(Tip1-Tb2)+alfarad_b2if*Ab2*Fb2iq1*(Tiq1-Tb2)+alfarad_b2ig*Ab2*Fb2ir1*(Tir1-Tb2)+alfarad_b2ih*Ab2*Fb2is1*(Tis1-Tb2)+alfarad_b2ij*Ab2*Fb2it1*(Tit1-Tb2)+alfarad_b2ik*Ab2*Fb2iu1*(Tiu1-Tb2)+alfarad_b2il*Ab2*Fb2iv1*(Tiv1-Tb2)+alfarad_b2im*Ab2*Fb2iw1*(Tiw1-Tb2)+alfarad_b2in*Ab2*Fb2ix1*(Tix1-Tb2)+alfarad_b2io*Ab2*Fb2iy1*(Tiy1-Tb2)+alfarad_b2ip*Ab2*Fb2iz1*(Tiz1-Tb2)+alfarad_b2iq*Ab2*Fb2ja1*(Tja1-Tb2)+alfarad_b2ir*Ab2*Fb2jb1*(Tjb1-Tb2)+alfarad_b2is*Ab2*Fb2jc1*(Tjc1-Tb2)+alfarad_b2it*Ab2*Fb2jd1*(Tjd1-Tb2)+alfarad_b2iu*Ab2*Fb2je1*(Tje1-Tb2)+alfarad_b2iv*Ab2*Fb2jf1*(Tjf1-Tb2)+alfarad_b2iw*Ab2*Fb2jg1*(Tjg1-Tb2)+alfarad_b2ix*Ab2*Fb2jh1*(Tjh1-Tb2)+alfarad_b2iy*Ab2*Fb2ji1*(Tji1-Tb2)+alfarad_b2iz*Ab2*Fb2jk1*(Tjk1-Tb2)+alfarad_b2ja*Ab2*Fb2jl1*(Tjl1-Tb2)+alfarad_b2jb*Ab2*Fb2jm1*(Tjm1-Tb2)+alfarad_b2jc*Ab2*Fb2jn1*(Tjn1-Tb2)+alfarad_b2jd*Ab2*Fb2jo1*(Tjo1-Tb2)+alfarad_b2je*Ab2*Fb2jp1*(Tjp1-Tb2)+alfarad_b2jf*Ab2*Fb2jq1*(Tjq1-Tb2)+alfarad_b2jg*Ab2*Fb2jr1*(Tjr1-Tb2)+alfarad_b2jh*Ab2*Fb2js1*(Tjs1-Tb2)+alfarad_b2ji*Ab2*Fb2jt1*(Tjt1-Tb2)+alfarad_b2jk*Ab2*Fb2ju1*(Tju1-Tb2)+alfarad_b2jl*Ab2*Fb2jv1*(Tjv1-Tb2)+alfarad_b2jm*Ab2*Fb2jw1*(Tjw1-Tb2)+alfarad_b2jn*Ab2*Fb2jx1*(Tjx1-Tb2)+alfarad_b2jo*Ab2*Fb2jy1*(Tjy1-Tb2)+alfarad_b2jp*Ab2*Fb2jz1*(Tjz1-Tb2)+alfarad_b2jq*Ab2*Fb2ka1*(Tka1-Tb2)+alfarad_b2jr*Ab2*Fb2kb1*(Tkb1-Tb2)+alfarad_b2js*Ab2*Fb2kc1*(Tkc1-Tb2)+alfarad_b2jt*Ab2*Fb2kd1*(Tkd1-Tb2)+alfarad_b2ju*Ab2*Fb2ke1*(Tke1-Tb2)+alfarad_b2jv*Ab2*Fb2kf1*(Tkf1-Tb2)+alfarad_b2jw*Ab2*Fb2kg1*(Tkg1-Tb2)+alfarad_b2jx*Ab2*Fb2kh1*(Tkh1-Tb2)+alfarad_b2jy*Ab2*Fb2ki1*(Tki1-Tb2)+alfarad_b2jz*Ab2*Fb2kl1*(Tkl1-Tb2)+alfarad_b2ka*Ab2*Fb2km1*(Tkm1-Tb2)+alfarad_b2kb*Ab2*Fb2kn1*(Tkn1-Tb2)+alfarad_b2kc*Ab2*Fb2ko1*(Tko1-Tb2)+alfarad_b2kd*Ab2*Fb2kp1*(Tkp1-Tb2)+alfarad_b2ke*Ab2*Fb2kq1*(Tkq1-Tb2)+alfarad_b2kf*Ab2*Fb2kr1*(Tkr1-Tb2)+alfarad_b2kh*Ab2*Fb2ks1*(Tks1-Tb2)+alfarad_b2ki*Ab2*Fb2kt1*(Tkt1-Tb2)+alfarad_b2kj*Ab2*Fb2ku1*(Tku1-Tb2)+alfarad_b2kl*Ab2*Fb2kv1*(Tkv1-Tb2)+alfarad_b2km*Ab2*Fb2kw1*(Tkw1-Tb2)+alfarad_b2kn*Ab2*Fb2kx1*(Tkx1-Tb2)+alfarad_b2ko*Ab2*Fb2ky1*(Tky1-Tb2)+alfarad_b2kp*Ab2*Fb2kz1*(Tkz1-Tb2)+alfarad_b2kq*Ab2*Fb2la1*(Tla1-Tb2)+alfarad_b2kr*Ab2*Fb2lb1*(Tlb1-Tb2)+alfarad_b2ks*Ab2*Fb2lc1*(Tlc1-Tb2)+alfarad_b2kt*Ab2*Fb2ld1*(Tld1-Tb2)+alfarad_b2ku*Ab2*Fb2le1*(Tle1-Tb2)+alfarad_b2kv*Ab2*Fb2lf1*(Tlf1-Tb2)+alfarad_b2kw*Ab2*Fb2lg1*(Tlg1-Tb2)+alfarad_b2kx*Ab2*Fb2lh1*(Tlh1-Tb2)+alfarad_b2ky*Ab2*Fb2li1*(Tli1-Tb2)+alfarad_b2kz*Ab2*Fb2lj1*(Tlj1-Tb2)+alfarad_b2la*Ab2*Fb2lk1*(Tlk1-Tb2)+alfarad_b2lb*Ab2*Fb2lm1*(Tlm1-Tb2)+alfarad_b2lc*Ab2*Fb2ln1*(Tln1-Tb2)+alfarad_b2ld*Ab2*Fb2lo1*(Tlo1-Tb2)+alfarad_b2le*Ab2*Fb2lp1*(Tlp1-Tb2)+alfarad_b2lf*Ab2*Fb2lq1*(Tlq1-Tb2)+alfarad_b2lh*Ab2*Fb2lr1*(Tlr1-Tb2)+alfarad_b2li*Ab2*Fb2ls1*(Tls1-Tb2)+alfarad_b2lj*Ab2*Fb2lt1*(Tlt1-Tb2)+alfarad_b2lk*Ab2*Fb2lu1*(Tlu1-Tb2)+alfarad_b2lm*Ab2*Fb2lv1*(Tlv1-Tb2)+alfarad_b2ln*Ab2*Fb2lw1*(Tlw1-Tb2)+alfarad_b2lo*Ab2*Fb2lx1*(Tlx1-Tb2)+alfarad_b2lp*Ab2*Fb2ly1*(Tly1-Tb2)+alfarad_b2lq*Ab2*Fb2lz1*(Tlz1-Tb2)+alfarad_b2lq*Ab2*Fb2ma1*(Tma1-Tb2)+alfarad_b2lr*Ab2*Fb2mb1*(Tmb1-Tb2)+alfarad_b2ls*Ab2*Fb2mc1*(Tmc1-Tb2)+alfarad_b2lt*Ab2*Fb2md1*(Tmd1-Tb2)+alfarad_b2lu*Ab2*Fb2me1*(Tme1-Tb2)+alfarad_b2lv*Ab2*Fb2mf1*(Tmf1-Tb2)+alfarad_b2lw*Ab2*Fb2mg1*(Tmg1-Tb2)+alfarad_b2lx*Ab2*Fb2mh1*(Tmh1-Tb2)+alfarad_b2ly*Ab2*Fb2mi1*(Tmi1-Tb2)+alfarad_b2lz*Ab2*Fb2mj1*(Tmj1-Tb2)+alfarad_b2ma*Ab2*Fb2mk1*(Tmk1-Tb2)+alfarad_b2mb*Ab2*Fb2ml1*(Tml1-Tb2)+alfarad_b2mc*Ab2*Fb2mn1*(Tmn1-Tb2)+alfarad_b2md*Ab2*Fb2mo1*(Tmo1-Tb2)+alfarad_b2me*Ab2*Fb2mp1*(Tmp1-Tb2)+alfarad_b2mf*Ab2*Fb2mq1*(Tmq1-Tb2)+alfarad_b2mh*Ab2*Fb2mr1*(Tmr1-Tb2)+alfarad_b2mi*Ab2*Fb2ms1*(Tms1-Tb2)+alfarad_b2mj*Ab2*Fb2mt1*(Tmt1-Tb2)+alfarad_b2mk*Ab2*Fb2mu1*(Tmu1-Tb2)+alfarad_b2ml*Ab2*Fb2mv1*(Tmv1-Tb2)+alfarad_b2mn*Ab2*Fb2mw1*(Tmw1-Tb2)+alfarad_b2mo*Ab2*Fb2mx1*(Tmx1-Tb2)+alfarad_b2mp*Ab2*Fb2my1*(Tmy1-Tb2)+alfarad_b2mq*Ab2*Fb2mz1*(Tmz1-Tb2)+alfarad_b2mq*Ab2*Fb2na1*(Tna1-Tb2)+alfarad_b2mr*Ab2*Fb2nb1*(Tnb1-Tb2)+alfarad_b2ms*Ab2*Fb2nc1*(Tnc1-Tb2)+alfarad_b2mt*Ab2*Fb2nd1*(Tnd1-Tb2)+alfarad_b2mu*Ab2*Fb2ne1*(Tne1-Tb2)+alfarad_b2mv*Ab2*Fb2nf1*(Tnf1-Tb2)+alfarad_b2mw*Ab2*Fb2ng1*(Tng1-Tb2)+alfarad_b2mx*Ab2*Fb2nh1*(Tnh1-Tb2)+alfarad_b2my*Ab2*Fb2ni1*(Tni1-Tb2)+alfarad_b2mz*Ab2*Fb2nj1*(Tnj1-Tb2)+alfarad_b2na*Ab2*Fb2nk1*(Tnk1-Tb2)+alfarad_b2nb*Ab2*Fb2nl1*(Tnl1-Tb2)+alfarad_b2nc*Ab2*Fb2no1*(Tno1-Tb2)+alfarad_b2nd*Ab								

wall h2		window j2		inned floor		inner wall	
NODE h2	Ah2*(Xcor_h2*Tpast)	NODE j2	0	NODE n	An*(Xcor_n*Tpast)	NODE p	Ap*(Xcor_p*Tpast)
solar from section 1		solar from section 1		convection and conduction		convection and conduction	
SOLAR_wb1	Ab1*D1*Qz*Fb1h2	SOLAR_wb1	Ab1*A1*Qz*Fb1j2	CONVECTION_j	alfaconv_ni*An*(Ti-Tn)	CONVECTION_j	alfaconv_pi*Ap*(Ti-Tp)
SOLAR_wd1	Ad1*D1*Qz*Fd1h2	SOLAR_wd1	Ad1*A1*Qz*Fd1j2	ABSORPTION	An*X0_n*In	ABSORPTION	Ap*X0_p*Ip
SOLAR_wf1	Af1*D1*Qz*Ff1h2	SOLAR_wf1	Af1*A1*Qz*Ff1j2	ABSORPTION_n	An*(Xcor_n*Tpast)	ABSORPTION_n	Ap*(Xcor_p*Tpast)
SOLAR_wk1	Ak1*D1*Qz*Fk1h2	SOLAR_wk1	Ak1*A1*Qz*Fk1j2	solar from section 1		solar from section 1	
solar from section 2		solar from section 2		SOLAR_wb1	Ab1*D1*Qz*Fb1n	SOLAR_wb1	Ab1*D1*Qz*Fb1p
SOLAR_wa2	Aa2*D1*Qz*Fa2h2	SOLAR_wa2	Aj2*A1*Qz	SOLAR_wd1	Ad1*D1*Qz*Fd1n	SOLAR_wd1	Ad1*D1*Qz*Fd1p
convection and conduction		convection and conduction		SOLAR_wf1	Af1*D1*Qz*Ff1n	SOLAR_wf1	Af1*D1*Qz*Ff1p
CONVECTION_o	alfaconv_h2o*Ah2*(To-Th2)	CONVECTION_o	Aa2*A1*Qz*Fa2j2	SOLAR_wk1	Ak1*D1*Qz*Fk1n	SOLAR_wk1	Ak1*D1*Qz*Fk1p
CONVECTION_j	alfaconv_h2i*Ah2*(Ti-Th2)	CONVECTION_o	alfaconv_j2o*Aj2*(To-Tj2)	solar from section 2		solar from section 2	
CONDUCTION	(1/(1/alfaov_h2)+Rc_h2))*Ah2*(To-Th2)	CONVECTION_j	alfaconv_j2i*Aj2*(Ti-Tj2)	SOLAR_wa2	Aa2*D1*Qz*Fa2n	SOLAR_wa2	Aa2*D1*Qz*Fa2p
ABSORPTION	Ah2*X0_h2*Th2	radiation to section 1		SOLAR_wj2	Aj2*D1*Qz*Fj2n	SOLAR_wj2	Aj2*D1*Qz*Fj2p
ABSORPTION_n	Ah2*(Xcor_h2*Tpast)	RADIATION_a1	alfarad_j2*Aj2*Fj2a1*(Ta1-Tj2)	radiation to section 1		radiation to section 1	
radiation to section 1		RADIATION_b1	alfarad_j2*Aj2*Fj2b1*(Tb1-Tj2)	RADIATION_a1	alfarad_n*An*Fna1*(Ta1-Tn)	RADIATION_a1	alfarad_p*Ap*Fpa1*(Ta1-Tp)
RADIATION_a1	alfarad_h2*Ah2*Fh2a1*(Ta1-Th2)	RADIATION_c1	alfarad_j2*Aj2*Fj2c1*(Tc1-Tj2)	RADIATION_b1	alfarad_n*An*Fnb1*(Tb1-Tn)	RADIATION_b1	alfarad_p*Ap*Fpb1*(Tb1-Tp)
RADIATION_b1	alfarad_h2*Ah2*Fh2b1*(Tb1-Th2)	RADIATION_d1	alfarad_j2*Aj2*Fj2d1*(Td1-Tj2)	RADIATION_c1	alfarad_n*An*Fnc1*(Tc1-Tn)	RADIATION_c1	alfarad_p*Ap*Fpc1*(Tc1-Tp)
RADIATION_c1	alfarad_h2*Ah2*Fh2c1*(Tc1-Th2)	RADIATION_f1	alfarad_j2*Aj2*Fj2f1*(Tf1-Tj2)	RADIATION_d1	alfarad_n*An*Fnd1*(Td1-Tn)	RADIATION_d1	alfarad_p*Ap*Fpd1*(Td1-Tp)
RADIATION_d1	alfarad_h2*Ah2*Fh2d1*(Td1-Th2)	RADIATION_g1	alfarad_j2*Aj2*Fj2g1*(Tg1-Tj2)	RADIATION_f1	alfarad_n*An*Fnf1*(Tf1-Tn)	RADIATION_f1	alfarad_p*Ap*Fpf1*(Tf1-Tp)
RADIATION_f1	alfarad_h2*Ah2*Fh2f1*(Tf1-Th2)	RADIATION_h1	alfarad_j2*Aj2*Fj2h1*(Th1-Tj2)	RADIATION_g1	alfarad_n*An*Fng1*(Tg1-Tn)	RADIATION_g1	alfarad_p*Ap*Fpg1*(Tg1-Tp)
RADIATION_g1	alfarad_h2*Ah2*Fh2g1*(Tg1-Th2)	RADIATION_j1	alfarad_j2*Aj2*Fj2j1*(Tj1-Tj2)	RADIATION_h1	alfarad_n*An*Fnh1*(Th1-Tn)	RADIATION_h1	alfarad_p*Ap*Fph1*(Th1-Tp)
RADIATION_h1	alfarad_h2*Ah2*Fh2h1*(Th1-Th2)	RADIATION_k1	alfarad_j2*Aj2*Fj2k1*(Tk1-Tj2)	RADIATION_j1	alfarad_n*An*Fnj1*(Tj1-Tn)	RADIATION_j1	alfarad_p*Ap*Fpj1*(Tj1-Tp)
RADIATION_j1	alfarad_h2*Ah2*Fh2j1*(Tj1-Th2)	RADIATION_m1	alfarad_j2*Aj2*Fj2m1*(Tm1-Tj2)	RADIATION_k1	alfarad_n*An*Fnk1*(Tk1-Tn)	RADIATION_k1	alfarad_p*Ap*Fpk1*(Tk1-Tp)
RADIATION_k1	alfarad_h2*Ah2*Fh2k1*(Tk1-Th2)	radiation to section 2		RADIATION_m1	alfarad_n*An*Fnm1*(Tm1-Tn)	RADIATION_m1	alfarad_p*Ap*Fpm1*(Tm1-Tp)
RADIATION_m1	alfarad_h2*Ah2*Fh2m1*(Tm1-Th2)	RADIATION_a2	alfarad_j2*Aj2*Fj2a2*(Ta2-Tj2)	radiation to section 2		radiation to section 2	
radiation to section 2		RADIATION_b2	alfarad_j2*Aj2*Fj2b2*(Tb2-Tj2)	RADIATION_a2	alfarad_n*An*Fna2*(Ta2-Tn)	RADIATION_a2	alfarad_p*Ap*Fpa2*(Ta2-Tp)
RADIATION_a2	alfarad_h2*Ah2*Fh2a2*(Ta2-Th2)	RADIATION_c2	alfarad_j2*Aj2*Fj2c2*(Tc2-Tj2)	RADIATION_b2	alfarad_n*An*Fnb2*(Tb2-Tn)	RADIATION_b2	alfarad_p*Ap*Fpb2*(Tb2-Tp)
RADIATION_b2	alfarad_h2*Ah2*Fh2b2*(Tb2-Th2)	RADIATION_d2	alfarad_j2*Aj2*Fj2d2*(Td2-Tj2)	RADIATION_c2	alfarad_n*An*Fnc2*(Tc2-Tn)	RADIATION_c2	alfarad_p*Ap*Fpc2*(Tc2-Tp)
RADIATION_c2	alfarad_h2*Ah2*Fh2c2*(Tc2-Th2)	radiation to roof i and floor e		RADIATION_d2	alfarad_n*An*Fnd2*(Td2-Tn)	RADIATION_d2	alfarad_p*Ap*Fpd2*(Td2-Tp)
RADIATION_d2	alfarad_h2*Ah2*Fh2d2*(Td2-Th2)	RADIATION_e	alfarad_j2*Aj2*Fj2e*(Te-Tj2)	RADIATION_f2	alfarad_n*An*Fnf2*(Tf2-Tn)	RADIATION_f2	alfarad_p*Ap*Fpf2*(Tf2-Tp)
radiation to roof i and floor e		RADIATION_j	alfarad_j2*Aj2*Fj2j*(Tj-Tj2)	RADIATION_g2	alfarad_n*An*Fng2*(Tg2-Tn)	RADIATION_g2	alfarad_p*Ap*Fpg2*(Tg2-Tp)
RADIATION_e	alfarad_h2*Ah2*Fh2e*(Te-Th2)	RADIATION_i		RADIATION_h2	alfarad_n*An*Fnh2*(Th2-Tn)	RADIATION_h2	alfarad_p*Ap*Fph2*(Th2-Tp)
RADIATION_j	alfarad_h2*Ah2*Fh2j*(Tj-Th2)			RADIATION_j2	alfarad_n*An*Fnj2*(Tj2-Tn)	RADIATION_j2	alfarad_p*Ap*Fpj2*(Tj2-Tp)
				radiation to roof i and floor e		radiation to roof i and floor e	
				RADIATION_e	alfarad_n*An*Fne*(Te-Tn)	RADIATION_e	alfarad_p*Ap*Fpe*(Te-Tp)
				RADIATION_j	alfarad_n*An*Fnj*(Tj-Tn)	RADIATION_j	alfarad_p*Ap*Fpj*(Tj-Tp)
				RADIATION_p	alfarad_n*An*Fnp*(Tp-Tn)	RADIATION_n	alfarad_p*Ap*Fpn*(Tp-Tp)

right equation	Ab1*D1*Qz*Fb1h2+Ad1*D1*Qz*Fd1h2+Af1*D1*Qz*Ff1h2+Ak1*D1*Qz*Fk1h2+Aa2*D1*Qz*Fa2h2+alfaconv_h2o*Ah2*(To-Th2)+alfaconv_h2i*Ah2*(Ti-Th2)+(1/(1/alfaov_h2)+Rc_h2))*Ah2*(To-Th2)+Ah2*X0_h2*Th2+alfarad_h2*Ah2*Fh2a1*(Ta1-Th2)+alfarad_h2*Ah2*Fh2b1*(Tb1-Th2)+alfarad_h2*Ah2*Fh2c1*(Tc1-Th2)+alfarad_h2*Ah2*Fh2d1*(Td1-Th2)+alfarad_h2*Ah2*Fh2e*(Te-Th2)+alfarad_h2*Ah2*Fh2f1*(Tf1-Th2)+alfarad_h2*Ah2*Fh2g1*(Tg1-Th2)+alfarad_h2*Ah2*Fh2h1*(Th1-Th2)+alfarad_h2*Ah2*Fh2j1*(Tj1-Th2)+alfarad_h2*Ah2*Fh2k1*(Tk1-Th2)+alfarad_h2*Ah2*Fh2m1*(Tm1-Th2)+alfarad_h2*Ah2*Fh2a2*(Ta2-Th2)+alfarad_h2*Ah2*Fh2b2*(Tb2-Th2)+alfarad_h2*Ah2*Fh2c2*(Tc2-Th2)+alfarad_h2*Ah2*Fh2d2*(Td2-Th2)+alfarad_h2*Ah2*Fh2e*(Te-Th2)+alfarad_h2*Ah2*Fh2j*(Tj-Th2)	right equation	Ab1*A1*Qz*Fb1j2+Ad1*A1*Qz*Fd1j2+Af1*A1*Qz*Ff1j2+Ak1*A1*Qz*Fk1j2+Aa2*A1*Qz*Fa2j2+alfaconv_j2o*Aj2*(To-Tj2)+alfaconv_j2i*Aj2*(Ti-Tj2)+alfarad_j2*Aj2*Fj2a1*(Ta1-Tj2)+alfarad_j2*Aj2*Fj2b1*(Tb1-Tj2)+alfarad_j2*Aj2*Fj2c1*(Tc1-Tj2)+alfarad_j2*Aj2*Fj2d1*(Td1-Tj2)+alfarad_j2*Aj2*Fj2e*(Tf1-Tj2)+alfarad_j2*Aj2*Fj2f1*(Tf1-Tj2)+alfarad_j2*Aj2*Fj2g1*(Tg1-Tj2)+alfarad_j2*Aj2*Fj2h1*(Th1-Tj2)+alfarad_j2*Aj2*Fj2j1*(Tj1-Tj2)+alfarad_j2*Aj2*Fj2k1*(Tk1-Tj2)+alfarad_j2*Aj2*Fj2m1*(Tm1-Tj2)	right equation	alfaconv_ni*An*(Ti-Tn)+An*X0_n*In+Ab1*D1*Qz*Fb1n+Ad1*D1*Qz*Fd1n+Af1*D1*Qz*Ff1n+Ak1*D1*Qz*Fk1n+Aa2*D1*Qz*Fa2n+alfaconv_ni*An*(Ti-Tn)+alfaconv_ni*An*Fna1*(Ta1-Tn)+alfaconv_ni*An*Fnb1*(Tb1-Tn)+alfaconv_ni*An*Fnc1*(Tc1-Tn)+alfaconv_ni*An*Fnd1*(Td1-Tn)+alfaconv_ni*An*Fnf1*(Tf1-Tn)+alfaconv_ni*An*Fng1*(Tg1-Tn)+alfaconv_ni*An*Fnh1*(Th1-Tn)+alfaconv_ni*An*Fnj1*(Tj1-Tn)+alfarad_n*An*Fna1*(Ta1-Tn)+alfarad_n*An*Fnb1*(Tb1-Tn)+alfarad_n*An*Fnc1*(Tc1-Tn)+alfarad_n*An*Fnd1*(Td1-Tn)+alfarad_n*An*Fnf1*(Tf1-Tn)+alfarad_n*An*Fng1*(Tg1-Tn)+alfarad_n*An*Fnh1*(Th1-Tn)+alfarad_n*An*Fnj1*(Tj1-Tn)+alfarad_n*An*Fne*(Te-Tn)+alfarad_n*An*Fni*(Ti-Tn)+alfarad_n*An*Fnp*(Tp-Tn)	right equation	alfaconv_pi*Ap*(Ti-Tp)+Ap*X0_p*Ip+Ab1*D1*Qz*Fb1p+Ad1*D1*Qz*Fd1p+Af1*D1*Qz*Ff1p+Ak1*D1*Qz*Fk1p+Aa2*D1*Qz*Fa2p+alfaconv_pi*Ap*(Ti-Tp)+alfaconv_pi*Ap*Fpa1*(Ta1-Tp)+alfaconv_pi*Ap*Fpb1*(Tb1-Tp)+alfaconv_pi*Ap*Fpc1*(Tc1-Tp)+alfaconv_pi*Ap*Fpd1*(Td1-Tp)+alfaconv_pi*Ap*Fpf1*(Tf1-Tp)+alfaconv_pi*Ap*Fpg1*(Tg1-Tp)+alfaconv_pi*Ap*Fph1*(Th1-Tp)+alfaconv_pi*Ap*Fpj1*(Tj1-Tp)+alfarad_p*Ap*Fpa1*(Ta1-Tp)+alfarad_p*Ap*Fpb1*(Tb1-Tp)+alfarad_p*Ap*Fpc1*(Tc1-Tp)+alfarad_p*Ap*Fpd1*(Td1-Tp)+alfarad_p*Ap*Fpe*(Te-Tp)+alfarad_p*Ap*Fpf1*(Tf1-Tp)+alfarad_p*Ap*Fpg1*(Tg1-Tp)+alfarad_p*Ap*Fph1*(Th1-Tp)+alfarad_p*Ap*Fpj1*(Tj1-Tp)+alfarad_p*Ap*Fpn*(Tp-Tp)
left equation	Ah2*(Xcor_h2*Tpast)	left equation	0	left equation	An*(Xcor_n*Tpast)	left equation	Ap*(Xcor_p*Tpast)

Appendix H

Model version 3

wall floor roof	0	window b	1	indoor air	2	inner floor	3	inner wall	4
NODE a	$Aa \cdot Xcor_a \cdot Tpast$	NODE b	0	NODE i	0	NODE c	$Ac \cdot Xcor_c \cdot Tpast$	NODE d	$Ad \cdot Xcor_d \cdot Tpast$
solar from section 1		solar from section 1		ventilation		convection and conduction		convection and conduction	
SOLAR	$Aa \cdot D1 \cdot Qz$	SOLAR	$Ab \cdot A1 \cdot Qz$	ADVECTION	$vent \cdot person \cdot rho_air \cdot Cp_air \cdot (To - Ti)$	CONVECTION_i	$alfaconv_ai \cdot Ac \cdot (Ti - Tc)$	CONVECTION_i	$alfaconv_ai \cdot Ad \cdot (Ti - Td)$
SOLAR_wb	$Ab \cdot D1 \cdot Qz \cdot Fba$	convection and conduction		convection with section 1		ABSORPTION	$Ac \cdot X0_c \cdot Tc$	ABSORPTION	$Ad \cdot X0_d \cdot Td$
convection and conduction		CONVECTION_o	$alfaconv_bo \cdot Ab \cdot (To - Tb)$	CONVECTION_a	$alfaconv_ai \cdot Aa \cdot (Ta - Ti)$	ABSORPTION_n	$Ac \cdot Xcor_c \cdot Tpast$	ABSORPTION_n	$Ad \cdot Xcor_d \cdot Tpast$
CONVECTION_o	$alfaconv_ao \cdot Aa \cdot (To - Ta)$	CONVECTION_i	$alfaconv_bi \cdot Ab \cdot (Ti - Tb)$	CONVECTION_b	$alfaconv_bi \cdot Ab \cdot (Tb - Ti)$	radiation to section 1		radiation to section 1	
CONVECTION_i	$alfaconv_ai \cdot Aa \cdot (Ti - Ta)$	radiation to section 1		heat load		RADIATION_a	$alfarad_c \cdot Ac \cdot Fca \cdot (Ta - Tc)$	RADIATION_a	$alfarad_d \cdot Ad \cdot Fda \cdot (Ta - Td)$
CONDUCTION		RADIATION_a	$alfarad_b \cdot Ab \cdot Fba \cdot (Ta - Tb)$	INTERNAL LOAD	Qint	RADIATION_b	$alfarad_c \cdot Ac \cdot Fcb \cdot (Tb - Tc)$	RADIATION_b	$alfarad_d \cdot Ad \cdot Fdb \cdot (Tb - Td)$
ABSORPTION	$Aa \cdot X0_a \cdot Ta$	RADIATION_c	$alfarad_b \cdot Ab \cdot Fbc \cdot (Tc - Tb)$	H/C LOAD	Qheat	RADIATION_d	$alfarad_c \cdot Ac \cdot Fcd \cdot (Td - Tc)$	RADIATION_c	$alfarad_d \cdot Ad \cdot Fdc \cdot (Tc - Td)$
ABSORPTION_n	$Aa \cdot Xcor_a \cdot Tpast$	RADIATION_d	$alfarad_b \cdot Ab \cdot Fbd \cdot (Td - Tb)$	convection with inner wall and floor					
radiation to section 1		conduction	$Ub \cdot Ab \cdot (To - Tb)$	CONVECTION_c	$alfaconv_ai \cdot Ac \cdot (Tc - Ti)$				
RADIATION_b	$alfarad_a \cdot Aa \cdot Fab \cdot (Tb - Ta)$	CONDUCTION		CONVECTION_d	$alfaconv_ai \cdot Ad \cdot (Td - Ti)$				
RADIATION_c	$alfarad_a \cdot Aa \cdot Fac \cdot (Tc - Ta)$								
RADIATION_d	$alfarad_a \cdot Aa \cdot Fad \cdot (Td - Ta)$								
CONDUCTION	$Ua \cdot Aa \cdot (To - Ta)$								
right equation	$Aa \cdot D1 \cdot Qz + Ab \cdot D1 \cdot Qz \cdot Fba + alfaconv_ao \cdot Aa \cdot (To - Ta) + alfaconv_ai \cdot Aa \cdot (Ti - Ta) + Aa \cdot X0_a \cdot Ta + alfarad_a \cdot Aa \cdot Fab \cdot (Tb - Ta) + alfarad_a \cdot Aa \cdot Fac \cdot (Tc - Ta) + alfarad_a \cdot Aa \cdot Fad \cdot (Td - Ta) + Ua \cdot Aa \cdot (To - Ta)$	right equation	$Ab \cdot A1 \cdot Qz + alfaconv_bo \cdot Ab \cdot (To - Tb) + alfaconv_bi \cdot Ab \cdot (Ti - Tb) + alfarad_b \cdot Ab \cdot Fba \cdot (Ta - Tb) + alfarad_b \cdot Ab \cdot Fbc \cdot (Tc - Tb) + alfarad_b \cdot Ab \cdot Fbd \cdot (Td - Tb) + Ub \cdot Ab \cdot (To - Tb)$	right equation	$vent \cdot person \cdot rho_air \cdot Cp_air \cdot (To - Ti) + alfaconv_ai \cdot Aa \cdot (Ta - Ti) + alfaconv_bi \cdot Ab \cdot (Tb - Ti) + Qint + Qheat + alfaconv_ai \cdot Ac \cdot (Tc - Ti) + alfaconv_ai \cdot Ad \cdot (Td - Ti)$	right equation	$alfaconv_ai \cdot Ac \cdot (Ti - Tc) + Ac \cdot X0_c \cdot Tc + alfarad_c \cdot Ac \cdot Fca \cdot (Ta - Tc) + alfarad_c \cdot Ac \cdot Fcb \cdot (Tb - Tc) + alfarad_c \cdot Ac \cdot Fcd \cdot (Td - Tc)$	right equation	$alfaconv_ai \cdot Ad \cdot (Ti - Td) + Ad \cdot X0_d \cdot Td + alfarad_d \cdot Ad \cdot Fda \cdot (Ta - Td) + alfarad_d \cdot Ad \cdot Fdb \cdot (Tb - Td) + alfarad_d \cdot Ad \cdot Fdc \cdot (Tc - Td)$
left equation	$Aa \cdot Xcor_a \cdot Tpast$	left equation	0	left equation	0	left equation	$Ac \cdot Xcor_c \cdot Tpast$	left equation	$Ad \cdot Xcor_d \cdot Tpast$

Appendix I

3M - Thinsulate Climate Control 75 Low-E Film (system 1)

	U-Value Before	U-Value After	Improvement	SHGC Before	SHGC After	Improvement
Single Pane (1/4")	1.03	0.62	40%	0.82	0.53	35%
Double Pane (1/4"; 1/2" air gap, 1/4")	0.47	0.35	26%	0.70	0.51	27%

Solar Screen - Solar 80C Insulating Film (system 2)

Technical Datasheet

Data from a product applied to a clear 3 mm glass (* on double glazing 4-16-4)








Ultraviolet Transmission	1%		
Visible Light Transmission	15%		
Reflection Of External Visible Light	53%		
Reflection Of Internal Visible Light	61%		
Total Solar Energy Rejected	82%		
Total Solar Energy Rejected 2*	86%		
Solar Ratio :		Heat Loss Reduction (Winter)	34%
Solar Energy Reflection	63%	Shading Coefficient	0.62
Solar Energy Absorption	25%	Installation Type	Interior
Solar Energy Transmission	15%	Roll Length	30.5 mètres
Reduction In Solar Glare	83%	Film Composition	PET
G-Value	0.18	Thickness	50µ
U-Value	3.8	Colour From The Outside	SILVER

Sotex Bolero Turquoise 53 (system 5)



BOLERO Turquoise 53

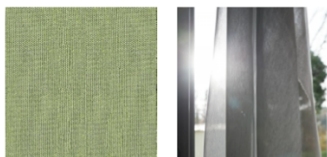
Technical properties

	
Flame retardant	Thermal
Applications Roman blinds - Curtains	
Composition 100% FR polyester	
Weight 400 g/m ²	Width 290 cm
Fabric direction Room high or standard direction	
Fitting +- cm 1 cm	
Maintenance advice     	
Certifications OEKO-TEX STANDARD 100 (CQ 1006/1)	
Minimum order 1 linear(s) meter(s)	

Technical characteristics

Flame retardant	M1 / B1 / IMO PASS / UNI 8456 / 9174 Classe Uno
Optical index	Light reflexion : 56 % Light absorption : 44 % Light transmission : 0 %
Thermal index	Solar reflexion : 55 % Solar absorption : 44 % Solar transmission : 1 % UV transmission : 0 % Gtot : Gt 39 % Fc 66 %
Resilience	Lightfastness (units Class/B) 5

Sotex M140 ALU Anis 62 (system 6)



M140 ALU Anis 62

Technical properties



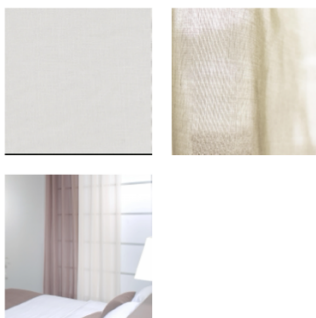


Flame retardant Thermal Sheer
Applications Roman blinds - Panel curtains - Curtains
Composition 100% aluminized FR polyester
Weight 70 g/m² **Width** 280 cm
Fabric direction Room high or standard direction **Fitting** ↔ cm ↓ cm
Maintenance advice    
Minimum order 1 linear(s) meter(s)

Technical characteristics

Flame retardant	M1 / IMO PASS
Optical index	Light reflexion : 32 %
	Light absorption : 40 %
	Light transmission : 28 %
Transparent veil	Yes
Thermal index	Solar reflexion : 34 %
	Solar absorption : 36 %
	Solar transmission : 30 %
	UV transmission : 28 %
	Gtot : Gt 46 % Fc 78 %
Resilience	Lightfastness (units Class/8) 6
	Dimensional Stability (%)
	Warp -0,5
	Weft 0
	Breaking Elongation
	Warp 14
	Weft 33
	Breaking load (daN)
	Warp 45
	Weft 41

Sotex ETAMINE Champagne 02 (system 7)



ETAMINE Champagne 02

This light and airy sheer curtain comes in several plain colours.

Technical properties




Flame retardant Sheer
Applications Roman blinds - Panel curtains - Curtains
Composition 100% FR polyester
Weight 95 g/m² **Width** 300 cm
Fabric direction Room high or standard direction **Fitting** ↔ cm ↓ cm
Maintenance advice    
Labels France Terre Textile (R016)
Certifications OEKO-TEX STANDARD 100 (CO 1006/1)
Minimum order 1 linear(s) meter(s)

Technical characteristics

Flame retardant	M1 / B1 / IMO PASS / UNI 8456 / 9174 Classe Uno
Optical index	Light reflexion : 42 %
	Light absorption : 4 %
	Light transmission : 54 %
Transparent veil	Yes
Thermal index	Solar reflexion : 43 %
	Solar absorption : 3 %
	Solar transmission : 54 %
	UV transmission : 52 %
	Gtot : Gt 44 % Fc 75 %
Resilience	Lightfastness (units Class/8) 6
	Dimensional Stability (%)
	Warp 0
	Weft 0
	Breaking Elongation
	Warp 46
	Weft 13
	Breaking load (daN)
	Warp 41
	Weft 40

Appendix J

Parameter estimation 1st attempt

L-BFGS-B

```
Optimization Result: message: CONVERGENCE: NORM_OF_PROJECTED_GRADIENT_<=_PGTOL
  success: True
  status: 0
  fun: 0.26550112817129595
  x: [ 4.000e-01  2.500e-01]
  nit: 0
  jac: [ 0.000e+00  0.000e+00]
  nfev: 3
  njev: 1
  hess_inv: <2x2 LbfgsInvHessProduct with dtype=float64>
```

SLSQP

```
Iter  obj      A1      D1
  1  0.565501  0.400000  0.250000
Optimization terminated successfully (Exit mode 0)
  Current function value: 0.26550112817129595
  Iterations: 1
  Function evaluations: 3
  Gradient evaluations: 1
Optimization Result: message: Optimization terminated successfully
  success: True
  status: 0
  fun: 0.26550112817129595
  x: [ 4.000e-01  2.500e-01]
  nit: 1
  jac: [ 0.000e+00  0.000e+00]
  nfev: 3
  njev: 1
```

Nelder-Mead

```
  2  0.565501  0.400000  0.250000
  3  0.565501  0.400000  0.250000
  4  0.565501  0.400000  0.250000
  5  0.565501  0.400000  0.250000
  6  0.565501  0.400000  0.250000
  7  0.565501  0.400000  0.250000
  8  0.565501  0.400000  0.250000
  9  0.565501  0.400000  0.250000
 10  0.565501  0.400000  0.250000
 11  0.565501  0.400000  0.250000
 12  0.565501  0.400000  0.250000
 13  0.565501  0.400000  0.250000
 14  0.565501  0.400000  0.250000
 15  0.565501  0.400000  0.250000
 16  0.565501  0.400000  0.250000
 17  0.565501  0.400000  0.250000
Optimization terminated successfully.
  Current function value: 0.265501
  Iterations: 16
  Function evaluations: 63
Optimization Result: message: Optimization terminated successfully.
  success: True
  status: 0
  fun: 0.26550112817129595
  x: [ 4.000e-01  2.500e-01]
  nit: 16
  nfev: 63
final_simplex: (array([[ 4.000e-01,  2.500e-01],
 [ 4.000e-01,  2.500e-01],
 [ 4.000e-01,  2.500e-01]]), array([ 2.655e-01,  2.655e-01,  2.655e-01]))
```

Appendix K

Parameter estimation 2nd attempt

L-BFGS-B

```
Iter   obj      A1      D1
  1   0.549380  0.389913  0.239922
Optimization Result:  message: CONVERGENCE: REL_REDUCTION_OF_F_<= _FACTR*EPSMCH
success: True
status: 0
  fun: 0.5493795420907299
  x: [ 3.899e-01  2.399e-01]
  nit: 1
  jac: [ 8.723e-05  7.793e-05]
  nfev: 6
  njev: 2
  hess_inv: <2x2 LbfgsInvHessProduct with dtype=float64>
```

SLSQP

```
  2   0.549380  0.390000  0.240000
Optimization terminated successfully (Exit mode 0)
  Current function value: 0.5493795557781799
  Iterations: 1
  Function evaluations: 3
  Gradient evaluations: 1
Optimization Result:  message: Optimization terminated successfully
success: True
status: 0
  fun: 0.5493795557781799
  x: [ 3.900e-01  2.400e-01]
  nit: 1
  jac: [ 8.725e-05  7.795e-05]
  nfev: 3
  njev: 1
```

Nelder-Mead

```
  3   0.549378  0.351000  0.258000
  4   0.549375  0.331500  0.243000
  5   0.549370  0.243750  0.271500
  6   0.549366  0.200000  0.255750
  7   0.549366  0.200000  0.255750
  8   0.549366  0.200000  0.255750
  9   0.549363  0.200000  0.217875
 10   0.549361  0.200000  0.173438
 11   0.549358  0.200000  0.125000
 12   0.549358  0.200000  0.125000
 13   0.549358  0.200000  0.125000
 14   0.549358  0.200000  0.125000
Optimization terminated successfully.
  Current function value: 0.549358
  Iterations: 12
  Function evaluations: 22
Optimization Result:  message: Optimization terminated successfully.
success: True
status: 0
  fun: 0.5493581675739961
  x: [ 2.000e-01  1.250e-01]
  nit: 12
  nfev: 22
final_simplex: (array([[ 2.000e-01,  1.250e-01],
 [ 2.000e-01,  1.250e-01],
 [ 2.000e-01,  1.250e-01]]), array([ 5.494e-01,  5.494e-01,  5.494e-01]))
```

Appendix L

Parameter estimation 3rd attempt

L-BFGS-B

```
Iter  obj  A1  D1  X0_a  X0_c  X0_d
1  0.549380  0.389913  0.239922  3.916000  11.002000  3.916000
Optimization Result: message: CONVERGENCE: REL_REDUCTION_OF_F_<= _FACTR*EPSMCH
success: True
status: 0
fun: 0.5493795420907299
x: [ 3.899e-01  2.399e-01  3.916e+00  1.100e+01  3.916e+00]
nit: 1
jac: [ 8.723e-05  7.793e-05  0.000e+00  0.000e+00  0.000e+00]
nfev: 12
njev: 2
hess_inv: <5x5 LbfgsInvHessProduct with dtype=float64>
```

SLSQP

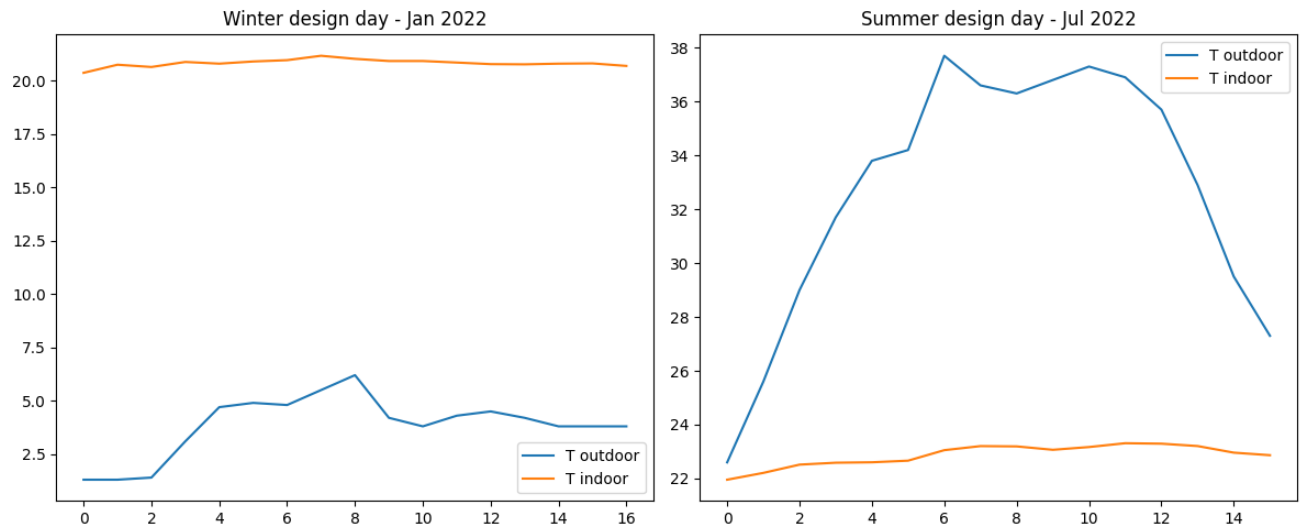
```
2  0.549380  0.390000  0.240000  3.916000  11.002000  3.916000
Optimization terminated successfully (Exit mode 0)
Current function value: 0.5493795557781799
Iterations: 1
Function evaluations: 6
Gradient evaluations: 1
Optimization Result: message: Optimization terminated successfully
success: True
status: 0
fun: 0.5493795557781799
x: [ 3.900e-01  2.400e-01  3.916e+00  1.100e+01  3.916e+00]
nit: 1
jac: [ 8.725e-05  7.795e-05  0.000e+00  0.000e+00  0.000e+00]
nfev: 6
njev: 1
```

Nelder-Mead

```
3  0.549377  0.351000  0.247200  4.033480  11.332060  4.033480  37  0.549358  0.200000  0.125000  7.832000  18.335233  7.832000
4  0.549377  0.351000  0.247200  4.033480  11.332060  4.033480  38  0.549358  0.200000  0.125000  7.832000  18.335233  7.832000
5  0.549377  0.351000  0.247200  4.033480  11.332060  4.033480  39  0.549358  0.200000  0.125000  7.832000  18.335233  7.832000
6  0.549377  0.351000  0.247200  4.033480  11.332060  4.033480  40  0.549358  0.200000  0.125000  7.832000  18.335233  7.832000
7  0.549374  0.325790  0.237742  4.149832  11.342094  4.431784  41  0.549358  0.200000  0.125000  7.832000  18.335233  7.832000
8  0.549371  0.287265  0.236387  4.290132  11.546150  4.232175  42  0.549358  0.200000  0.125000  7.832000  18.335233  7.832000
9  0.549371  0.287265  0.236387  4.290132  11.546150  4.232175  43  0.549358  0.200000  0.125000  7.832000  18.335233  7.832000
10  0.549371  0.287265  0.236387  4.290132  11.546150  4.232175  44  0.549358  0.200000  0.125000  7.832000  18.335233  7.832000
11  0.549366  0.213813  0.246147  4.629269  12.339351  4.502340  45  0.549358  0.200000  0.125000  7.832000  18.335233  7.832000
12  0.549364  0.200000  0.228965  4.694765  12.607504  5.039919  46  0.549358  0.200000  0.125000  7.832000  18.335233  7.832000
13  0.549364  0.200000  0.228965  4.694765  12.607504  5.039919  47  0.549358  0.200000  0.125000  7.832000  18.335233  7.832000
14  0.549364  0.200000  0.228965  4.694765  12.607504  5.039919  48  0.549358  0.200000  0.125000  7.832000  18.335233  7.832000
15  0.549364  0.200000  0.228965  4.694765  12.607504  5.039919  49  0.549358  0.200000  0.125000  7.832000  18.335233  7.832000
16  0.549364  0.200000  0.228965  4.694765  12.607504  5.039919  50  0.549358  0.200000  0.125000  7.832000  18.335233  7.832000
17  0.549363  0.200000  0.217125  5.421881  13.886901  5.718067  51  0.549358  0.200000  0.125000  7.832000  18.335233  7.832000
18  0.549363  0.200000  0.217125  5.421881  13.886901  5.718067  52  0.549358  0.200000  0.125000  7.832000  18.335233  7.832000
19  0.549362  0.200000  0.199051  6.212624  14.933015  6.638988  Optimization terminated successfully.
20  0.549361  0.200000  0.178286  5.444859  13.778383  6.008154  Current function value: 0.549358
21  0.549361  0.200000  0.178286  5.444859  13.778383  6.008154  Iterations: 50
22  0.549359  0.200000  0.142753  7.359306  17.543898  7.832000  Function evaluations: 198
23  0.549359  0.200000  0.142753  7.359306  17.543898  7.832000  Optimization Result: message: Optimization terminated successfully.
24  0.549358  0.200000  0.125000  7.832000  18.335233  7.832000  success: True
25  0.549358  0.200000  0.125000  7.832000  18.335233  7.832000  status: 0
26  0.549358  0.200000  0.125000  7.832000  18.335233  7.832000  fun: 0.5493581675730961
27  0.549358  0.200000  0.125000  7.832000  18.335233  7.832000  x: [ 2.000e-01  1.250e-01  7.832e+00  1.834e+01  7.832e+00]
28  0.549358  0.200000  0.125000  7.832000  18.335233  7.832000  nit: 50
29  0.549358  0.200000  0.125000  7.832000  18.335233  7.832000  nfev: 198
30  0.549358  0.200000  0.125000  7.832000  18.335233  7.832000  final_simplex: (array([[ 2.000e-01,  1.250e-01, ...,  1.834e+01,
31  0.549358  0.200000  0.125000  7.832000  18.335233  7.832000  [ 2.000e-01,  1.250e-01, ...,  1.834e+01,
32  0.549358  0.200000  0.125000  7.832000  18.335233  7.832000  [ 2.000e-01,  1.250e-01, ...,  1.834e+01,
33  0.549358  0.200000  0.125000  7.832000  18.335233  7.832000  [ 2.000e-01,  1.250e-01, ...,  1.834e+01,
34  0.549358  0.200000  0.125000  7.832000  18.335233  7.832000  [ 2.000e-01,  1.250e-01, ...,  1.834e+01,
35  0.549358  0.200000  0.125000  7.832000  18.335233  7.832000  [ 2.000e-01,  1.250e-01, ...,  1.834e+01,
36  0.549358  0.200000  0.125000  7.832000  18.335233  7.832000  [ 2.000e-01,  1.250e-01, ...,  1.834e+01,
5.494e-01,  5.494e-01,  5.494e-01,  5.494e-01,  5.494e-01,  5.494e-01]))
```

Appendix M

Design Days



Appendix N

Cooling and heating load comparison values (on design days)

Base summer: 2,182.28

Base winter: 5,941.62

Seasons	Cooling and heating load reduction compared to baseline							
	B_C	B_S	sys5	sys5_C	sys5_S	sys8	sys8_C	sys8_S
Summer	373.82	382.80	1,097.28	373.85	382.15	978.34	373.86	382.19
Winter	3,590.63	5,482.61	4,993.94	3,437.42	5,402.41	3,721.01	3,404.08	5,055.29